Volume 6, Number 4, 2006 ISSN 1562-8353

NONLINEAR DYNAMICS AND SYSTEMS THEORY
An International Journal of Research and Surveys

Volume 6 Number 4 2006

CONTENTS

 ISSN 1562-8353 Printed in Ukraine
To receive contents and abstracts by e-mail, visit our Website at: **http://www.e-ndst.kiev.ua**

NONLINEAR DYNAMICS & SYSTEMS THEORY Volume 6, No. 4, 2006

Nonlinear Dynamics and Systems Theory

An International Journal of Research and Surveys

Academic Periodical Press

Nonlinear Dynamics and Systems Theory
An International Journal of Research and Surveys

NONLINEAR DYNAMICS AND SYSTEMS THEORY
An International Journal of Research and Surveys

INSTRUCTIONS FOR CONTRIBUTORS

(1) General. The Journal will publish original carefully refereed papers, brief notes and reviews on a wide range of nonlinear dynamics and systems theory problems. Contributions will be considered for publication in ND&ST if they have not been published previously. Before preparing your submission, it is essential that you consult our style guide; please visit our website: http://www.e-ndst.kiev.ua

(2) Manuscript and Correspondence. Contributions are welcome from all countries and should be written in English. Two copies of the manuscript, double spaced one column format, and the electronic version by AMSTEX, TEX or LATEX program (on diskette) should be sent directly to

Professor A.A. Martynyuk
Institute of Mechanics,
Nesterov str.3, 03057, MSP 680
Kiev-57, Ukraine
(e-mail: anmart@stability.kiev.ua)

or to one of the Editors or to a member of the Editorial Board.

The title of the article must include: author(s) name, name of institution, department, address, FAX, and e-mail; an Abstract of 50-100 words should not include any formulas and citations; key words, and AMS subject classifications number(s). The size for regular paper should be 10-14 pages, survey (up to 24 pages), short papers, letter to the editor and book reviews (2-3 pages).

(3) Tables, Graphs and Illustrations. All figures must be suitable for reproduction without being retouched or redrawn and must include a title. Line drawings should include all relevant details and should be drawn in black ink on plain white drawing paper. In addition to a hard copy of the artwork, it is necessary to attach a PC diskette with files of the artwork (preferably in PCX format).

(4) References. Each entry must be cited in the text by author(s) and number or by number alone. All references should be listed in their alphabetic order. Use please the following style:

Journal: [1] Poincaré, H. Title of the article. *Title of the Journal* **Vol.1**(No.1) (year) pages. [Language].
Book: [2] Liapunov, A.M. *Title of the book.* Name of the Publishers, Town, year.
Proceeding: [3] Bellman, R. Title of the article. In: *Title of the book.* (Eds.). Name of the Publishers, Town, year, pages. [Language].

(5) Proofs and Reprints. Proofs sent to authors should be returned to the Editor with corrections within three days after receipt. Acceptance of the paper entitles the author to 10 free reprints.

(6) Editorial Policy. Every paper is reviewed by the regional editor, and/or a referee, and it may be returned for revision or rejected if considered unsuitable for publication.

(7) Copyright Assignment. When a paper is accepted for publication, author(s) will be requested to sign a form assigning copyright to Informath Publishing Group. Failure to do it promptly may delay the publication.

NONLINEAR DYNAMICS AND SYSTEMS THEORY
An International Journal of Research and Surveys
Published since 2001

Volume 6 Number 4 2006

CONTENTS

Founded by A.A. Martynyuk in 2001.
Registered in Ukraine Number: KB № 5267 / 04.07.2001.

NONLINEAR DYNAMICS AND SYSTEMS THEORY

An International Journal of Research and Surveys

Nonlinear Dynamics and Systems Theory (ISSN 1562-8353 (Print), ISSN 1813-7385 (Online)) is an international journal published under the auspices of the S.P.Timoshenko Institute of Mechanics of National Academy of Sciences of Ukraine and the Laboratory for Industrial and Applied Mathematics (LIAM) at York University (Toronto, Canada). It is aimed at publishing high quality original scientific papers and surveys in area of nonlinear dynamics and systems theory and technical reports on solving practical problems. The scope of the journal is very broad covering:

SCOPE OF THE JOURNAL

Analysis of uncertain systems • Bifurcations and instability in dynamical behaviors • Celestial mechanics, variable mass processes, rockets • Control of chaotic systems • Controllability, observability, and structural properties • Deterministic and random vibrations • Differential games • Dynamical systems on manifolds • Dynamics of systems of particles • Hamilton and Lagrange equations • Hysteresis • Identification and adaptive control of stochastic systems • Modeling of real phenomena by ODE, FDE and PDE • Nonlinear boundary problems • Nonlinear control systems, guided systems • Nonlinear dynamics in biological systems • Nonlinear fluid dynamics • Nonlinear oscillations and waves • Nonlinear stability in continuum mechanics • Non-smooth dynamical systems with impacts or discontinuities • Numerical methods and simulation • Optimal control and applications • Qualitative analysis of systems with aftereffect • Robustness, sensitivity and disturbance rejection • Soft computing: artificial intelligence, neural networks, fuzzy logic, genetic algorithms, etc. • Stability of discrete systems • Stability of impulsive systems • Stability of large-scale power systems • Stability of linear and nonlinear control systems • Stochastic approximation and optimization • Symmetries and conservation laws

PUBLICATION AND SUBSCRIPTION INFORMATION

The **Nonlinear Dynamics and Systems Theory** is published four times per year in 2006. Base list subscription price per volume: US$ 149.00. This price is available only to individuals whose library subscribes to the journal OR who warrant that the Journal is for their own use and provide a home address for mailing. Separate rates apply to academic and corporate/government institutions. Our charge includes postage, packing, handling and airmail delivery of all issues. Mail order and inquires to: Department of Processes Stability, S.P.Timoshenko Institute of Mechanics NAS of Ukraine, Nesterov str., 3, 03057, Kiev-57, MSP 680, Ukraine, Tel: ++38-044-456-6140, Fax: ++38-044-456-0319, E-mail: anchern@stability.kiev.ua, http://www.sciencearea.com.ua; http://www.e-ndst.kiev.ua

ABSTRACTING AND INDEXING SERVICES

EBSCO Databases, Swets Information Services, Mathematical Reviews/MathSciNet, Zentralblatt MATH/Mathematics Abstracts.

Nonlinear Dynamics and Systems Theory, **6** (4) (2006) 309–318

INFORMATH Publishing Group

PERSONAGE IN SCIENCE

Academician Yu.A. Mitropolskii

V. Lakshmikantham[1], A.A. Martynyuk[2*] and J.H. Dshalalow[1]

[1] *Department of Mathematical Sciences, Florida Institute of Technology, Melbourne, FL 32901, USA*
[2] *Institute of Mechanics, National Academy of Sciences of Ukraine, Nesterov Str., 3, Kiev, 03057, MSP-680, Ukraine*

On January 3, 2007, Professor Yurii Alexeevich Mitropolskii, the Member of the National Academy of Sciences of Ukraine and Member of Russian Academy of Sciences, will turn 90. The Editorial Board of the International Scientific Journal "Nonlinear Dynamics and Systems Theory" wishes him many happy returns of this day and a great health and prosperity. To honor Professor Mitropolskii, the Editorial Board of "Nonlinear Dynamics and Systems Theory" presents here a biographical sketch highlighting Mitropolskii's research and scholarly activities.

1 Brief Outline of Mitropolskii's Life

Yurii Alexeevich Mitropolskii was born on January 3, 1917 in the Charnysh's estate located in Kobelyakskiy district of Poltava province. Shortly thereafter he was baptized in Shishaki village, Kobelyakskiy district of the same province where his birth certificate was issued. This is why Shishaki village is erroneously referred to as his place of birth.

Yurii Alexeevich's grandfather on his father's side, Savva Alexeevich Mitropolskii, graduated from St. Petersburg Military Medical Academy and then served at Michailovskoye Artillery Academy. In 1906 he retired at the rank of a general.

Yurii Alexeevich's father, Alexey Savvich, enrolled St. Petersburg University, department of physics and mathematics, but later changed his major to law and graduated 1906 with a law degree. Yurii Alexeevich's mother, Vera Vasilievna (whose maiden name was Charnysh) was born to a noble family. Her great-grandfather, Ivan Vasilievich Charnysh, was the chairman of the noble community in Poltava province. His grandson, Vasiliy Nikolaevich Charnysh, the father of Vera Vasilievna, at the age of 17, voluntarily joined the Russian Imperial army during the Russian-Turkish war to liberate Bulgaria from the Ottoman oppression. In 1878, in the battle at Plevna (Bulgaria), he was severely wounded. He died in 1906 at the age of 46.

* Corresponding author: anmart@stability.kiev.ua

Alexey Savvich served in the Russian Army during the First World War. Later he joined the Red Army and continued to serve there until his retirement in 1926.

During the civil war (in 1918), the Charnysh's residence was completely destroyed. It was common for that time. Consequently, the Mitropolskii's moved to Kiev. In 1932, Yurii Alexeevich finished a 7-years school in Kiev followed by his employment at a cannery. In 1938, Yurii Alexeevich graduated from a high school with honors. In the same year, he was accepted at Kiev University in the department of mathematics and physics. During that time, lectures were taught by B.Ya. Bukreev, G.F. Pfeiffer, and V.E. Dyachenko, while N.N.Bogoliubov and M.A.Lavrentiev were among young instructors.

Upon completion of his third year at Kiev University, when on the day of June 22, 1941, the fascist Germany attacked the Soviet Union, Yurii Alexeevich married his university mate Alexandra Ivanovna to live together happily for more than 60 years. All this time, Alexandra Ivanovna has been his loyal friend and a guardian angel. Yurii Alexeevich and Alexandra Ivanovna have two children: son Alexey (born in 1942) and daughter Nadezhda (born in 1948).

On July 7, 1941 Yurii Alexeevich joined the Soviet Army and was stationed in an armor division in the city of Chuguyev. In October of 1941, according to the decree issued by the Defense Secretary S.K. Timoshenko, all fourth and fifth years college students were eligible to continue their degrees at the corresponding universities, with forthcoming appointments at military academies. Yurii Alexeevich was sent to the city of Kzyl-Orda in Kazakhstan where Kiev University was evacuated to. In March of 1942, Yurii Alexeevich successfully passed all exams and graduated from Kazakh University and then was sent to Ryazan Artillery Academy in the city of Talgar, which he graduated from in March of 1943 in the rank of a lieutenant. He was sent to the Stepnoy battlefield thereafter.

In 1946, after being discharged from the army, Yurii Alexeevich joined the Ukrainian Academy of Sciences in Kiev in the capacity of a Junior Scientist. In 1948 Yurii Alexeevich received his Candidate of Science degree (the Western equivalent of a Ph.D. degree). His thesis was titled "Investigation of resonance phenomena in nonlinear systems with variable frequencies." In the same year he joined the Institute of Constructive Mechanics of the Ukrainian Academy of Sciences (now S.P. Timoshenko's Institute of Mechanics of the National Academy of Sciences of Ukraine) in the capacity of a Senior Scientist under the supervision of N.N. Bogoliubov.

In 1951 he was awarded a Doctor of Science degree (the Western and Eastern European equivalent of Habilitation Degree). His thesis was titled "Slow processes in nonlinear oscillatory systems with many degrees of freedom." Earlier he moved to the Institute of Mathematics of the Ukrainian Academy of Sciences where he was appointed a Senior Scientist. In 1953 Yurii Alexeevich was promoted to the rank of Professor and Department Head in the same Institute. In 1956 he became the Associate Provost of Science of this Institute and in 1958 he was appointed its Director. He remained in this capacity up until 1988. Since1988 he has served as the Honorary Director of the Institute of Mathematics.

In 1958, Yurii Alexeevich was elected the Corresponding Member of the Academy of Sciences of Ukrainian SSR and in 1961 he was elected the Full Member of the Academy of Sciences of the USSR (now the Russian Academy of Sciences), then the most prestigious academic title in the USSR.

2 Basic Trends of His Scientific Work

During the years of his scientific activity, Yurii Alexeevich Mitropolskii has obtained numerous fundamental results in nonlinear mechanics and differential equations. The results of his prolific research were manifested in more than 700 articles and 50 monographs, of which most essential are "Nonstationary Processes in Nonlinear Oscillating Systems" (1955), "Asymptotic Methods in the Theory of Nonlinear Oscillations" (1964), "Averaging Method in Nonlinear Mechanics" (1971), and "Nonlinear Mechanics. Single-Frequency Oscillations" (1997).

We present an overview of his most significant work.

2.1 Development of Asymptotic Methods in Nonlinear Mechanics

Along with N.M. Krylov and N.N. Bogoliubov, Mitropolskii was one of the first to develop asymptotic methods in nonlinear mechanics. More specifically, he studied nonstationary processes under variations of frequency, mass and other parameters of nonlinear systems.

Imposing the condition on the system parameters to be of slow variation relative to the characteristic period of oscillations, Mitropolskii created a very efficient approach. In fact, this condition turned out to be very practical and it often applies to various problems of physics and engineering. By means of this approach, he obtained significant results in many real world situations for models with one and many degrees of freedom that pass through a resonance.

Due to the successful applications of this method, a number of phenomena in nonlinear oscillating systems (for example, amplitude delay, breakdowns and abrupt changes of amplitude, beats, etc.) were finally explained.

An important application of this method was the calculation of resonance. This method has also led to the description of the formation of a noise in a cyclotron built in the United Institute of Nuclear Research located in Dubna (Russia). Calculation of turbo-engine rotor oscillations and of centrifuge oscillations were among other notable applications of the method.

A historical development of this method was described in his monographs [1-3, 12, 14, 15, 26, 30, 36, 38, 40, 47, 48] written in Russian. Some of them were translated into many languages worldwide (see [6, 7, 10, 11, 17, 43, 46]).

2.2 The Development of the Single-Frequency Method

In 1948, when investigating an autonomous system with many degrees of freedom, N.N. Bogoliubov suggested a scheme of partial solution for equations describing single-frequency oscillations. The proposed scheme was based on the averaging method. Having used the same averaging method, Mitropolskii developed a technique of an asymptotic solution in the form of a series. A remarkable advantage of the series method is that one can construct a differential equation to define the amplitude and phase with no need of precise motion equations.

Mitropolskii extended the single-frequency method to distributed parameter systems and systems with gyroscopic terms. A version of one-frequency method developed by him for equations in a symbolic form turned out to be effective in the investigation of nonstationary oscillations of crank-shafts, systems of transmissions, and electrical circuits.

The method is well established in a series of papers by Mitropolskii as well as in his monograph [42].

2.3 Contribution to the Method of Integral Manifolds

Another major area of Mitropolskii's research was initiated in his work on the method of integral manifolds. In the early 50th, he proposed and laid the foundation to the method involving the construction of a two-parametric family of partial solutions to systems with many degrees of freedom and slowly varying parameters.

His most important contribution to this subject of study includes establishing an existence criteria for integral manifolds in systems of nonlinear differential equations with variable coefficients and in resonance systems. In particular, these existence criteria were related to the regions of parametric resonance in resonance systems. Furthermore, Mitropolskii came across the quasisyncronization phenomenon. He also extended the method of integral manifolds from finite- to infinite-dimensional systems, distributed parameter systems, and singularly perturbed systems, to name a few.

The results obtained along this topic have been presented in monographs [13, 19, 24].

2.4 The Method of Accelerated Convergence

His work on accelerated of convergence corresponds to yet another direction in Mitropolskii's research. It was initially suggested by N.N. Bogoliubov, and it was based on a combination of the accelerated convergence method and the method of integral manifolds. This approach was essentially developed by Mitropolskii and recently applied to numerous problems in nonlinear mechanics.

Let us mention some of them: the problem of reducibility of a nonlinear system of differential equations to a linear system with constant coefficients, the problem on reducibility of linear systems with quasiperiodical coefficients to linear systems with constant coefficients, investigation of trajectories on tora, and others. The basic results obtained along this subject have been summarized in monograph [22] (see also [27]).

2.5 The Averaging Method

Mitropolskii's studies on the averaging method also generated a new direction in his intense research activities. The initiation of a rigorous theory of the averaging method was due to N.N. Bogoliubov. In Mitropolskii's work, the Bogoliubov's technique became further enhanced and adopted to new classes of differential equations containing small and large parameters, as well as to equations in functional spaces, equations with deviating arguments, and to integro-differential and stochastic differential equations. For the investigation of partial differential equations of a quasi-hyperbolic type he developed a particular version of averaging and shortening technique for infinite-dimensional systems. This begot an investigation of distributed parameter systems and systems with slowly varying parameters.

Numerous results obtained along this line have been brought together in monograph [23] (see also [31, 32, 35, 44] in Russian and [25, 37] in other languages).

2.6 Asymptotic Methods and Averaging Method for Distributed Parameter Systems

Another notable direction in Mitropolskii's research includes his studies on distributed parameter systems. Based on N.M. Krylov's and N.N. Bogoliubov's suggestions to use

asymptotic expansion method for distributed parameter systems, Mitropolskii explored their ideas beginning with a rigorous mathematical formalism. In a combination of the single-frequency method with Fourier method of separation of variables and the averaging method, Mitropolskii developed a very efficient and innovative approach.

This enabled him and his followers to construct approximate solutions for distributed parameter systems under nonlinearity, random perturbations, delays, nonlinearity with boundary conditions, and slowly varying parameters.

All of these led to the creation of the energy method, which is based on the construction of first and second approximation equations for the amplitude and phase of a single-frequency oscillating process. Instead of some preliminary construction of a precise quasi-hyperbolic partial differential equation, the use of the new approach enabled one to proceed immediately to an expression for potential and kinetic energy.

All related results have appeared in Mitropolskii's numerous papers and they were summarized in his monographs [34, 37, 41].

2.7 Contribution to the Theory of Systems with Delay and Small Parameter

The development of the theory of systems with delay and small parameter proves a unique versatility of Mitropolskii's analytical mind.

In this area he established existence conditions for periodic and quasiperiodic solutions for various classes of equations, he rendered stability analysis of these solutions, constructed toroidal manifolds and investigated the path behavior on them. He also solved problems of reducibility of difference equations with quasiperiodic coefficients to a linear system of differential equations, studied quasi-hyperbolic partial differential equations with delay, and constructed periodic solutions for neutral systems.

The results obtained in this area have been the subject to some special courses at Kiev University and they have appeared in monographs [21, 31].

2.8 Development of the Theory of Random Oscillating Processes

Mitropolskii developed asymptotic methods of nonlinear mechanics in the area of oscillating stochastic processes. He investigated the white noise effect on autonomous and nonautonomous quasilinear oscillating systems described by various equations and found various characteristics of oscillating stochastic processes.

The main results obtained along this line have been presented in monograph [36].

2.9 Contribution to the Theory of Decomposition of Systems

Recently, under the guidance of Mitropolskii and with his direct participation, a group of his students and collaborators developed the theory of multi-frequence oscillating processes and theory of decomposition for a wide class of large scale systems of ordinary differential equations. Mitropolskii and his research team developed a group theory approach when studying the solution structure of systems of ordinary differential equations. They constructed an enveloping Lie algebra generated by an initial system and its associated enveloping pseudogroup. Furthermore, they studied systems of linear and nonlinear differential equations with constant and variable coefficients, established conditions for their decompositions, and developed algorithms of some specific decompositions. The results obtained in the direction have been applied in physics and engineering.

The results obtained along this line were summarized in monograph [32] (see also [39]).

At the end of our survey on the main directions of investigations by Mitropolskii it should be noted that one of the characteristic features of his profound and prolific research is his versatility starting with a rigorous problem setting, continuing with analytical solution, and ending with an algorithm including numerical illustrative examples.

3 Research-Organizational and Pedagogical Activity

Since 1958, Mitropolskii has focused his attention on the development of the Institute of Mathematics of Academy of Science of the USSR. He initiated new departments setting up to facilitate research in the areas of algebra, probability theory, real and functional analysis, and mechanics of special systems.

During this period of time, the post-graduate enrollment was substantially expanded. As the result of Mitropolskii's efforts, the Institute produced about 500 candidates of science (equivalent to Ph.D. degrees in the US) and more than 80 doctors of science (equivalent to Habilitation Degree in Eastern and Western Europe) for their further employments at national universities and research labs in Ukraine, Russia, and other countries.

As a consequences of Mitropolskii's colossal scholarly activity, the Institute of Mathematics of Academy of Science of Ukranian SSR has become the leading scientific center of mathematical research in Ukraine.

Mitropolskii began his pedagogical activity in 1948 at Kiev university to extend it up to 1989. During all these years, along with the regular courses at the department of mechanics and mathematics he taught a variety of special courses in nonlinear mechanics, mathematical physics, and differential equations. Under Mitropolskii's supervision the Institute of Mathematics offered seminars, summer mathematical schools, and organized international conferences which all have had an enormous impact upon youth of all ages, including high school students.

Mitropolskii himself supervised and directed 100 Ph.D. and 25 Habilitation theses in physical and mathematical sciences.

From 1961 until 1992 Mitropolskii had been the Head of the Department of mathematics, mechanics and cybernetics at Academy of Sciences of Ukrainian SSR. Over this period of time he paid much attention to the development of mathematical schools in various Ukrainian districts where new scientific research institutes were opened and new programs were launched, all majoring in mathematics and physics.

In 1992 Mitropolskii was appointed the director of the International mathematical center of National Academy of Science of Ukraine and Counselor of Presidium of National Academy of Science of Ukraine. This position he continues to hold to this day.

4 Editorial Activity

Mitropolskii has been much involved in editorial work. He has initiated the publication of works by Academician N.M. Krylov and selected works by Academician N.N. Bogoliubov. In the years 1961 through 1968, the Institute of Mathematics of Academy of Science of Ukrainian SSR copyrighted and published Proceedings of seminars held at the Institute of Mathematics under Mitropolskii's direct editorship.

Since 1967, Mitropolskii has been the Editor-in Chief of the "Ukrainian Mathematical Journal" whose English translation is regularly published in the US. Since 1961, he has been an editorial board member of three Russian and three international journals.

Mitropolskii was among main contributors to a 12-volume selected works by N.N. Bogoliubov in the area of mathematics and nonlinear mechanics. Three volumes of this edition has been already published by the Russian Academy of Sciences.

Mitropolskii dedicated much of his time and efforts to popularize mathematics to the general public. He gave popular lectures, talks, and wrote articles on various topics in mathematics for newspapers and popular magazines. He also held the city hearings on urgent mathematical problems.

5 International Scientific Activity

The first international talk Mitropolskii gave in 1956 at the International congress of mathematicians in Bucharest, Romania. Since 1958, he has been an invited speaker to the International Mathematical Congresses held in Edinburgh, Scotland (1958), Stockholm Sweden (1962), Moscow, Russia (1966), Niece, France (1970), Vancouver, Canada (1974), Warsaw, Poland (1983), Berkeley, USA (1986), and Kyoto, Japan (1990).

In 1960, Mitropolskii spoke at the plenary meeting of 10th International Congress on theoretical and applied mechanics at Streza, Italy, to present the main achievements and unsolved problems in asymptotic methods of nonlinear mechanics. In 1970 he took part in the 1st Pan-African Mathematical Congress.

In 1961, Mitropolskii gave a plenary talk on the method of integral manifolds in nonlinear mechanics at the International Conference held in Colorado Springs, USA. His talk was synchronously translated by Professor S.A. Lefshets. A series of lectures and talks on individual problems in nonlinear mechanics was given by Mitropolskii at various universities in the USA, China, Vietnam, Czechoslovakia, Poland, Mexico, Canada, Italy, and Yugoslavia and numerous international conferences.

His active cooperation over the past two decades with Vietnamese scientists in the area of nonlinear mechanics and theory of differential equations is worth mentioning. Due to this cooperation, they have opened an active scientific school of nonlinear mechanics in Ukraine.

6 Awards

Mitropolskii has been one of the most celebrated scientists who has ever lived in Ukraine and Russia. Consequently, his research, scholarly, pedagogical activities and public service have been highly revered. He was awarded by almost all known highest and most prestigious prizes ever given to a Soviet citizen. Here is the list of some of them:

Hero of the Socialist Labor;
Honored Activist of Science of UkrSSR;
Lenin Prize Laureate;
State Prize Laureate of Ukraine;
Federal Prize Laureate of Soviet Union;
Lyapunov Golden Medal;
Certificate of the Soviet Supreme Presidium;
Certificate of Presidium of Supreme Soviet of UkrSSR;
Lenin Golden Medal;
Two Red Star Orders;
October Revolution Medal;
Labor Red Banner Medal;

Second-Degree Great Patriotic War Medal;

The Fifth Degree Yaroslav Mudryi Order;

Bogdan Hmelnitskiy Medal;

N.M. Krylov, N.N. Bogoliubov and M.A. Lavrentiev prizes of Presidium of the Academy of Sciences of Ukrainian SSR.

Also, outside Ukraine and Russia, Mitropolskii has been treated with a high respect. In 1971, he was elected the foreign member of Bologna Academy of Sciences (Italy) and awarded with a Silver Medal of Czechoslovak Academy of Sciences "For Achievements in Science and Deeds for the Mankind". The government of Vietnam awarded him with the "Friendship" Medals in 1987 and 2001.

Completing our survey of scientific, scientific-organizational and pedagogical activities of Mitropolskii we acknowledge his undisputable achievements in mathematics, his remarkable versatility, novelty and depth of his mathematical thinking, his profound contributions to the development of nonlinear mechanics and theory of differential equations, his loyalty and tireless efforts towards mathematical sciences, that all qualifies him as one of the most distinguished mathematicians of the twentieth century.

List of Monographs and Books by Yu.A. Mitropolskii

[1] *Asymptotical Methods in the Theory of Nonlinear Oscillations*, Gostekhizdat, Moscow, 1955. (with N.N.Bogoliubov)

[2] *Nonstationary Processes in Nonlinear Oscillating Systems*, Izd-vo Acad. nauk Ukr.SSR, Kiev, 1955.

[3] *Asymptotic Methods in the Theory of Nonlinear Oscillations*, Second Edition, Revised and Expanded, Fizmatgiz, Moscow, 1958. (with N.N.Bogoliubov)

[4] *Nonstationary Processes in Nonlinear Oscillating Systems*, Publ. of Acad. of Sci., Beijin, 1958. (Chinese)

[5] *Investigations of Oscillations in the Systems of Distributed Parameters: Asymptotical Methods*, Publ. of Kiev. Univ., Kiev, 1961. (with B.I.Moseenkov). (Ukrainian)

[6] *Asymptotic Methods in the Theory of Nonlinear Oscillations*, Gordon and Breach Science Publ., New York, (Delhi Hindustan Publishing Corp. India), 1961. (with N.N.Bogoliubov)

[7] *Asymptotic Methods in the Theory of Nonlinear Oscillations*, Math. Soc. of Japan, Tokyo, 1961. (Japanese)

[8] *Nonstationary Processes in Non-linear Oscillatory Systems*, Air Technical Intelligence Translation ATIC–270579 F–9085/V., 1961.

[9] *Nonstationary Processes in Nonlinear Oscillating Systems*, Math. Soc of Japan, y, 1962. (Japanese)

[10] *Les mthodes asymptotiques et thorie des oscillations non lineaires*, Gauthier-Villars, Paris, 1962. (with N.N.Bogoliubov) (France)

[11] *Asymptotic Methods in the Theory of Nonlinear Oscillations*, Publ. Acad. of Sci., Beijin, 1962. (with N.N.Bogoliubov) (Chinese)

[12] *Asymptotic Methods in the Theory of Nonlinear Oscillations*, Third Edition, Revised and Expanded, Fizmatgiz, Moscow, 1963. (with N.N. Bogoliubov) (Russian)

[13] *The Method of Integral Manifolds in Nonlinear Mechanics*, In: Contributions to Differential Equations. Wiley, New York, 1963. Vol. 2. P. 123-196. (with N.N.Bogoliubov)

[14] *The Problems of Asymptotic Theory of Nonstationary Vibrations*, Nauka, Moscow, 1964. (Russian)

[15] *Asymptotische Methoden in der Theorie der nichtlinearen Schwin-gungen*, Acad. Verlag, Berlin, 1965. (with N.N.Bogoliubov) (Germany)

[16] *Problems of the Asymptotic Theory of Nonstationary Vibrations*. Davey, New York, 1965.

[17] *Problemes de la Theorie Asymptotique des Oscillations Nonstationaires*, Quathier Villars, Paris, 1966. (France)

[18] *The Mono-frequency Method in the Dynamic Analysis of Structures*, A Special Research Report, New York, 1967. (with B.I. Moseenkov)

[19] *Lectures on the Method of Integral Manifolds*, Inst. of Math. Acad. nauk UkrSSR, Kiev, 1968. (with O.B.Lykova)

[20] *Lectures on Applications of Asymptotic Methods to Solution of Partial Differential Equations*, Inst. Math. Acad nauk UkrSSR, Kiev, 1968. (with B.I.Moseenkov)

[21] *Lecturs on the Theory of Vibrations of Delay Systems*, Inst. Math. Acad nauk UkrSSR, Kiev, 1969. (with D.I.Martynyuk)

[22] *Method of Accelerated Convergence in Nonlinear Mechanics*, Naukova Dumka, Kiev, 1969. (with N.N.Bogoliubov and A.M.Samoilenko)

[23] *Method of Averaging in Nonlinear Mechanics*, Naukova Dumka, Kiev, 1971.

[24] *Integral Manifolds in Nonlinear Mechanics*, Nauka, Moscow, 1973. (with O.B.Lykova)

[25] *Certains aspects des progress de la methode de centrage*, In: Nonlinear Mechanics, Centro intern. mat. estivo. CIME. Edizioni Cremonese, Roma. 1973. P. 173–313.

[26] *Asymptotic Methods in the Theory of Nonlinear Oscillations*, 4th Edition, Nauka, Moscow, 1974. (with N.N.Bogoliubov)

[27] *Method of Accelerated Convergence in Nonlinear Mechanics*, Springer Verlag, Berlin, 1976. (with N.N.Bogoliubov and A.M.Samoilenko)

[28] *Periodic and Quasiperiodic Oscillations od Delay Systems*, Vushch Shcola, Kiev, 1979. (with D.I.Martynyuk)

[29] *Machine Analysis of Nonlinear Resonance Circuit*, Naukova Dumka, Kiev, 1981. (with I.N.Molchanov)

[30] *Mathematical Justification of Asymptotic Methods of Nonlinear Mechanics*, Naukova Dumka, Kiev, 1983. (with G.P.Khoma)

[31] *Systems of Evolution Equations with Periodic and Conditionally Periodic Coefficients*, Naukova Dumka, Kiev, 1984. (with A.M.Samoilenko and D.I.Martynyuk)

[32] *Group-Theoretic Approach in Asymptotic Methods of Nonlinear Mechanics*, Naukova Dumka, Kiev, 1988. (with A.K.Lopatin)

[33] *Investigation of Dichotomie of Lianear Systems Differential Equations via Liapunov Functions*, Naukova Dumka, Kiev, 1990. (with A.M.Samoilenko and V.L.Kulik)

[34] *Asymptotic Methods of Investigations of Quasi-Wave Equations of Hyperbolic Type*, Naukova Dumka, Kiev, 1991. (with G.P.Khoma and M.I.Gromiak)

[35] *Method of Averaging in the Investigations of Resonance Systems*, Nauka, Moscow, 1992. (with E.A.Grebenikov and Yu.A.Riabov)

[36] *Nonlinear Oscillations in Quasilinear Dynamical Systems*, Naukova Dumka, Kiev, 1992. (with Nguen Van Dao and Nguen Dong Ann')

[37] *Systems of Evolution Equations with Periodic and Quasiperiodic Coefficiennts*, Kluwer Akademic Publishers, Dordrecht, 1993. (with A.M.Samoilenko and D.I.Martynyuk)

[38] *Applied Asymptotic Methods in Nonlinear Oscillations*, Hanoi, 1994. (with Nguen Van Dao)

[39] *Nonlinear Mechanics, Groups and Symmetry*, Kluwer Academic Publishers, Dordrecht, 1995. (with A.K.Lopatin)

[40] *Nonlinear Mechanics. Asymptotic Methods*, Inst. Math. NAS of Ukraine, Kiev, 1995.

[41] *Asymptotic Methods for Investigating Quasiwave Equations of Hyperbolic Type*, Kluwer Academic Publishers, Dordrecht, 1997. (with G.Khoma and M.Gromiak)

[42] *Nonlinear Mechanics. One-frequency Oscillations*, Inst. Math. NAS of Ukraine, Kiev, 1997.

[43] *Applied Asymptotic Methods in Nonlinear Oscillations*, Kluwer Academic Publishers, Dordrecht, 1997. (with Nguen Van Dao)

[44] *Introduction to Resonance Analytical Dynamics*, Janus-K., Moscow, 1999. (with E.A.Grebenikov and Yu.A.Riabov)

[45] *Dichotomies and Stability in Nonautonomous Linear Systems*, Taylor and Trancis, London and New York, 2003. (with A.M.Samoilenko and V.L.Kulik)

[46] *Lectures on Asymptotic Methods of Nonlinear Dynamics*, Victnam Nat. Univ. Publ. House, Hanoi, 2003. (with Nguyen Van Dao)

[47] *Methods of Nonlinear Dynamics*, Naukova Dumka, Kiev, 2005. (Ukrainian)

[48] *Asymptotical Methods in the Theory of Nonlinear Oscillations*, In: Collection of Scientific Works in 12 volumes by N.N. Bogoliubov, Mathematics and Nonlinear Mechanics, Vol.3, Nauka, Moscow, 2005. 8–600 p. (with N.N.Bogoliubov) (Russian)

Nonlinear Dynamics and Systems Theory, **6** (4) (2006) 319–336

Synchronization of Discrete-Time Hyperchaotic Systems Through Extended Kalman Filtering

A. Y. Aguilar-Bustos [1] and C. Cruz-Hernández [2*]

[1] *Electronics & Telecommunications Department*
[2] *Telematics Direction*
Scientific Research and Advanced Studies of Ensenada (CICESE)
Km. 107 Carretera Tijuana-Ensenada, 22860 Ensenada, B.C., México

Received: August 22, 2006; Revised: September 25, 2006

Abstract: In this paper, we use an extended Kalman filter (EKF) to sinchronize discrete-time hyperchaotic systems. In particular, we consider unidirectionally coupled maps corrupted by noise. Approximate synchronization is obtained between master and slave maps in case that the slave is designed as an EKF which is driven by a noisy drive signal from a noisy master dynamics. Two numerical examples are provided to illustrate the efficiency of the proposed approach.

Keywords: *Synchronization; hyperchaotic maps; discrete-time systems; extended Kalman filter; Lyapunov stability; convergence analysis.*

Mathematics Subject Classification (2000): 34C15, 34C28, 37B25, 37D45, 60G35, 93C55, 93E11.

1 Introduction

Synchronization of chaotic oscillations has attracted in recent decades much attention. Different approaches have been reported in the literature see, e.g. [1-14] and references therein. This phenomenon is supposed to have interesting applications in secure communications, see for example [14-23]. However, it has been shown [24, 25] that masking information signals by means of comparatively simple chaos with only one positive Lyapunov exponent does not ensure a sufficient level of security. In some cases, extracting of the information can be performed using common signal processing techniques. For **higher security** the **hyperchaotic systems** characterized by more than one positive Lyapunov exponent **are advantageous** over "simple" chaotic systems. Two factors of primordial importance in security considerations related to chaotic communication systems are:

* Corresponding author: ccruz@cicese.mx

i) *the dimensionality of the chaotic attractor, and*

ii) *the effort required to obtain the necessary parameters for the matching of a slave dynamics.*

One way to enhance the level of encryption security of the communication system consists in applying proper cryptographic techniques to the information signal in combination with chaos [26, 27]. Another way to solve this security problem is to encrypt the information by using high dimensional chaotic attractors, or hyperchaotic attractors, which take advantage of the increased randomness and unpredictabilily of the higher dimensional dynamics. In such option, one generally encounters multiple positive Lyapunov exponents. However, *hyperchaotic synchronization is a much more difficult problem*, see for example [28-30] and [11] for discrete-time context. Other alternative of synchronize hyperchaotic dynamics is using delay differential (or difference) equations, such systems have an infinite-dimensional state space and produce hyperchaos with an arbitrary large number of positive Lyapunov exponents [22, 23].

On the other hand, most of the previous work done on chaos synchronization has been concentrated on continuous-time chaotic systems. Discrete-time systems used for chaos synchronization though, having potential in applications of discrete communications, have not been thoroughly discussed. While a lot of work is available in the control of chaotic mappings, only a few works face the problem of synchronization of discrete-time chaotic systems.

Moreover, parameter uncertainty or unstructured uncertainty in the master dynamics and coupling signal, **noise** may appear due to measurement noise or uncertainties in the dynamics. In this case, synchronization becomes a more difficult problem, certainly no exact state reconstruction will be possible. Nevertheless, a **filtering** approach may be very suitable in this case, see [31] and in the discrete-time context [6, 7].

On the basis of these considerations, the objective of this paper is to extend the approach developed in [6, 7] to the synchronization of hyperchaotic noisy maps with noisy coupling signal. Our goal is achieved by designing an EKF as a slave. In this work, we show that synchronization of discrete-time hyperchaotic systems is indeed suitable from this viewpoint and, moreover, we proceed to apply this approach to synchronize two noisy maps as illustrative examples.

The paper is organized as follows. In Section 2 we state the problem under consideration, the noisy synchronization of discrete-time systems. In Section 3, based on Lyapunov theory, we present an analysis of asymptotic convergence of the EKF. To illustrate the proposed approach, we use in Section 4 an EKF as a slave to synchronize two noisy hyperchaotic maps. Finally, some conclusions are drawn in Section 5.

2 Problem Statement

We consider **noisy master dynamics** given by the state equation

$$x(k+1) = f(x(k)) + w(k), \qquad x(0) = x_0, \tag{1}$$

with coupling signal

$$y(k) = h(x(k)) + v(k). \tag{2}$$

In system (1), $w(k)$ represents the noise in the dynamics of the master system, which is assumed to be a zero mean noise process with $E\left[w(k)\, w^T(l)\right] = Q\delta_{kl} > 0$, with δ_{kl} the Kronecker delta function. Also $v(k)$ is a zero mean noise process with $E[v(k)\, v(l)] = R\delta_{kl} > 0$; the processes $v(k)$ and $w(k)$ are assumed to be independent.

The EKF that we use as **slave dynamics** for (1) with noisy coupling signal (2) is described as follows [32]:
Measurement update equations:

$$\hat{x}(k) = \hat{x}(k/k-1) + K_{\hat{x}}(k)\left[y(k) - h\left(\hat{x}(k/k-1)\right)\right], \tag{3}$$

where the vector $\hat{x}(k)$ is referred as the *filtered* estimate for the master state vector $x(k)$ at time k. The covariance of the error in $\hat{x}(k)$ is given by

$$P_{\hat{x}}(k) = \left[I - K_{\hat{x}}(k)\, H_{\hat{x}}(k)\right] P_{\hat{x}}(k/k-1). \tag{4}$$

Time update equations:
The (one-step ahead) *predictor* of $\hat{x}(k+1)$ is given by

$$\hat{x}(k+1/k) = f\left(\hat{x}(k)\right), \tag{5}$$

the covariance matrix of the prediction error is

$$P_{\hat{x}}(k+1/k) = F_{\hat{x}}(k)\, P_{\hat{x}}(k)\, F_{\hat{x}}^T(k) + Q, \tag{6}$$

where

$$K_{\hat{x}}(k) = P_{\hat{x}}(k/k-1)\, H_{\hat{x}}^T(k)\left[H_{\hat{x}}(k)\, P_{\hat{x}}(k/k-1)\, H_{\hat{x}}^T(k) + R\right]^{-1} \tag{7}$$

is the *Kalman gain matrix*, and

$$\begin{aligned} F_{\hat{x}}(k) &= \left.\frac{\partial\, f(x(k))}{\partial\, x(k)}\right|_{x(k)=\,\hat{x}(k)}, \\ H_{\hat{x}}(k) &= \left.\frac{\partial\, h(x(k))}{\partial\, x(k)}\right|_{x(k)=\,\hat{x}(k/k-1)}. \end{aligned} \tag{8}$$

In this paper, our main objective is: Given a noisy master system, and a noisy coupling signal; we want to design a suitable EKF for synchronization in the master-slave framework, such that the following problem is solved.

Definition (*Noisy synchronization*). *The slave dynamics (3)-(8)* ***synchronizes*** *with the noisy master dynamics (1) with noisy drive signal (2), if*

$$\|x(k) - \hat{x}(k)\| \le \rho, \qquad \forall k \ge \tau, \tag{9}$$

where ρ should be related to Q and R and is a constant of the synchronization/estimation error. If for a given ρ there exists a time instant τ (to be called the ***synchronization time****) such that condition (9) is fulfilled, then the noisy master (1) and the EKF slave (3)-(8) are* ***approximately synchronized*** *with level ρ.*

One might also consider as an adequate condition for approximate (or noisy) synchronization, if there exists a positive constant τ such that

$$E\left\{\|(x(k) - \hat{x}(k))\|^2\right\} \le \rho, \qquad \forall k \ge \tau.$$

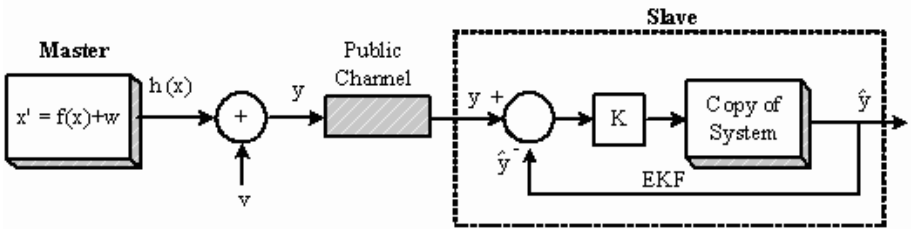

Figure 2.1: Master-slave coupling scheme for noisy hyperchaotic maps: where $x' = x(k+1)$ is the state master, w and v are independent noise processes, y the coupling signal, and $\hat{y}$ the output of EKF.

In particular, this may be a more relevant requirement if $w(k)$ is not necessarily bounded. Since we will assume that $v(k)$ and $w(k)$ are bounded, then is sufficient to take condition (9). Figure 2.1 shows the master-slave coupling scheme for approximate (or noisy) synchronization of maps (1) and (3)-(8) when the noisy drive signal (2) is used. Also, in all subsequent simulations we check the condition (9) over a long but finite time interval $[0, t_f]$.

3 Convergence Analysis of the EKF for Synchronization

In this section, based on Lyapunov theory, we make an analysis of the convergence of the synchronization error. Define the *estimation (synchronization) error* as

$$e(k) = x(k) - \hat{x}(k), \tag{10}$$

and the error between the state and the prediction of the estimation as

$$e(k/k-1) = x(k) - \hat{x}(k/k-1).$$

If we assume that f and h are C^1 functions, then f can be expanded (using Taylor's Theorem) as follows,

$$f(x) = f(\hat{x}) + F(k)[x(k) - \hat{x}(k)] + \varphi(x(k), \hat{x}(k)), \tag{11}$$

where $f(\hat{x})$ represents the copy of the system $f(x)$, $F = \partial f(x)/\partial x$ the first derivative of $f(x)$, and $\varphi(x, \hat{x})$ the remainder after the first order expansion of $f(x)$.

The dynamics of the error between the state of the master and the prediction are given by the equation,

$$\begin{aligned} e(k+1/k) &= x(k+1) - \hat{x}(k+1/k) \\ &= f(x(k)) + w(k) - f(\hat{x}(k)) \\ &= F(k)\, e(k) + \varphi(x(k), \hat{x}(k)) + w(k) \end{aligned}$$

and the dynamics of the state estimation (synchronization) error system are governed by

the following equation

$$\begin{aligned} e(k+1) &= x(k+1) - \hat{x}(k+1) \\ &= f(x(k)) + w(k) - f(\hat{x}(k)) - K(k+1)[y(k+1) - H\hat{x}(k+1/k)] \\ &= [I - K(k+1)H]F(k)e(k) + [I - K(k+1)H]\varphi(x(k), \hat{x}(k)) \\ &\quad + [I - K(k+1)H]w(k) - K(k+1)v(k+1), \\ e(k+1) &= [I - K(k+1)H]F(k)e(k) + r(k) + s(k), \end{aligned} \tag{12}$$

where

$$\begin{aligned} r(k) &= [I - K(k+1)H]\varphi(x(k), \hat{x}(k)), \\ s(k) &= [I - K(k+1)H]w(k) - K(k+1)v(k+1). \end{aligned}$$

Before going to analyze the stability of the error system (12) we make the following assumptions:

(A1) *There exist positive constants* $\bar{f}$, $\bar{h}$, p_1, *and* p_2 *such that the following bounds hold for all* $k \geq 0$:

$$\|F(k)\| \leq \bar{f}, \tag{13}$$

$$\|H(k)\| \leq \bar{h}, \tag{14}$$

$$p_1 I \leq P(k) \leq p_2 I, \tag{15}$$

$$qI \leq Q, \tag{16}$$

$$rI \leq R. \tag{17}$$

(A2) $F(k)$ *is nonsingular for all* $k \geq 0$.

(A3) *There exist positive constants* ϵ *and* κ *such that the function* $\varphi(x(k), \hat{x}(k))$ *in (11) is bounded by*

$$\|\varphi(x(k), \hat{x}(k))\| \leq \kappa \|x(k) - \hat{x}(k)\|^2,$$

for $x(k), \hat{x}(k) \in \mathbb{R}^n$ *with* $\|x(k) - \hat{x}(k)\| \leq \epsilon$.

In addition to this, we demonstrate the following lemmas to be required to establish the necessary conditions on stability of the estimation (synchronization) error given by the EKF.

Lemma 3.1 *Under the boundedness conditions (13)-(17) there exists a real number* $0 < \alpha < 1$ *such that* $P^{-1}(k)$ *satisfies the inequality*

$$F^T(k)[I - K(k+1)H]^T P^{-1}(k+1)[I - K(k+1)H]F(k) \leq (1-\alpha)P^{-1}(k)$$

for all $k \geq 0$.

Proof The term $P(k+1) = [I - K(k+1)H]\left[F(k)P(k)F^T(k) + Q\right]$ can be rewritten as follows

$$\begin{aligned} P(k+1) &= [I - K(k+1)H]F(k)P(k)F^T(k)[I - K(k+1)H]^T \\ &\quad + [I - K(k+1)H]Q[I - K(k+1)H]^T \\ &\quad + [I - K(k+1)H]\left[Q + F(k)P(k)F^T(k)\right]H^T K^T(k+1), \end{aligned} \tag{18}$$

where $[I - K(k+1)H]\left[Q + F(k)P(k)F^T(k)\right]$ is a symmetric matrix. Making use of the matrix inversion Lemma, we obtain

$$\begin{aligned}[I - K(k+1)H]\left[Q + F(k)P(k)F^T(k)\right] &= \\ \left[\left(Q + F(k)P(k)F^T(k)\right)^{-1} + H^T R^{-1} H\right]^{-1} &> 0, \end{aligned} \tag{19}$$

from Eq. (19) it follows that

$$[I - K(k+1)H]\left[Q + F(k)P(k)F^T(k)\right]H^T K^T(k+1) \geq 0, \tag{20}$$

using the condition (20) and eliminating that term of (18), the following inequality holds

$$\begin{aligned}P(k+1) \geq\ & [I - K(k+1)H]F(k)P(k)F^T(k)[I - K(k+1)H]^T \\ & + [I - K(k+1)H]Q[I - K(k+1)H]^T.\end{aligned}$$

Now, the above inequality can be rewritten as follows

$$P(k+1) \geq [I - K(k+1)H]F(k)\left[P(k) + F^{-1}(k)QF^{-T}(k)\right]F^T(k)[I - K(k+1)H]^T.$$

Using the conditions (13), (15), and (16), we have that

$$P(k+1) \geq [I - K(k+1)H]F(k)\left(I + \frac{qI}{\bar{f}^2 p_2}\right)P(k)F^T(k)[I - K(k+1)H]^T \tag{21}$$

and taking the inverse in both sides of inequality (21) and multiplying by $F^T(k)[I - K(k+1)H]^T$ and $[I - K(k+1)H]F(k)$, we have that

$$F^T(k)[I - K(k+1)H]^T P^{-1}(k+1)[I - K(k+1)H]F(k) \leq \left(1 + \frac{q}{p_2 \bar{f}^2}\right)^{-1} P^{-1}(k)$$

with $(1-\alpha) = \left(1 + \frac{q}{p_2 \bar{f}^2}\right)^{-1}$.

Lemma 3.2 *Since conditions (13)-(17) hold. Then, there exist positive constants ϵ and k_{nom} such that*

$$r^T(k)P^{-1}(k)\left[\,2[I - K(k+1)H]F(k)e(k) + r(k)\,\right] \leq k_{nom}\|e(k)\|^3$$

holds for all $\|e(k)\| \leq \epsilon$.

Proof Since $r(k) = [I - K(k+1)H]\varphi(x(k), \hat{x}(k))$ and by Assumption (A3), we have that $\|\varphi(x(k), \hat{x}(k))\| \leq \kappa\|e(k)\|^2$ in addition, considering $Q \leq \delta_1 I$ it follows that

$$\begin{aligned}\|K(k+1)\| &\leq \left\|\left[F(k)P(k)F^T(k) + Q\right]H^T\left[H\left[F(k)P(k)F^T(k) + Q\right]H^T + R\right]^{-1}\right\| \\ &\leq \left\|\left[F(k)P(k)F^T(k) + Q\right]\right\|\left\|H^T\right\|\left\|\left[H\left[F(k)P(k)F^T(k) + Q\right]H^T + R\right]^{-1}\right\| \\ &\leq \left\|\left[F(k)P(k)F^T(k) + Q\right]\right\|\left\|H^T\right\|\left\|\left[H\left[F(k)P(k)F^T(k) + Q\right]H^T + R\right]^{-1}\right\| \\ &\leq \left(\bar{f}^2 p_2 + \delta_1\right)\frac{\bar{h}}{r}.\end{aligned}$$

The term $\|K(k+1)\|$ can be expressed as $\|K(k+1)\| \leq \rho_1 + \rho_2\delta_1$ with $\rho_1 = \frac{\bar{f}^2 p_2 \bar{h}}{r}$ and $\rho_2 = \frac{\bar{h}}{r}$. Therefore, we obtain

$$\begin{aligned}
\|r(k)\| &\leq \|I - K(k+1)H\| \, \|\varphi(x(k), \hat{x}(k))\| \\
&\leq \|I - K(k+1)H\| \, \kappa \|e(k)\|^2 \\
&\leq [\|I\| + \|K(k+1)H\|] \, \kappa \|e(k)\|^2 \\
&\leq [1 + \|K(k+1)\| \, \|H\|] \, \kappa \|e(k)\|^2 \\
&\leq \left(1 + \rho_1\bar{h} + \rho_2\bar{h}\delta_1\right) \kappa \|e(k)\|^2 \qquad (22)
\end{aligned}$$

and making use of inequality (22), we have that

$$\begin{aligned}
& r^T(k) P^{-1}(k) [2[I - K(k+1)H]F(k) e(k) + r(k)] \\
\leq \; & \left\| r^T(k) P^{-1}(k) [2[I - K(k+1)H]F(k) e(k) + r(k)] \right\| \\
\leq \; & \left\| r^T(k) \right\| \left\| P^{-1}(k) \right\| \| [2[I - K(k+1)H]F(k) e(k) + r(k)] \| \\
\leq \; & \left(1 + \rho_1\bar{h} + \rho_2\bar{h}\delta_1\right) \kappa \|e(k)\|^2 \left(\frac{1}{p_1}\right) \\
& \times \left[2\left(1 + \rho_1\bar{h} + \rho_2\bar{h}\delta_1\right) \bar{f} \|e(k)\| + \left(1 + \rho_1\bar{h} + \rho_2\bar{h}\delta_1\right) \kappa \|e(k)\|^2\right] \\
\leq \; & \left(1 + \rho_1\bar{h} + \rho_2\bar{h}\delta_1\right)^2 \kappa \left(\frac{1}{p_1}\right) \left(2\bar{f} + \kappa\epsilon\right) \|e(k)\|^3 \\
\leq \; & k_{nom} \|e(k)\|^3
\end{aligned}$$

with

$$k_{nom} = \left(1 + \rho_1\bar{h} + \rho_2\bar{h}\delta\right)^2 \kappa \left(\frac{1}{p_1}\right) \left(2\bar{f} + \kappa\epsilon\right) \quad \text{and} \quad \delta = \delta_1.$$

Lemma 3.3 *Under the boundedness conditions (13)-(17). There exist positive real numbers ρ_3, ρ_4, and ρ_5 independent of δ, such that*

$$E\left\{s^T(k) P^{-1}(k+1) s(k)\right\} \leq \rho_3\delta^3 + \rho_4\delta^2 + \rho_5\delta$$

holds for some constant $\delta > 0$.

Proof Firstly, we have that

$$\begin{aligned}
s^T(k) P^{-1}(k+1) s(k) = \; & w^T(k)[I - K(k+1)H]^T P^{-1}(k+1)[I - K(k+1)H]w(k) \qquad (23) \\
& - w^T(k)[I - K(k+1)H]P^{-1}(k+1) K(k+1) v(k) \\
& - v^T(k) K^T(k+1) P^{-1}(k+1)[I - K(k+1)H]w(k) \\
& + v^T(k) K^T(k+1) P^{-1}(k+1) K(k+1) v(k)
\end{aligned}$$

since $w(k)$ and $v(k)$ are uncorrelated signals, the expression (23) becomes,

$$\begin{aligned}
s^T(k) P^{-1}(k+1) s(k) = \; & w^T(k)[I - K(k+1)H]^T P^{-1}(k+1)[I - K(k+1)H]w(k) \\
& + v^T(k) K^T(k+1) P^{-1}(k+1) K(k+1) v(k).
\end{aligned}$$

From Lemma 3.2, we have obtained that $\|K(k+1)\| \leq \rho_1 + \rho_2\delta_1$ with $\rho_1 = \frac{\bar{f}^2 p_2 \bar{h}}{r}$ and $\rho_2 = \frac{\bar{h}}{r}$ and, considering again that $Q \leq \delta_1 I$ and $R \leq \delta_2 I$, we have

$$\begin{aligned}
s^T(k) P^{-1}(k+1) s(k) \; &\leq \; \left(1 + \rho_1\bar{h} + \rho_2\bar{h}\delta_1\right)^2 \frac{1}{p_1} w^T(k) w(k) + (\rho_1 + \rho_2\delta_1)^2 \frac{1}{p_1} v^T(k) v(k) \\
&\leq \; \left(1 + \rho_1\bar{h} + \rho_2\bar{h}\delta_1\right)^2 \frac{1}{p_1}\delta_2 + (\rho_1 + \rho_2\delta_1)^2 \frac{1}{p_1}\delta_1 \qquad (24)
\end{aligned}$$

considering $\delta_1 = \delta_2 = \delta$ the above inequality can be rewritten as follows,

$$s^T(k) P^{-1}(k+1) s(k) \leq \rho_3 \delta^3 + \rho_4 \delta^2 + \rho_5 \delta$$

with

$$\rho_3 = \frac{\rho_2^2 \left(1 + \bar{h}^2\right)}{p_1}, \quad \rho_4 = \frac{2\rho_2 \left(\bar{h} + \rho_1 \bar{h}^2 + \rho_1\right)}{p_1}, \quad \rho_5 = \frac{1 + 2\rho_1 \bar{h} + \rho_1^2 \bar{h}^2 + \rho_1^2}{p_1}.$$

Lemma 3.4 ([35]) *Suppose that $V(e(k))$ is a stochastic process and that exist real numbers v_1, v_2, $\mu > 0$, and $0 < \alpha' \leq 1$ such that:*

$$v_1 \|e(k)\|^2 \leq V(e(k)) \leq v_2 \|e(k)\|^2,$$

$$E\{V(e(k+1))/e(k)\} - V(e(k)) \leq \mu - \alpha' V(e(k))$$

hold for all solution of Eq. (12). Then, the stochastic process is exponentially bounded as follows

$$E\left\{\|e(k)\|^2\right\} \leq \frac{v_2}{v_1} E\left\{\|e(0)\|^2\right\} (1-\alpha)^k + \frac{\mu}{v_1 \alpha'}.$$

In order to prove stability of the estimation (synchronization) error (10), we propose the following function as a Lyapunov function candidate

$$V(e(k)) = e^T(k) P^{-1}(k) e(k) \tag{25}$$

since $P(k)$ is a positive definite matrix, then $P^{-1}(k)$ is another positive definite matrix, and therefore $V(e(k))$ is positive definite, hence Lyapunov function candidate. From (15), we can obtain

$$\frac{1}{p_2} \|e(k)\|^2 \leq V(e(k)) \leq \frac{1}{p_1} \|e(k)\|^2,$$

iterating both sides of (25), we have

$$\begin{aligned} V(e(k+1)) &= e(k+1)^T P^{-1}(k+1) e(k+1) \\ &= e^T(k) F^T(k) [I - K(k+1) H]^T P^{-1}(k+1) [I - K(k+1) H] F(k) e(k) \\ &\quad + r^T(k) P^{-1}(k+1) [2[I - K(k+1) H] F(k) e(k) + r(k)] \\ &\quad + 2s^T(k) P^{-1}(k+1) [[I - K(k+1) H] F(k) e(k) + r(k)] \\ &\quad + s^T(k) P^{-1}(k+1) s(k). \end{aligned}$$

Using the Lemma 3.1, we obtain

$$\begin{aligned} V(e(k+1)) \leq\ & (1-\alpha) V(e(k)) \\ & + r^T(k) P^{-1}(k+1) [2[I - K(k+1) H] F(k) e(k) + r(k)] \\ & + 2s^T(k) P^{-1}(k+1) [[I - K(k+1) H] F(k) e(k) + r(k)] \\ & + s^T(k) P^{-1}(k+1) s(k). \end{aligned}$$

Taking the conditional expectation $E\{V(e(k+1))/e(k)\}$ and considering the properties of the white Gaussian random process, it is not difficult to see that the term

$$E\left\{2s^T(k) P^{-1}(k+1) [[I - K(k+1) H] F(k) e(k) + r(k)] | e(k)\right\}$$

vanishes. Thus, we have that

$$\begin{aligned} E\left\{V\left(e\left(k+1\right)\right)/e\left(k\right)\right\} &\leq \left(1-\alpha\right)V\left(e\left(k\right)\right)+s^{T}\left(k\right)P^{-1}\left(k+1\right)s\left(k\right) \\ &\quad + r^{T}\left(k\right)P^{-1}\left(k+1\right)\left[2[I-K\left(k+1\right)H]F\left(k\right)e\left(k\right)+r\left(k\right)\right]. \end{aligned}$$

Now, invoking to Lemmas 3.2 and 3.3, we obtain that

$$E\left\{V\left(e\left(k+1\right)\right)/e\left(k\right)\right\} \leq V\left(e\left(k\right)\right)-\alpha V\left(e\left(k\right)\right)+\rho_3\delta^3+\rho_4\delta^2+\rho_5\delta+\ k_{nom}\left\|e\left(k\right)\right\|^3 \quad (26)$$

or equivalently,

$$E\left\{V\left(e\left(k+1\right)\right)/e\left(k\right)\right\}-V\left(e\left(k\right)\right) \leq -\frac{\alpha}{p_2}\left\|e\left(k\right)\right\|^2+\rho_3\delta^3+\rho_4\delta^2+\rho_5\delta+\ k_{nom}\left\|e\left(k\right)\right\|^3. \quad (27)$$

The function (27) will be negative semidefinite if satisfies:

$$k_{nom}\left\|e\left(k\right)\right\| \leq \frac{\alpha}{2p_2}, \quad (28)$$

$$\rho_3\delta^3+\rho_4\delta^2+\rho_5\delta \leq \frac{\alpha}{2p_2}\left\|e\left(k\right)\right\|^2, \quad (29)$$

the expression (29) can be replaced by

$$\left(1+\rho_1\bar{h}+\rho_2\bar{h}\delta_1\right)^2\frac{1}{p_1}\delta_2+\left(\rho_1+\rho_2\delta_1\right)^2\frac{1}{p_1}\delta_1 \leq \frac{\alpha}{2p_2}\left\|e\left(k\right)\right\|^2,$$

if we do not consider $\delta_1=\delta_2=\delta$. Defining $\varepsilon=\min\left(\epsilon,\frac{\alpha}{2p_2k_{nom}}\right)$ and using it in (26), the following inequality

$$E\left\{V\left(e\left(k+1\right)\right)/e\left(k\right)\right\}-V\left(e\left(k\right)\right) \leq -\frac{\alpha}{2}V\left(e\left(k\right)\right)+\rho_3\delta^3+\rho_4\delta^2+\rho_5\delta$$

holds for all $\left\|e\left(k\right)\right\| \leq \varepsilon$. Now, invoking to Lemma 3.4 with $\left\|e\left(0\right)\right\| \leq \varepsilon$, $v_1=\frac{1}{p_2}$, $v_2=\frac{1}{p_1}$, $\alpha'=\frac{\alpha}{2}$, and $\mu=\rho_3\delta^3+\rho_4\delta^2+\rho_5\delta$ to quantify the estimation/synchronization error $e\left(k\right)$.

The previous results can be combined to obtain the main result of this paper on the stability of the estimation (synchronization) error given by EKF, when it is applied to hyperchaotic synchronization of stochastic discrete-time systems, which is established in the following theorem.

Theorem 3.1 *Consider a stochastic nonlineal system defined by (1) with noisy coupling signal (2). In addition, consider an extended Kalman filter described by (3)-(8). Assume that Assumptions (A1)-(A3) hold. Then, the estimation (synchronization) error* $e\left(k\right)$ *given by (10) is exponentially bounded, if the initial error satisfies*

$$\left\|e\left(0\right)\right\| \leq \varepsilon,$$

and the covariance matrices of the noise terms are bounded by

$$\begin{aligned} Q &\leq \delta_1 I, \\ R &\leq \delta_2 I \end{aligned}$$

for some constants δ_1, δ_2, $\varepsilon>0$.

The above result shows that the stability of the estimation (synchronization) error depends on the nature of the nonlinearities and of the size of the noise in the processes, thus as of the boundedness of the initial estimation error. Therefore, this result can be used to design nonlinear filters (EKF) with stability to approximate synchronize noisy hyperchaotic maps, as will be shown in the next section. In addition to this, we mention that other bounds on the error dynamics of the EKF can be obtained with a prescribed degree of stability from [33–35].

4 Synchronization of Noisy Hyperchaotic Maps

Example 1. Consider the following discrete-time system

$$\begin{aligned} x_1(k+1) &= x_2(k) + a x_1(k), \\ x_2(k+1) &= x_1(k)^2 + b \end{aligned} \tag{30}$$

with parameter values $a = -0.1$ and $b = -1.7$, the map (30) exhibits hyperchaotic dynamics [12]. Figure 4.1 shows the hyperchaotic attractor generates for the map (30). In the sequel, based on this mapping, we show approximate synchronization, by using an EKF as slave dynamics, which will try to estimate the master dynamics (30) corrupted by noise, described by

$$\begin{aligned} x_1(k+1) &= x_2(k) + a x_1(k) + w_1(k), \\ x_2(k+1) &= x_1(k)^2 + b + w_2(k), \end{aligned} \tag{31}$$

with output corrupted by noise defined by

$$y(k) = x_1(k) + v(k).$$

The EKF will generate the estate estimates $\hat{x}_i(k)$, $i = 1, 2$ for the master states $x_i(k)$. The state equations of EKF as *slave,* are described by

$$\begin{aligned} \hat{x}_1(k) &= \hat{x}_1(k/k-1) + K_1(k)\left[y(k) - \hat{x}_1(k/k-1)\right], \\ \hat{x}_2(k) &= \hat{x}_2(k/k-1) + K_2(k)\left[y(k) - \hat{x}_1(k/k-1)\right], \end{aligned} \tag{32}$$

where the Kalman gain $(K_1(k), K_2(k))^T$ is given by (7).

For the noisy map (31) with the above parameter values, we obtain that: $\bar{h} = 1$, $\bar{f} = 4$, $p_1 = 4.52 \times 10^{-6}$, $p_2 = 5.52 \times 10^{-6}$, and $\kappa = 2$. By computer simulations, we take $\delta_1 = 0.0005$ such that the system remains with hyperchaotic dynamics. In addition, we propose the values for q and r as $q = r = \frac{\delta_1}{100}$. With previous data and by using conditions (28) and (29), we obtain the values $\delta_2 = 0.0001$ and $\|e(0)\| \leq 0.02$ which satisfy the mentioned conditions. In the sequel, we show some computer simulations.

We take $x(0) = (0.1, 0.1)$, $P_0 = \text{diag}\{p_{0i}\}$, $p_{0_i} = 5 \times 10^{-6}$. Figure 4.2 shows the time evolution of synchronization errors $e_1(k)$ and $e_2(k)$ for $\hat{x}(0) = (0.13, 0.13)$ for one realization of the noise, where approximate synchronization is achieved for $\tau = 0$ when the level of synchronization $\rho = 0.06$ was considered. While, in Figure 4.3 we can see the time evolution of synchronization errors $e_1(k)$ and $e_2(k)$ for one realization of the noise, starting at $\hat{x}(0) = (0.31, 0.31)$, in this case approximate synchronization is achieved for $\tau = 7$ when $\rho = 0.06$ was considered.

To evaluate the performance of EKF from the point of view of sensitivity to initial error and noise, twenty different Monte Carlo runs were taken in order to obtain root-mean-square error statistics. The results are summarized in Table 4.1, where SSE_i is the *sum of square errors* for each realization of the noise given by

$$SSE_i = \sum_{k=0}^{N} \left(x_i\left(k\right) - \hat{x}_i\left(k\right)\right)^2, \qquad i = 1, 2, ..., n$$

where $x_i\left(k\right)$ and $\hat{x}_i\left(k\right)$ are the true and estimated states, respectively, and N the number of time steps. So, t*he mean-square error (MSE$_i$)* is obtained as $\frac{1}{N+1}\left(SSE_i\right)$. Therefore, the *Monte Carlo sum of square errors* $\left(SSE_i\right)_{MC}$ is given by

$$\left(SSE_i\right)_{MC} = \frac{1}{20}\sum_{j=1}^{20} \left(SSE_i\right)_j \ , \qquad i = 1, 2, ..., n.$$

With the purpose of knowing the same statistics, when the transient has died out we define the *truncated mean-square error* $\left(TMSE_i\right)$ for each realization of the noise as

$$TMSE_i = \frac{1}{N+1-\tau} \sum_{k=\tau}^{N} \left(x_i\left(k\right) - \hat{x}_i\left(k\right)\right)^2, \qquad i = 1, 2, ..., n,$$

so, the *Monte Carlo truncated mean-square error* is obtained as

$$\left(TMSE_i\right)_{MC} = \frac{1}{20}\sum_{j=1}^{20} \left(TMSE_i\right)_j, \qquad i = 1, 2, ..., n,$$

and the *Monte Carlo synchronization time* τ_{MC} by

$$\tau_{MC} = \frac{1}{20}\sum_{j=1}^{20} \max\left(\tau_i\left(\rho\right)\right)_j, \qquad i = 1, 2, ..., n.$$

From Table 4.1, it possible to appreciate the suitable performance of the EKF as slave for the estimation/synchronization of the noisy master (31), when the conditions $e\left(0\right) < \varepsilon$ and $R < \delta_1$ and $Q < \delta_2$ are satisfied. Note that last three lines in Table 4.1, we take the initial error values $e\left(0\right) > \varepsilon$, nevertheless the EKF achieves approximate synchronization, due to the bounds used are conservatives.

Example 2. Consider the hyperchaotic Rössler map

$$\begin{aligned} x_1\left(k+1\right) &= \alpha x_1\left(k\right)\left(1 - x_1\left(k\right)\right) - \beta\left(x_3\left(k\right) + \gamma\right)\left(1 - 2x_2\left(k\right)\right), \\ x_2\left(k+1\right) &= \delta x_2\left(k\right)\left(1 - x_2\left(k\right)\right) + \zeta x_3\left(k\right), \\ x_3\left(k+1\right) &= \eta\left(\left(x_3\left(k\right) + \gamma\right)\left(1 - 2x_2\left(k\right)\right) - 1\right)\left(1 - \theta x_1\left(k\right)\right), \end{aligned} \tag{33}$$

with the set of parameter values: $\alpha = 3.8$, $\beta = 0.05$, $\gamma = 0.35$, $\delta = 3.78$, $\zeta = 0.2$, $\eta = 0.1$, and $\theta = 1.9$ the Rössler map (33) exhibits hyperchaotic dynamics [12]. Figure 4.4 shows

Table 4.1: Monte Carlo sum of square errors $(SSE_i)_{MC}$, Monte Carlo truncated mean-square error $(TMSE_i)_{MC}$, and synchronization time (τ_{MC}) for Example 1 with $p_{0_i} = 5\times10^{-6}$, $i = 1, 2$, $Q = R = 5 \times 10^{-5}$, $\rho = 0.06$, and $N = 100$.

$e(0)$	$(SSE_1)_{MC}$	$(SSE_2)_{MC}$	$(TMSE_1)_{MC}$	$(TMSE_2)_{MC}$	(τ_{MC})
$(0.2, 0.2)$	0.0043	0.0595	0.0035	0.0203	2
$(0.05, 0.05)$	0.0065	0.0235	0.0064	0.0228	0
$(0.01, 0.01)$	0.0040	0.0219	0.0042	0.0210	1
$(-0.01, -0.01)$	0.0038	0.0204	0.0042	0.0213	0
$(-0.05, -0.05)$	0.0065	0.0243	0.0064	0.0262	0
$(-0.1, -0.1)$	0.0141	0.0319	0.0055	0.0216	2
$(-0.2, -0.2)$	0.0450	0.0721	0.0042	0.0229	4
$(-0.5, -0.5)$	0.2676	0.4756	0.0040	0.0214	6
$(-1, -1)$	1.1183	3.09	0.0052	0.0230	7
$(-5, -5)$	30.37	544.12	0.0038	0.0194	10

several hyperchaotic attractors generate for the Rössler map (33). Consider the noisy master map

$$\begin{aligned} x_1(k+1) &= \alpha x_1(k)(1-x_1(k)) - \beta(x_3(k)+\gamma)(1-2x_2(k)) + w_1(k), \quad (34)\\ x_2(k+1) &= \delta x_2(k)(1-x_2(k)) + \zeta x_3(k) + w_2(k),\\ x_3(k+1) &= \eta((x_3(k)+\gamma)(1-2x_2(k))-1)(1-\theta x_1(k)) + w_3(k), \end{aligned}$$

and the noisy drive signal

$$y(k) = x_1(k) + v(k). \quad (35)$$

The covariance Q and variance R were fixed at $R = Q = 1 \times 10^{-6}$. The slave system (EKF) will generate the state estimates $\hat{x}_i(k)$, $i = 1, 2, 3$ for each $x_i(k)$, which is designed as

$$\begin{aligned} \hat{x}_1(k+1) &= \alpha\hat{x}_1(k)(1-\hat{x}_1(k)) - \beta(\hat{x}_3(k)+\gamma)(1-2\hat{x}_2(k)) + k_1(k)(y(k)-\hat{x}_1(k)), \quad (36)\\ \hat{x}_2(k+1) &= \delta\hat{x}_2(k)(1-\hat{x}_2(k)) + \zeta\hat{x}_3(k) + k_2(k)(y(k)-\hat{x}_1(k)),\\ \hat{x}_3(k+1) &= \eta((\hat{x}_3(k)+\gamma)(1-2\hat{x}_2(k))-1)(1-\theta\hat{x}_1(k)) + k_3(k)(y(k)-\hat{x}_1(k)), \end{aligned}$$

where $(k_1(k), k_2(k), k_3(k))^T$ is given by (7).

For noisy Rössler map (34), we obtain that: $\bar{h} = 1$, $\bar{f} = 3.84$, $p_1 = 5.5 \times 10^{-3}$, $p_2 = 248$, and $\kappa = 7.6$. By computer simulations, we take $\delta_1 = 0.00005$ such that the mapping remains with hyperchaotic dynamics. We propose $q = r = \delta_1/1000$ and using (28) and (29), we have that $\delta_2 = 1 \times 10^{-7}$ and $\|e(0)\| \leq 0.03$ which satisfy these conditions. In the following simulations we take $x(0) = (0.95, 0.9, 0)$, $P_0 = \text{diag}\{p_{0_i}\}$, $p_{0_i} = 500$, $i = 1, 2, 3$. Figure 4.5 shows the synchronization error evolution between (34) and (36) for $\hat{x}(0) = (0.9, 0.95, 0.05)$ for one realization of the noise. We can see, after some transient behavior, that approximate synchronization is achieved at time $\tau = 3$ when $\rho = 0.05$ was considered. Tables 4.2 and 4.3 show the suitable behavior of EKF as a estimator of the state vector of noisy hyperchaotic map (34).

Table 4.2: Monte Carlo sum of square errors $(SSE_i)_{MC}$ and synchronization time (τ_{MC}) for Example 2 with $p_{0_i} = 500$, $i = 1, 2, 3$, $Q = R = 1 \times 10^{-6}$, $\rho = 0.05$, and $N = 100$.

$e(0)$	$(SSE_1)_{MC}$	$(SSE_2)_{MC}$	$(SSE_3)_{MC}$	τ_{MC}
$(0.1, 0.1, 0.1)$	0.0100	0.1066	0.0110	6
$(0.05, 0.05, 0.05)$	0.0025	0.0532	0.0035	5
$(0.01, 0.01, 0.01)$	1.0095×10^{-4}	0.0142	0.0010	4
$(-0.01, -0.01, -0.01)$	1.0100×10^{-4}	0.0176	0.0011	3

Table 4.3: Monte Carlo truncated mean-square error and synchronization time (τ_{MC}) for Example 2 with $p_{0_i} = 500$, $i = 1, 2, 3$, $Q = R = 1 \times 10^{-6}$, $\rho = 0.05$, and $N = 100$.

$e(0)$	$(TMSE_1)_{MC}$	$(TMSE_2)_{MC}$	$(TMSE_3)_{MC}$	τ_{MC}
$(0.1, 0.1, 0.1)$	1.0205×10^{-6}	0.0131	9.7194×10^{-4}	6
$(0.05, 0.05, 0.05)$	9.6606×10^{-7}	0.0128	9.7529×10^{-4}	5
$(0.01, 0.01, 0.01)$	8.5910×10^{-5}	0.0117	9.8750×10^{-4}	4
$(-0.01, -0.01, -0.01)$	9.5976×10^{-5}	0.0148	0.0011	3

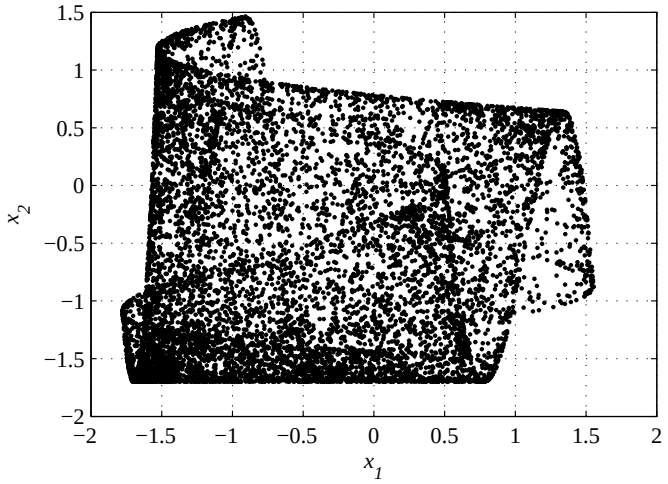

Figure 4.1: Hyperchaotic attractor of discrete-time system (30).

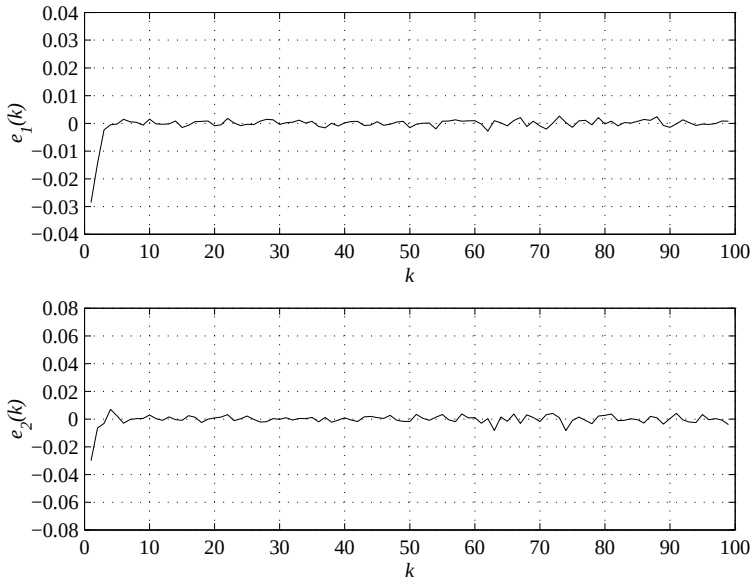

Figure 4.2: Time evolution of synchronization errors $e_1(k)$ and $e_2(k)$ for $\hat{x}(0) = (0.13, 0.13)$; $\tau = 0$ when $\rho = 0.06$ was considered (for one realization of the noise).

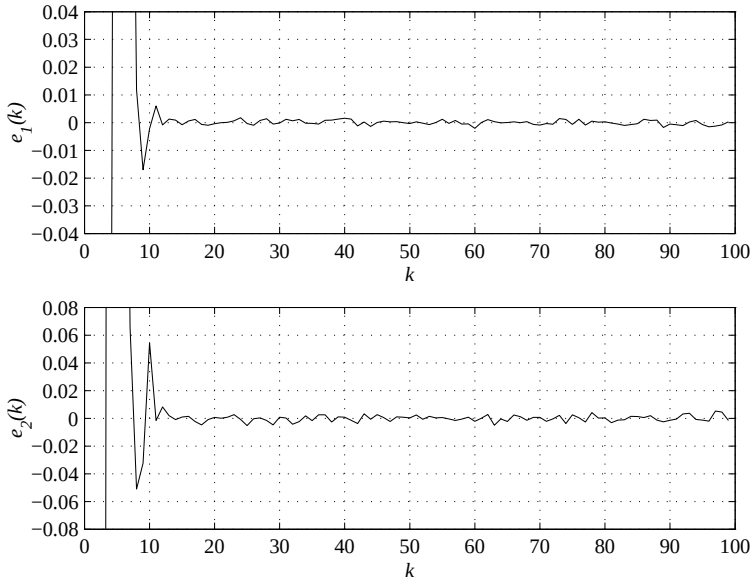

Figure 4.3: Time evolution of synchronization errors $e_1(k)$ and $e_2(k)$ for $\hat{x}(0) = (0.31, 0.31)$; $\tau = 7$ when $\rho = 0.06$ was considered (for one realization of the noise).

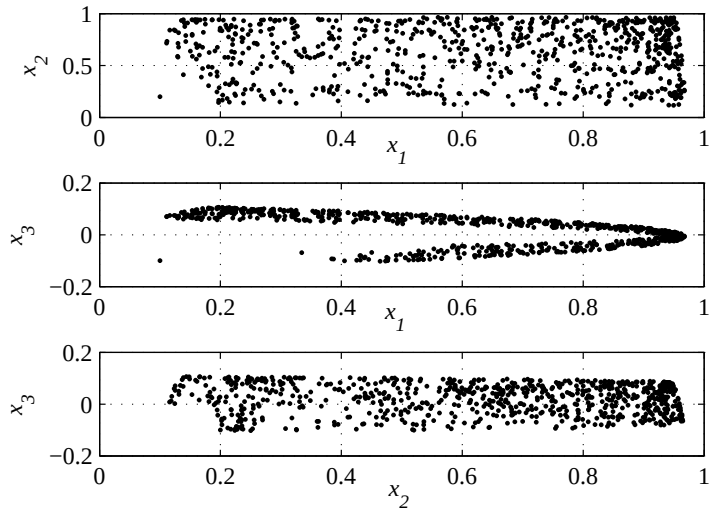

Figure 4.4: Hyperchaotic attractors of Rössler map (33).

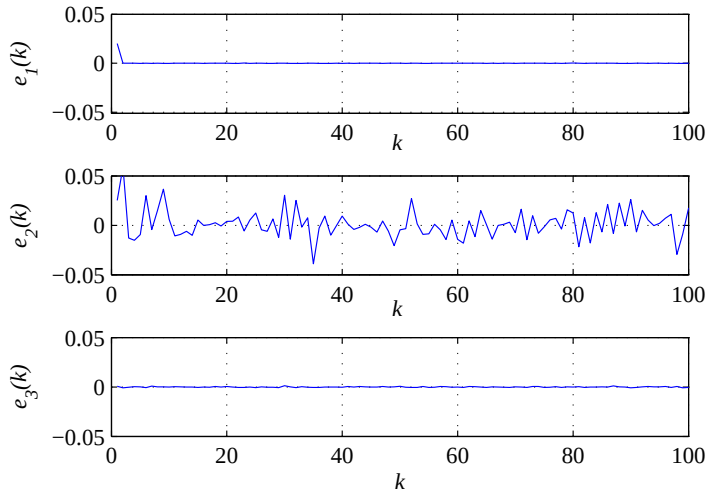

Figure 4.5: Time evolution of the estimation errors $e_i(k)$, $i = 1, 2, 3$ between (34) and (36) for $\hat{x}(0) = (0.9, 0.95, 0.05)$ (for one realization of the noise).

5 Conclusions

In this paper, we have approached the problem of synchronization of discrete-time hyperchaotic systems from the perspective of an extended Kalman filter (EKF) designed as slave. Approximate synchronization was obtained between a noisy master and slave dynamics when the slave was driven by a noisy drive signal from the master. Based on Lyapunov theory, we have demonstrated stability of the estimation/synchronization error, this result provides necessary conditions to achieve approximate synchronization. By extensive computer simulations, we have shown that the filter/slave is indeed suitable for synchronization of noisy hyperchaotic maps, it was illustrated by means of two numerical examples. The adopted approach shows great potential for actual communication systems in which the encoding is required to be secure. In a forthcoming article we will be concerned with the application to secure communication, and with the quantization of the degree of safety of the proposal in actual communication systems. Finally, we comment that this type of approximate synchronization method can be applied to secure chaotic communication, by using similar idea developed in [6, 7] and for continuous case in [31].

Acknowledgements

This work was supported by the CONACYT, México under Research Grants No. J49593-Y and P50051-Y.

References

[1] Pecora, L.M. and Carroll, T.L. Synchronization in chaotic systems. *Phys. Rev. Lett.* **64** (1990) 821–824.

[2] Feldmann, U., Hasler, M. and Schwarz, W. Communication by chaotic signals: the inverse system approach. *Int. J. Circuits Theory and Applications* **24** (1996) 551–579.

[3] Nijmeijer H. and Mareels I.M.Y. An observer looks at synchronization. *IEEE Trans. Circuits Syst. I* **44** (10) (1997) 882–890.

[4] Special Issue on Chaos synchronization and control: Theory and applications. *IEEE Trans. Circuits Syst. I* **44** (10) (1997).

[5] Fradkov, A.L. and Pogromsky, A. Yu. *Introduction to control of oscillations and chaos*, World Scientific Publishing, Singapore, 1998.

[6] Cruz-Hernández, C. and Nijmeijer, H. Synchronization through extended Kalman filtering. In: *New Trends in Nonlinear Observer Design* (Eds: H. Nijmeijer, T.I. Fossen), Lecture Notes in Control and Information Sciences 244 Springer-Verlag, 1999, 469–490.

[7] Cruz-Hernández, C. and Nijmeijer, H. Synchronization through filtering. *Int. J. Bifurc. Chaos* **10** (4) (2000) 763–775.

[8] Special Issue on Control and synchronization of chaos. *Int. J. Bifurc. Chaos* **10** (3-4) (2000).

[9] Sira-Ramírez H. and Cruz-Hernández C. Synchronization of chaotic systems: A generalized Hamiltonian systems approach. *Int. J. Bifurc. Chaos* **11** (5) (2001) 1381-1395. And In: *Procs. of American Control Conference (ACC'2000)*, Chicago, USA, P. 769–773.

[10] Pikovsky, A., Rosenblum, M. and Kurths, J. *Synchronization: A universal concept in nonlinear sciences*, Cambridge University Press, 2001.

[11] Aguilar, A.Y. and Cruz-Hernández, C. Synchronization of two hyperchaotic Rössler systems: Model-matching approach. *WSEAS Transactions on Systems* **1** (2) (2002) 198–203.

[12] Itoh, M., Yang, T. and Chua, L.O. Conditions for impulsive synchronization of chaotic and hyperchaotic systems. *Int. J. Bifurc. Chaos* **11** (2) (2001) 551–560.

[13] López-Mancilla, D. and Cruz-Hernández C. An analysis of robustness on the synchronization of chaotic systems under nonvanishing perturbations using sliding modes. *WSEAS Transactions on Mathematics* **3** (2) (2004) 364–369.

[14] López-Mancilla, D. and Cruz-Hernández C. Output synchronization of chaotic systems: Model-matching approach with application to secure communication. *Nonlinear Dynamics and Systems Theory* **5** (2) (2005) 141–156.

[15] Parlitz, U., Chua, L.O., Kocarev, Lj., Halle, K.S. and Shang, A. Transmission of digital signals by chaotic synchronization. *Int. J. Bifurc. Chaos* **2** (4) (1992) 973–977.

[16] Cuomo, K.M., Oppenheim, A.V. and Strogratz, S.H. Synchronization of Lorenz-based chaotic circuits with applications to communications *IEEE Trans. Circuits Syst. II* **40** (10) (1993) 626–633.

[17] Dedieu, H., Kennedy, M.P., and Hasler, M. Chaotic shift keying: Modulation and demodulation of a chaotic carrier using self-synchronizing Chua's circuits. *IEEE Trans. Circuits Syst. II* **40** (10) (1993) 634–642.

[18] Yang, T., and Chua, L.O. Secure communication via chaotic parameter modulation. *IEEE Trans. Circuits Syst. I* **43** (9) (1996) 817–819.

[19] López-Mancilla, D. and Cruz-Hernández, C. A note on chaos-based communication schemes. *Revista Mexicana de Física* **51** (3) (2005) 265–269.

[20] López-Mancilla, D., Cruz-Hernández, C. and Posadas-Castillo, C. A modified chaos-based communication scheme using Hamiltonian forms and observer. *Journal of Physics: Conference Series* 23 (2005) 267–275.

[21] Cruz-Hernández, C., López-Mancilla, D., García, V., Serrano, H. and Núñez, R. Experimental realization of binary signal transmission using chaos *J. Circuits, Syst. Computers* **14** (3) (2005) 453–468.

[22] Cruz-Hernández, C. Synchronization of time-delay Chua's oscillator with application to secure communication. *Nonlinear Dynamics and Systems Theory* **4** (1) (2004) 1–13.

[23] Cruz-Hernández, C. and Romero-Haros, N. Communicating via synchronized time-delay Chua's circuits. To be published in: *Communications in Nonlinear Science and Numerical Simulation* (2006).

[24] Short, K.M. Steps towards unmasking chaotic communication. *Int. J. Bifurc. Chaos* **4** (4) (1994) 959–977.

[25] Pérez, G. and Cerdeira, H.A. Extracting messages masked by chaos. *Phys. Rev. Lett.* **74** (1995) 1970–1973.

[26] Yang, T, Wu, C.W. and Chua, L.O. Cryptography based on chaotic systems. *IEEE Trans. Circuits Syst. I* **44** (5) (1997) 469–472.

[27] Cruz-Hernández, C. and Serrano-Guerrero, H. Cryptosystems based on synchronized Chua's circuits. In *Procs. of the 16th IFAC World Congress*, July 3–8 (2005) Prague, Czech Republic.

[28] Brucoli, M., Cafagna, D. and Carnimeo, L. Synchronization of hyperchaotic circuits via continuous feedback control with application to secure communications. *Int. J. Bifurc. Chaos* **8** (10) (1998) 2031–2040.

[29] Peng, J.H., Ding, E.J., Ding, M. and Yang, W. Synchronizing hyperchaos with a scalar transmitted signal. *Phys. Rev. Lett.* **76** (6) (1996) 904–907.

[30] Cruz-Hernández, C., Posadas, C. and Sira-Ramírez, H. Synchronization of two hyperchaotic Chua circuits: A generalized Hamiltonian systems approach. *Procs. of the 15th IFAC World Congress*, July 21–26 (2002), Barcelona, Spain.

[31] Sobiski, D.J. and Thorp, J.S. PDMA-1: Chaotic communication via the extended Kalman filter. *IEEE Trans. Circuit Syst. I* **45** (2) (1998) 194–197.

[32] Anderson, B.D.O. and Moore, J.B. *Optimal Filtering*. Prentice-Hall, Englewood Cliffs, NJ, 1979.

[33] La Scala, B.F., Bitmead, R.R. and James, M.R. Conditions for stability of the extended Kalman filter and their application to the frequency tracking problem. *Math. Control Signals Systems* **8** (1) (1995) 1–26.

[34] Reif, K., Sonnemann, F. and Unbehauen, R. An EKF-based nonlinear observer with a prescribed degree of stability. *Automatica* **34** (9) (1998) 1119–1123.

[35] Reif, K., Günther, S. and Yaz, E. Stochastic stability of the discrete-time extended Kalman filter. *IEEE Trans. Automat. Contr.* **44** (4) (1999) 714–728.

Nonlinear Dynamics and Systems Theory, **6** (4) (2006) 337–342

Stable Communication Topologies of a Formation of Satellites

M. Dellnitz, O. Junge, A. Krishnamurthy and R. Preis *

Institute for Mathematics, University of Paderborn, Germany

Received: July 19, 2005; Revised: September 13, 2006

Abstract: Several currently planned space missions consist of a set of satellites flying in formation. While increasing the functionality, this concept introduces several new challenges with respect to the design of the mission. The topology of the sensing or communication network among the satellites can be a bottleneck in the operation because the transmission of information and the coordination of the formation relies on it. Here we study the robustness of the formation dynamics with respect to changes in the communication topology (like the failure of some communication links). Moreover, we propose a special variant of the notion of stability radius in order to measure the robustness of a certain topology.

Keywords: *Formation; stability; stability radius.*

Mathematics Subject Classification (2000): 70M20, 70K20.

1 Introduction

Space missions with several spacecraft flying in formation have received a lot of attention recently. Increased functionality and robustness of the mission are two key characteristics of this approach. Several currently planned space missions consist of a set of satellites flying in formation, like, e.g., the NASA mission *Terrestrial Planet Finder (TPF)* and the ESA mission *Darwin*. In both missions, a network of formation flying spacecraft builds up an infrared interferometer in order to detect and study planets in outer space.

One key challenge in the design of these missions is the question on how to efficiently attain and accurately maintain the desired formation. In [1, 5] it has been shown that formation-stabilizing control laws can be derived for the individual spacecraft that rely on local information only. The key idea is that, together with the stability properties of the dynamics of the individual spacecraft, the spectrum of the Laplacian associated

* Corresponding author: {dellnitz,arvind,robsy,junge}@upb.de

to the graph that describes which spacecraft communicate with which other spacecraft plays a crucial role in the design of this control law.

In this paper, by means of a network of six spacecraft with simple linear dynamics, we study the robustness of certain communication graphs with respect to the removal of edges (i.e. the failure of some communication links). Based on stabilizability statements from [1, 5] we analyse how many communication links can fail before the dynamics of the overall system becomes unstable. For more complicated situations we propose an adapted version of the concept of stability radius of a linear system in order to measure this robustness.

2 Model

In the current mission design for Darwin and TPF it is planned to inject the spacecraft into a Libration orbit around the Lagrange point L_2. Close to this orbit, a time-dependent linear model may be used in order to describe the motion of the spacecraft [4]. For the purposes of this paper we restrict ourselves to a time-independent model as used in [5], i.e. we model the dynamics of each of the N vehicles by

$$\dot{x}_i = Ax_i + Bu_i, \quad i = 1, \ldots, N, \tag{1}$$

where $x_i \in R^6$ is the state and $u_i \in R^p$ for some p is the control of vehicle i and A and B are real matrices of appropriate size. As shown in [5], a linear local feedback can be designed which drives the system asymptotically into a prescribed *formation*, i.e. the vehicles attain prescribed distances relative to each other as well as the same velocity. We follow [5] in the following description.

The feedback law is local in the sense that each vehicle i can generate its own control u_i from the determination of its state relative to the states of some subset $S_i \subset \{1, \ldots, N\}$ of all vehicles (obtained, e.g., by communicating with the vehicles in S_i). The i-th vehicle computes

$$z_i = (x_i - h_i) - \frac{1}{|S_i|} \sum_{j \in S_i} (x_j - h_j), \tag{2}$$

where $h_i \in R^6$ is some reference state for the i-th vehicle, and sets $u_i = Fz_i$ for some feedback matrix F.

Viewing the system as an undirected graph $G = (V, E)$, where the set of nodes $V = \{1, \ldots, N\}$ represent the vehicles and the set of edges E represent communication links (i.e. $E = \{(i, j) \colon j \in S_i\}$), one can compactly write the system in the form

$$\dot{x} = \hat{A}x + \hat{B}\hat{F}\hat{L}(x - h). \tag{3}$$

Here $x = (x_1, \ldots, x_N) \in R^{6N}$, $\hat{A} = I_N \otimes A$, $\hat{B} = I_N \otimes B$, $\hat{F} = I_N \otimes F$, $h = (h_1, \ldots, h_N)$ and $\hat{L} = L \otimes I_6$, with L being the Laplacian of the graph G, i.e.

$$L_{ij} = \begin{cases} 1: & i = j, \\ -\dfrac{1}{|S_i|}: & j \in S_i, \\ 0: & j \notin S_i. \end{cases} \tag{4}$$

3 Robustness of Communication Topologies

In [5] it is shown that the vehicles are in formation if and only if $\hat{L}(x-h)=0$ and (under certain assumptions) that if the matrix $A+\lambda BF$ is stable for each nonzero eigenvalue λ of L, then $\hat{L}(x(t)-h)\to 0$ as $t\to\infty$, i.e. the vehicles asymptotically attain the desired formation. For a given communication graph, this result thus gives a criterion on how to design the feedback matrix F. In fact, under certain assumptions on the uncontrolled dynamics of a single system, i.e. on the matrix A, one can show that for every connected graph one can find a feedback matrix F which renders the closed loop system stable ([5], Proposition 4.4). What is more, under these assumptions, feedback matrices can in fact be constructed which render the system stable regardless of how the communication graph is chosen — as long as it is connected.

However, the choice of the feedback matrix F will depend on the single system dynamics (i.e. the matrix A) and, in particular in our application context, in a non-autonomous setting it may happen that A is changing in such a way that the overall system dynamics becomes unstable. In this case, the question arises which communication topology is best suited in the sense that it will ensure stability of the formation for the largest "range" of single system dynamics. What is more, taking into account that communication links may fail, the question is which topology is most robust with respect to such failures, i.e. ensures stability of the system even when a certain number of links fail.

In order to make these considerations more precise we focus on the following basic setting from [5]: we assume that each coordinate of the system is modelled by the same second order dynamics, i.e. we have

$$A = I_3 \otimes \begin{pmatrix} 0 & 1 \\ 0 & a_{22} \end{pmatrix} \quad \text{and} \quad B = I_3 \otimes \begin{pmatrix} 0 \\ 1 \end{pmatrix}.$$

Using $F = I_3 \otimes (f_1 \ f_2)$ as the feedback matrix, our goal will thus be to render the matrix

$$H_\lambda = \begin{pmatrix} 0 & 1 \\ 0 & a_{22} \end{pmatrix} + \lambda \begin{pmatrix} 0 & 0 \\ f_1 & f_2 \end{pmatrix}$$

stable for each nonzero eigenvalue λ of the Laplacian L. This matrix will be stable if and only if

$$a_{22} + \lambda f_2 < 0 \quad \text{and} \quad \lambda f_1 < 0,$$

i.e. f_1 has to be chosen negative (since $\lambda \in [0,2]$ for all eigenvalues of L). If the single system dynamics is unstable, i.e. $a_{22} > 0$, then the eigenvalue λ of L which is closest to zero determines how f_2 has to be chosen in order to render the overall system stable.

Since we are assuming that all vehicles have identical dynamics and communication capabilities, it seems natural to restrict the choice of communication graphs to regular ones. Figure 3.1 shows all non-isomorphic connected regular (undirected) graphs with six nodes (see e.g. [6]). In the first column of Table 3.1 we list the corresponding minimal nonzero eigenvalues of the Laplacians (except for the 2-regular graph which becomes disconnected as soon as more than one edge is removed). The other columns show how these eigenvalues change when removing a certain number of edges from the corresponding graph (where we minimized over all possible removals).

From these values, the choice of the full graph appears to be the best one (as one might have expected), since it features the largest minimal nonzero eigenvalue (and thus, for a fixed f_2, allows for the largest value for a_{22}).

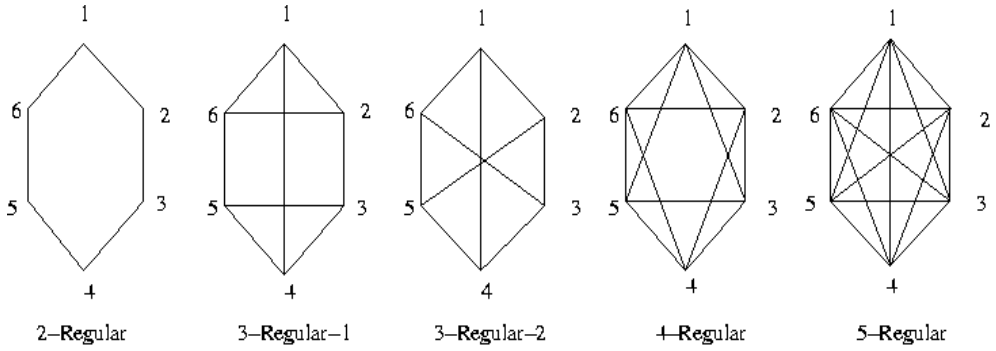

Figure 3.1: All non-isomorphic connected regular undirected graphs with six nodes.

graph \ # of edge failures	0	1	2	3	4
3 regular (1)	0.6670	0.4226	0.2047	0.1960	0.1910
3 regular (2)	1.0000	0.6670	0.5286	0.2929	0.1910
4 regular	1.0000	0.8104	0.6670	0.4610	0.2727
5 regular	1.2000	1.0000	0.8911	0.8104	0.7180

Table 3.1: The minimal nonzero eigenvalues for the communication graphs under consideration in dependence of the number of edge failures.

The full graph is also optimal if we choose f_2 dependent on the graph and ask for maximal robustness with respect to communication link failures, since the absolute decrease of the minimal nonzero eigenvalue is smallest for this graph. This fact is also visualized in Figure 3.2.

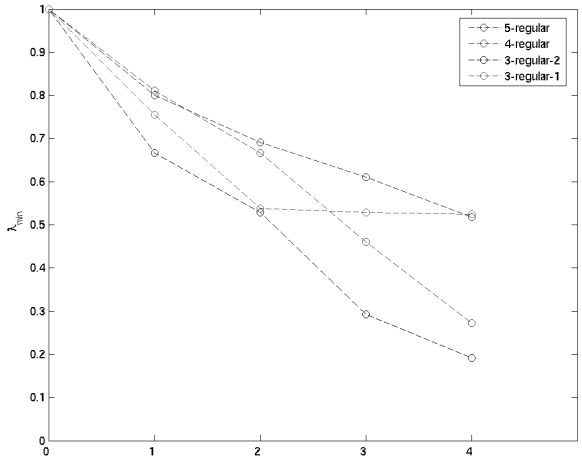

Figure 3.2: The plot of normalized λ_{min}.

4 Conclusion and Outlook

Stability radius. In the preceding section we have been considering a simple model in order to analyse robustness properties of certain communication topologies. In a more general setting it will be necessary to approach this question in a more systematic way. To this end, we propose to use the concept of the *stability radius* from control theory, see [3].

We denote by $\mathcal{U}_n$ the set of unstable real $n \times n$ matrices:

$$\mathcal{U}_n = \{U \in R^{n\times n} \colon\ \sigma(U) \cap \overline{\mathbb{C}}_+ \neq \varnothing\}, \tag{5}$$

where $\overline{\mathbb{C}}_+$ is the closed right half complex plane. For a general matrix $A \in R^{n\times n}$, the stability radius measures the distance $r(A)$ of A from the set $\mathcal{U}_n$ of unstable matrices,

$$r(A) = \inf_{U\in\mathcal{U}_n} \|A - U\|. \tag{6}$$

Proposition 4.1 ([2]) *Let $A \in R^{n\times n}$ be stable and normal with eigenvalues $\lambda_j = -\alpha_j \pm i\omega_j$, $\alpha_1 \geq \cdots \geq \alpha_n > 0$, then $r(A) = \alpha_n$.*

This proposition shows that for normal matrices A, the distance of A from the set of unstable matrices is given by the distance of its spectrum from the imaginary axis. If A is not normal, then the distance of $\sigma(A)$ from the imaginary axis can be a very misleading indicator of the "robustness" of A.

Motivated by an adaptation of this notion to structured systems [2] we we propose the following definition which is adapted to our context. Let $L(G)$ be the Laplacian associated with a given communication graph $G = (V, E)$ and let $\mathbb{L}(G)$ be the set of Laplacians associated with those graphs which result from G by removing some edges, i.e.

$$\mathbb{L}(G) = \{L(G') \colon\ G' = (V, E'), E' \subset E\}.$$

For some Laplacian $L' = L(G') \in \mathbb{L}(G)$ with $G' = (V, E')$ let

$$d(L') = |E| - |E'|$$

be the number of communication link failures. We define the stability radius $r(A, B, F, G)$ of a given system (A, B, F, G) as the minimum number of edges failures such that the system is unstable, i.e.

$$r(A, B, F, G) = \min_{L\in\mathbb{L}(G)} \{d(L) \colon\ \sigma(\hat{A} + \hat{B}\hat{F}\hat{L}) \cap \overline{\mathbb{C}_+} \neq \emptyset\}\,. \tag{7}$$

In future work we will explore the usefulness of this concept for the analysis of the robustness of certain communication topologies within systems with more complicated dynamics.

Conclusion. Using a simple linear model, we explored the robustness of different communication graphs with respect to failures of communication links. We introduced a variant of the notion of the stability radius of a given system as a means of systematically measuring the robustness for more complicated systems. It remains to explore this concept in an application scenario as well as to analyse nonautonomous systems like motivated by missions with formation flying spacecraft on Libration orbits.

References

[1] Fax, A.J. *Optimal and Cooperative Control of Vehicle Formations*. Ph.D. Thesis, California Institute of Technology, 2002.

[2] Hinrichsen, D. and Pritchard, A.J. Stability radius for structured perturbations and the algebraic Riccati equation. *Systems and Control Letters* **8** (1986) 105–113.

[3] Hinrichsen, D. and Pritchard, A.J. Stability radii of linear systems. *Systems and Control Letters* **7** (1986) 1–10.

[4] Junge, O., Levenhagen, J., Seifried, A. and Dellnitz, M. Identification of Halo orbits for energy efficient formation flying. In: *Proceedings of the International Symposium Formation Flying*. Toulouse, 2002.

[5] Lafferriere, G., Caughman, J. and Williams, A. Graph Theoretic Methods in the Stability of Vehicle Formations. In: *Proceedings of the American Control Conference*, 2004, P. 3729–3724.

[6] Preis, R. *Analyses and Design of Efficient Graph Partitioning Methods.* Ph.D. Thesis, University of Paderborn, Germany, 2000.

Nonlinear Dynamics and Systems Theory, **6** (4) (2006) 343–352

Optimal Reconfiguration of Spacecraft Formations Using a Variational Numerical Method

L. García [1] and J.J. Masdemont [2*]

[1] *Departament d'Informàtica i Matemàtica Aplicada, Universitat de Girona, Girona, Spain,*
[2] *IEEC & Departament de Matemàtica Aplicada I, Universitat Politècnica de Catalunya, Diagonal 647, 08028 Barcelona, Spain*

Received: July 19, 2005; Revised: September 14, 2006

Abstract: One of the key issues when working with formations of spacecraft is how to reconfigure the formation in order to change its orientation, its pointing or just to arrive to a given pattern. In this paper we treat these reconfiguration tasks as an optimal problem and set out the problem using the finite element method. Although the methodology is general, and suits to many different types of problems, the examples that have been considered focus in some basic maneuvers of the TPF and Darwin missions about the L_2 Lagrange point of the Earth-Sun system.

Keywords: *Formation flight; optimal reconfiguration; finite element method; spacecraft formations.*

Mathematics Subject Classification (2000): 70M20, 70G75, 65K10, 65L60.

1 Introduction

In the last few years, the interest in constellations of spacecraft and formation flight has been increasing. One of the major applications of this technique is for remote sensing missions, where using the formation it is possible to increase the resolution as a virtual antenna, resulting in a much larger one than using a single spacecraft. Examples of this procedure are missions such as Darwin of the ESA and TPF of the NASA (see [5, 3]).

Among others, one of the problems one must face when working with formations of spacecraft are the reconfiguration maneuvers. For instance, several situations where the need of reconfiguration of the formation appears are the following:

- There are some basic maneuvers that a formation must be capable to perform, such as expansions and contractions, or simply to change the pattern to perform specific tasks.

* Corresponding author: josep@barquins.upc.edu

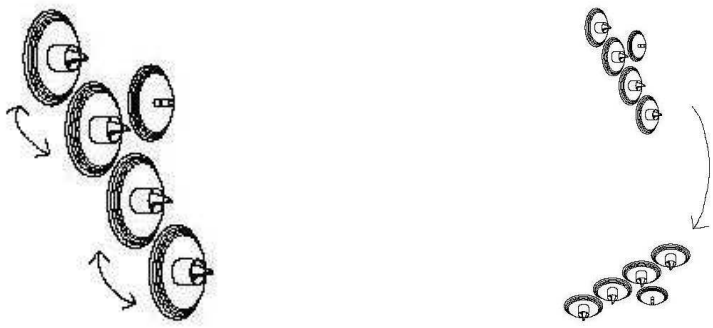

Figure 1.1: Two examples of reconfiguration of spacecraft. In the left-hand side, we change the position of the inner and outer spacecraft of the TPF formation. In the right-hand side we have a constellation pointing to a certain target and we reconfigure it to point to another one.

- The lifetime of a formation finishes when a spacecraft ends its fuel. Many times will be mandatory to equilibrate the consume of fuel of all the spacecraft to extend the lifetime of the formation. An example of this situation is the TPF formation, where the outer spacecraft consume more fuel than the inner ones. To exchange the position of the inner and outer spacecraft, as in Figure 1.1 may be a solution to the problem.

- In interferometry missions, the formation of spacecraft usually will have to point to many targets. It is necessary to reconfigure the formation in order to point to the next goal as it is represented in Figure 1.1.

- In some cases, due to the number of spacecraft of the formation, the deployment phase might follow after a rendezvous of several motherships. Deployments can be treated as special cases of reconfigurations where the satellites depart from different locations and configure a final pattern.

The objective of this work is to compute reconfigurations of the spacecraft in a systematic way and taking into account collision avoidance during the execution of the maneuvers. Earlier approaches with different methodologies can be found in the literature. For instance C.R. McInnes creates a local topology based on artificial potential functions (see [2]). The method is also used in the guidance of robots which move avoiding fixed objects or in the guidance of a robotic arm (see [7]). Singh and Hadaegh also treated the problem as an optimization one, modeling the trajectory with cubic splines (see [6]). However our proposed research in the use of finite element methods looks very promising due to the huge amount of knowledge on this area. The finite element method implements in a systematic and general way giving a full methodology. There is no need to look or adjust functions or parameters in special situations and different levels of approximation can be attained. Moreover it has a complete mathematical foundation in behind assuring nice properties such as convergence to solutions and adaptability.

2 The methodology

In the results we present, we assume that the spacecraft are in a L_2 Halo orbit of 120,000 km of z-amplitude in the Sun-Earth system. The model we use for the computations is the RTBP, but the procedure is easily generalized to any other one or to free space. Since we work with formations of a diameter of few hundred meters, the size of the formation with respect to the orbit is very small and it is feasible to use the linearized equations about the nonlinear orbit.

In this paper, the problem we consider is how to reconfigure a formation of N spacecraft in a selected time T. The formation will evolve in the vicinity of a given point on the halo orbit. Let us denote by X_i the position and velocity of the i-th spacecraft of the formation with respect to this point on the nominal halo orbit. The governing equations for the formation are:

$$\begin{cases} \dot{X}_i(t) = A(t)X_i(t) + U_i(t), \\ X_i(0) = X_i^0, \quad X_i(T) = X_i^T, \end{cases} \tag{1}$$

in the time interval $[0, T]$, for $i = 1 \dots N$. Here $A(t)$ is the Jacobian matrix of the equations of motion about the halo orbit and $U_i(t)$ is the control law to be applied to the i-th satellite, so it is of the form $U_i(t) = (0, 0, 0, u_i^x(t), u_i^y(t), u_i^z(t))^t$. The final goal is to find optimal controls, $U_1, \dots, U_N$, subjected to certain restrictions on mutual distances (i.e. Euclidean norms in the position components of $X_i(t)$) or being the satellites on a certain surface, manifold, etc. Restrictions can be also time dependent.

The finite element method could be applied directly to equations (1), but in order to work with the simplest equations, we introduce a change of coordinates which casts $A(t)$ into its Jordan form which is

$$\begin{pmatrix} \lambda_1(t) & & & & & \\ & -\lambda_1(t) & & & & \\ & & 0 & \lambda_2(t) & & \\ & & -\lambda_2(t) & 0 & & \\ & & & & 0 & \lambda_3(t) \\ & & & & -\lambda_3(t) & 0 \end{pmatrix}.$$

This change of variables reduces (1) into a new set of equations each one them of the form

$$\begin{cases} \ddot{x}(t) + \lambda(t)\,\dot{x}(t) + \tau(t)\,x(t) = u(t), \\ x(0) = x_0, \qquad x(T) = x_T, \\ \dot{x}(0) = v_0, \qquad \dot{x}(T) = v_T. \end{cases} \tag{2}$$

where $\lambda(t)$ and $\tau(t)$ are computed from a corresponding $\lambda_i(t)$ set. At this point it is also worth to mention that if one wants to consider the motion of the formation in free space, which is common in many studies of formation flight, we need only to take $\lambda(t) = \tau(t) \equiv 0$.

Assuming the time interval $[0, T]$ splitted in a given number, M, of smaller intervals (elements), $t_0 = 0$, $t_1, \dots, t_{M-1}, t_M = T$, we apply the Galerkin finite element method in time to the equations (2) by means of considering products by weight functions $w(t)$ and the usual weak form on each element is computed from the expression (see [8]):

$$\int_{t_k}^{t_{k+1}} w(t)\,(\ddot{x}(t) + \lambda(t)\,\dot{x}(t) + \tau(t)\,x(t))dt = \int_{t_k}^{t_{k+1}} w(t)\,u(t)dt, \quad k = 0, \dots, M-1.$$

As it is well known, depending on the order of the elements used in the procedure one obtains different linear systems of equations associated with them. In case of considering a linear

element, the system is

$$\begin{pmatrix} K_{11}^k & K_{12}^k \\ K_{21}^k & K_{22}^k \end{pmatrix} \begin{pmatrix} x_k \\ x_{k+1} \end{pmatrix} = \begin{pmatrix} \Delta v_k \\ \Delta v_{k+1} \end{pmatrix},$$

which essentially states a relation between the nodal values x_k and x_{k+1}, which are related to the positions of the reconfiguration trajectory, and the delta-v's, Δv_k and Δv_{k+1}, applied in the nodal places of the element. We note that at this moment x_k, x_{k+1}, Δv_k and Δv_{k+1} are unknowns and the K_{ij}^k are 3×3 known matrices which are systematically computed following Galerkin's method. Finally, assembling the elementary equations we obtain the relations between the all the nodal positions and delta-v's. For each one of the spacecraft of the formation $(i = 1 \dots N)$ we obtain a system of the form

$$\begin{pmatrix} K_{22}^0 + K_{11}^1 & K_{12}^1 & 0 & & \\ K_{21}^1 & K_{22}^1 + K_{11}^2 & K_{12}^2 & & \\ \ddots & \ddots & \ddots & & \\ & K_{21}^{M-3} & K_{22}^{M-3} + K_{11}^{M-2} & K_{12}^{M-2} & \\ & 0 & K_{21}^{M-2} & K_{22}^{M-2} + K_{11}^{M-1} & \end{pmatrix} \begin{pmatrix} x_{i,1} \\ x_{i,2} \\ \vdots \\ x_{i,M-2} \\ x_{i,M-1} \end{pmatrix} + \\ + \begin{pmatrix} K_{21}^0 x_{i,0} \\ 0 \\ \vdots \\ 0 \\ K_{12}^{M-2} x_{i,T} \end{pmatrix} = \begin{pmatrix} \Delta v_{i,1} \\ \Delta v_{i,2} \\ \vdots \\ \Delta v_{i,M-2} \\ \Delta v_{i,M-1} \end{pmatrix}, \tag{3}$$

for the interior nodes, while for the boundary ones we incorporate what is known as essential boundary conditions and results in

$$\Delta v_{i,0} = K_{11}^0 \, x_{i,0} + v_{i,0} + K_{12}^0 \, x_{i,1}, \quad \Delta v_{i,M} = K_{21}^{M-1} \, x_{i,M-1} + K_{2,2}^{M-1} \, x_{i,M} - v_{i,T}.$$

From now on we treat the problem as an optimal control problem, where the functional we minimize is a penalty on the delta-v of the spacecraft. Collision avoidance and any other type of requirements enters in the method as restriction functions in the $x_{i,k}$ and $v_{i,k}$.

The objective function

The solution to our reconfiguration problem must be found attending essentially to the fuel consumption of the satellites. For this purpose we have selected an objective function of the form

$$J(\Delta v_{1,0}, \dots, \Delta v_{N,M}) = \sum_{i=0}^{N} J_i, \quad \text{with} \quad J_i(\Delta v_{i,0}, \dots, \Delta v_{i,M}) = \sum_{k=0}^{M} \rho_{i,k} ||\Delta v_{i,k}||^2, \tag{4}$$

(here $|| * ||$ denotes Euclidean norm), because it is directly related with the fuel expenditure, moreover derivatives are easily computed.

We consider parameters $\rho_{i,k}$ because in some way can be selected to equilibrate the fuel consumption of the spacecraft. For instance, incrementing the values of ρ corresponding to a particular satellite the penalty function takes into account that for that particular satellite fuel consumption is more critical. We also note that parameters ρ can depend on time (through the subscript k), this fact may be used to penalize the delta-v in certain time intervals.

Collision avoidance and other restrictions

In the reconfiguration planning it is essential to avoid collision between spacecraft. A minimum security distance between them must be required while maneuvering. In our procedure this distance can be chosen constant for general purpose reconfigurations or variable in time for special situations. For instance, during deployment a variable security distance is needed because at the beginning of the maneuver the satellites are closer than the usual safety distance demanded for reconfigurations.

As we previously stated, collision avoidance enters in the variational method as constraints in the position coordinates of $X_i(t)$ of (1). Via the change of coordinates used to obtain (2) and the finite element discretization, the constraints translate into conditions on the $x_{i,k}$ nodal variables. The finite element discretization is used to compute the distance between each spacecraft on each element and to check that this distance is greater than the security distance.

In a similar way many other restrictions can be applied (provided that there exist compatibility with the requirements). For instance some other cases that we have been studying are the following

- It is possible to maintain a formation in a region determined by a geometrical condition, such as an sphere, a paraboloid or a plane in an optimal way.
- It is also possible to keep the geometrical condition during a formation reconfiguration. For instance satellites can be forced to move in a plane or in a sphere while maneuvering for the reconfiguration.
- We can impose that particular spacecraft do not perform maneuvers during certain time intervals. In this case restrictions are set fixing the values of some $\Delta v_{i,k}$ (to zero in this example).
- The procedure can be used to keep the formation pointing continuously to a selected goal.
- Satellites can be restricted to maintain only certain relative distances between them. For instance to keep an equilateral triangle or tetrahedron. When the relative distances do not depend on time, the formation will evolve like a solid.
- Moreover in all these cases the final position of the spacecraft of the formation can be selected fixed (as in the formulation given by equations (1)), restricted to certain conditions or free.

Computing the initial seed for the iterative procedure

The computation of the optimal value of the objective function (4) involves an iterative process which needs an initial seed. In our approach this initial seed is computed using the uncoupled systems (3) and without taking into account the restrictions. This is, the initial guess does not have to be compatible with distance requirements between spacecraft or other type of constraints.

We have chosen to minimize the each one of the values given by

$$\bar{J}_i = \sum_{k=0}^{M} ||\Delta v_{i,k}||^2, \quad i = 1 \dots N.$$

Note that we do not use the parameter ρ to find the initial seed. If we denote by $K\, x_i + b_i = \Delta v_i$, the system (3) the function $\bar{J}_i$ casts into the form

$$\bar{J}_i = (K\, x_i + b_i)^T (K\, x_i + b_i) + (\Delta v_0)^2 + (\Delta v_{_M})^2.$$

Then it is easy to see that the trajectory of the i-th satellite which minimizes $\bar{J}_i$, and it is represented by the nodal values x_i, is obtained solving a linear system

$$(K^T K + C_i)x_i + (K^T b_i + d_i) = 0,$$

where C is an sparse matrix and d is an sparse vector.

Other computational issues

In order to find reconfiguration paths, we have implemented a specific program in C which returns the optimal trajectory for a given discretization of finite elements in time. The program obtains the trajectory in an iterative way. Usually we start with a few number of elements (typically 6 elements in the first step) and then we refine it by more or less doubling the number of elements at each iteration.

Using a slow computer such as a Pentium 3, 1.5 GHz, the CPU time to find the initial optimal six element trajectory from the initial seed is less than 20 seconds for a formation of 5 or 6 satellites. Doubling the number of elements from 50 to 100 for the same formation requires less than 40 seconds. Of course these CPU times, specially for the initial iterations, depend strongly on the characteristics of the reconfiguration demanded, but these ones are in general good indicators.

In case that problems of convergence had appeared in the first iterations we could also have used continuation methods, for instance with respect to the security distance, but it has not been necessary in all the examples that we have tried.

3 Some examples of reconfigurations

To illustrate the procedure we have selected three examples, two of them related with current missions of the NASA and ESA agencies. The TPF Mission (Terrestrial Planet Finder) is one of the masterpieces of the NASA Origins Program. Its goal is the detection and characterization of Earth-like planets that orbit nearby stars (see [3], [1]). The TPF configuration is currently considered to be formed by five spacecraft contained in a plane. Four spacecraft are evenly distributed in a baseline of approximately 100 m. The fifth one, the collector, forms an equilater triangle with the two interior satellites of the baseline (see Figure 3.1).

The Darwin Mission is a project of the ESA with a similar objective of the TPF Mission. The Darwin configuration (see [5]) is formed by seven spacecraft contained in a plane. Six of them are on the vertices of a regular hexagon of radius about 100 m and the seventh one is located at the baricenter (see again Figure 3.1).

In the examples, and only for illustration purposes, of we have also computed the delta-v on/off necessary to reconfigure the formation. We note however that the on/off control does not take into account collision avoidance which is a major requirement in the following examples, where the satellites will irremediable collide using the on/off technique.

Changing inner-outer position in the TPF formation

In the TPF formation, the exterior spacecraft have a bigger fuel consumption than the interior ones (see [4]). To compensate the difference, we can consider changing their position at some moment in the lifetime of the mission. In Table 3.1 we present the cost, in terms of total delta-v (cm/s), for each satellite to accomplish the task. Relative trajectories and the profile of delta-v consumption is represented in Figure 3.2.

Figure 3.1: Representations of the TPF (left-hand side) and Darwin (right-hand side) configurations.

Satellite	1	2	3	4	5	Total (cm/s)
Δv	1.65	1.63	1.65	1.67	0.19	6.79
Δv on-off	0.23	0.23	0.23	0.23	0.00	0.92

Table 3.1: Change the position of the consecutive interior and exterior spacecraft of TPF in 8 hours. The formation is considered about a halo orbit of 120000 km of z-amplitude. The results corresponds to a discretization of each trajectory in 50 linear elements.

Exchanging positions of several spacecraft

In this example (see Figure 3.3), we have 4 small spacecraft in a square of length 40 meters and another one in the center of the it. Again the satellites are about a halo orbit of 120000 km of z-amplitude being the central one on the halo orbit. The example consist in switching the satellites located in the opposite vertices, while the central one returns to the same place after letting the other ones pass near the center. Total costs are displayed in Table 3.2.

Rendezvous and formation deployment

We consider the Darwin configuration to perform an example of rendezvous and deployment. We start with two groups of 3 and 4 spacecraft separated by a distance of 1000 m. The example is again about a halo orbit of 120000 km of z-amplitude about the L_2 Sun-Earth libration point. It turns out that the optimum place for the rendezvous is the relative point located in the center of mass of the initial configuration. We show the trajectory and the profiles of the delta-v expenditures in Figure 3.4. Total amounts of Δv are given in Table 3.3.

Satellite	1	2	3	4	5	Total (cm/s)
Δv	1.17	1.02	1.21	0.93	0.28	4.61
Δv on-off	0.39	0.39	0.39	0.39	0.00	1.56

Table 3.2: Delta-v expenditure to change the position of four satellites located in opposite corners of an square of 40 m. Reconfiguration time has been set to 8 hours. In this example 100 linear elements have been used.

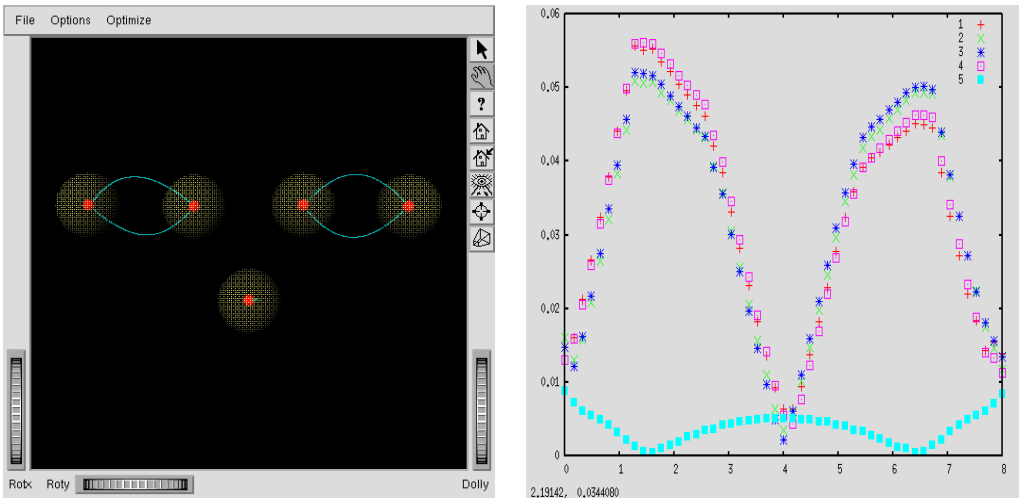

Figure 3.2: In the left-hand side plot we have the trajectory obtained when we change the consecutive interior and exterior spacecraft in the TPF configuration. Satellites are represented in the center of the collision avoidance spheres which cannot intersect during the maneuver (the radius of the sphere is half of the security distance considered). In the right hand side plot we show the profile of the Δv expenditure for each satellite. The corresponding total amounts are given in Table 3.1

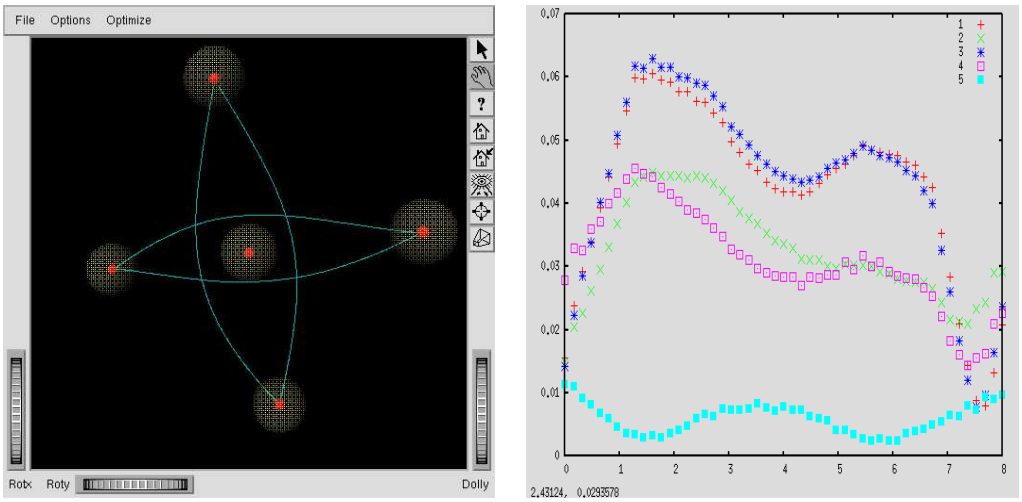

Figure 3.3: In the left-hand side plot we have the trajectory of the spacecraft when we change the position of the opposite spacecraft in a square. In the right hand side plot we have the profile of the Δv expenditure for each spacecraft. Total amounts of Δv are given in Table 3.2.

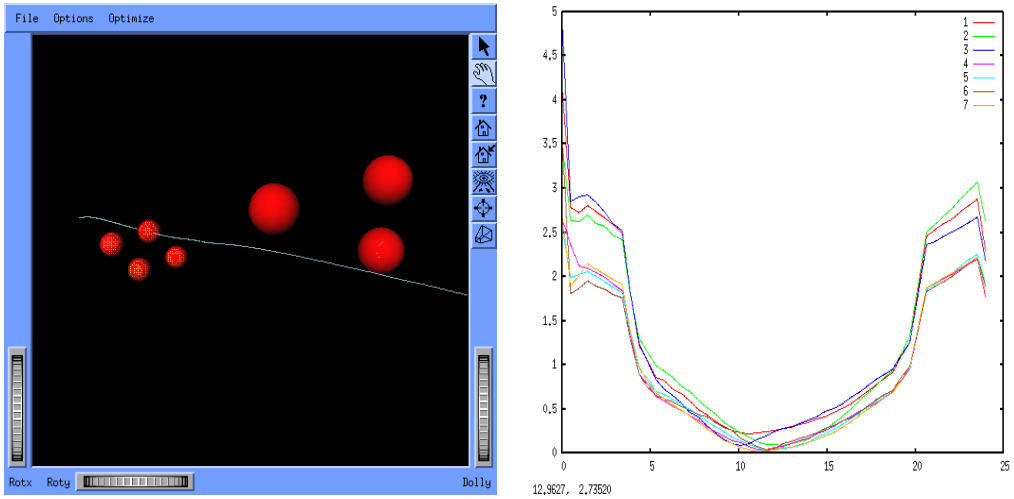

Figure 3.4: In the left-hand side we plot a snapshot of a rendezvous trajectory for the Darwin mission. In the right hand side plot we show the profile of the Δv expenditure for each spacecraft. Total amounts of Δv are given in Table 3.3

Satellite	1	2	3	4	5	6	7	Total (cm/s)
Δv	1.83	1.83	1.83	1.33	1.33	1.33	1.33	10.81
Δv on-off	1.32	1.32	1.32	0.99	0.99	0.99	0.99	7.92

Table 3.3: Δv cost corresponding to the rendezvous example for the Darwin formation. The two groups of satellites depart from 1000 m apart and perform rendezvous in one day. The example uses 50 linear elements for each satellite.

4 Conclusions

In this paper we present a technique for reconfigurations of spacecraft formations based in the use of the finite element method and optimal control. The finite element method provides a systematic approach to the discretization of the problem which tends to a low thrust continuous solution when the mesh of elements is refined. This approach has been presented in several examples concerning the TPF and Darwin missions with satisfactory results but much more general situations can be dealt using the methodology.

Acknowledgements

This research has been supported by the Spanish grant BFM2003-09504, and the Catalan grants CIRIT 2001SGR-70 and 2003XT-00021.

References

[1] Beichman, C., Gómez, G., Lo, M.W., Masdemont, J.J. and Romans, L. Searching for Life with the Terrestrial Planet Finder: Lagrange Point Options for a Formation Flying Interferometer. *Advances in Space Reseach* **34** (2004) 637–644.

[2] McInnes, C.R. Autonomous proximity manoeuvring using artificial potential functions. *ESA Journal* **17**(2) (1993) 159–169.

[3] The TPF Science Working Group. *The Terrestrial Planet Finder: A NASA Origins Program to Search for Habitable Planets*. JPL Publication 99-3, 1999.

[4] Gómez, G., Lo, M.W., Masdemont, J.J. and Museth, K. Simulation on Formation flight near Lagrange Points for the TPF mission. *Advances in the Astronautical Sciences* **109** (2002) 61–75.

[5] The Science and Technology Team of Darwin and Alcatel Study Team. *Darwin. The Infrared Space Interferometer. Concept and Feasibility Study Report*. European Space Agency, ESA-SCI(2000)12, iii+218, July 2000.

[6] Singh, G. and Hadaegh, F. Autonomous Path-Planning for Formation-Flying Applications. In: *International Symposium on Space Flight Dynamics*, 2001.

[7] Volpe, R.A. *Real and Artificial Forces in the Control of Manipulators: Theory and Experiments*. Ph.D. Thesis, Dept. of Physics, Carnegie Mellon University, September, 1990.

[8] Zienkiewicz, O.C. and Taylor, R.L. *The finite element method*. McGraw-Hill, New York, 1994.

Nonlinear Dynamics and Systems Theory, **6** (4) (2006) 353–366

Cause Effect Nonlinear Relations in Continuous Orbital Transfers under Superposed Pitch and Yaw Deviations

A.D.C. Jesus *

Universidade Estadual de Feira de Santana (UEFS), Departamento de Física
Caixa Postal 252-294, BR116-Norte, Km 3, 44.031-460, Feira de Santana, BA, Brazil

Received: June 13, 2006; Revised: October 10, 2006

Abstract: The thrust direction deviations effects in orbital transfers maneuvers cause linear and angular misalignments that displace the vehicle with respect to its nominal directions. Corrections maneuvers are realized, but these deviations are increasing during the vehicle life time due to the propulsion system consuming. The main of the corrections maneuvers are not reached during this period. The vehicle is lost due to the dissipatives forces and the thrusters systems deviations. The understanding of these deviations effects through the final orbit is very important to the mission control under pitch and yaw deviations. In this paper, we show the algebraic relations between these deviations and the keplerian elements of the vehicle final orbit. This analysis allowed to found the theoretical and exact nonlinear cause effect relation between the media values of the keplerian elements (final semi-major axis) and the superposed burn-direction deviations. The dissipatives forces effects were not considered with respect to these thrust deviations during the transfers maneuvers.

Keywords: *Pitch; yaw; thrust deviations; superposed; nonlinear relation.*

Mathematics Subject Classification (2000): 70M20.

* Corresponding author: adj@uefs.br

1 Introduction

The optimum orbital transfer problem of the space vehicle was studied initially by Goddard [1] in 1919, with his pioneer paper about the maximization of the final altitude of the rocket under the gravitation field and atmosphere drag. Hohmann [2] in 1925 found the minimum fuel solution for the bi-impulsive transfer problem between two space vehicle circular and coplanar orbits. This solution was considered the final solution for this problem until 1959. In this year Hoelker and Silber [3] published the minimum fuel condition for the Hohmann transfer limited to 11.94. This value is the ratio between the final orbit and initial orbit radius to the bi-impulsive maneuver. In the non-impulsives maneuvers is it very important to know one of the thrust burn point to avoid the misalignment's thrust. Lawden [4] in 1955 found optimum directions to thrust application and showed that the thrust direction would be tangente to the trajectory. There are others maneuvers of tri- and multi-impulsives under minimum fuel consumption condition and under others in-orbital restrictions, studied by many authors through several methods. Many authors used the propulsion system as control system to reach many purposes. See e.g., Kluever and Tanck [5] (1997), Javorsek II and Longuski [6] (1999), Vassar and Sherwood [7] (1985), Ulybyshev [8] (1998), etc. The orbital and rotational motions coupling effects through the transfer maneuvers were studied, e.g., Duboshin [9] (1958), Barkin [10] (1985), Beletski [11] (1990), Wang et alli [12] (1991), Wang et alii [13] (1992) and Maciejewski [14] (1995), etc.

Study of the superposition thrust deviations effects for the space vehicle trajectories is important, due to their technological importance and space missions feasibility to vehicle under thrusters burns. The poorly modeled maneuvers and/or non optimized to turn aside from nominal orbits and the correction or vehicle capture maneuvers can be unworkable, due to the operational expense and the fuel availability on board. The satellite orbits under non-ideal propulsion system are affected due to the non-superposed directions thrust. This results was verified by Jesus [15] in (1999) to orbital transfers planar maneuvers. The numerical analysis of the maneuvers under superposed and correlated thrust deviations were published in 2004 by Jesus and Santos [16] and the mission feasibility analysis under thrust direction deviations by Jesus et al. [17]. In this paper we realized the algebraic demonstration of the cause/effect relation between the semi-major axis deviations and the thrust superposed pitch and yaw deviations to orbital transfers maneuvers. Our results were found without restrictions on the kind of maneuvers with respect to the their altitude, power thrusters, etc.

2 Mathematical Formulation and Coordinate System

The mathematical problem is to find the motion equations of the space vehicle and show the cause/effect algebraic relation between superposed "pitch" α and "yaw" β, thrust direction deviations and the semi-major axis deviations of the orbital transfer trajectory. Besides this, the maneuvers were considered optimum as minimum fuel consumption condition. The Figure 2.1, shows the reference system where we wrote the Newton laws. The optimum problem associated with the space vehicle orbital dynamic is:

1) Globally minimize the performance index: $J = m(t_0) - m(t_f)$;

2) With respect to $\alpha : [t_0, t_f] \rightarrow R$ ("pitch" angle) and $\beta : [t_0, t_f] \rightarrow R$ ("yaw" angle) with α , $\beta \in C^{-1}$ in $[t_0, t_f]$;

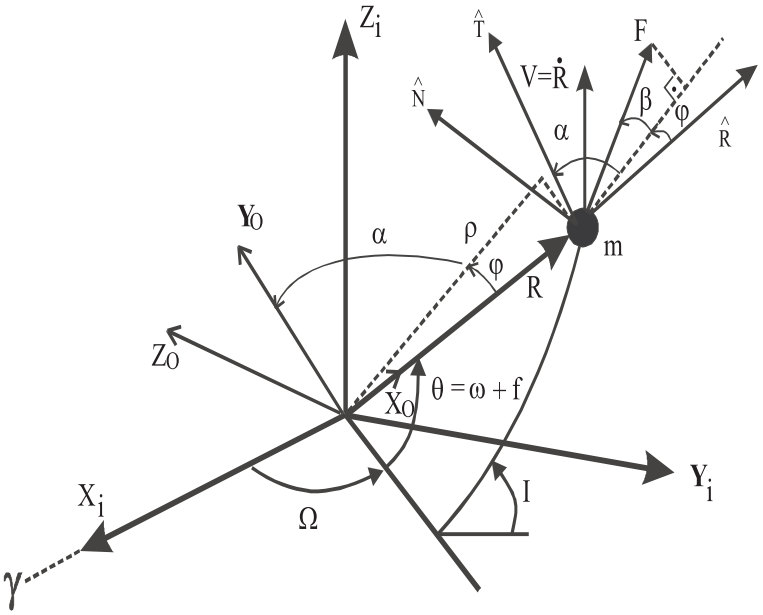

Figure 2.1: Reference systems used in this work.

3) Consideration of the dynamics in inertial coordinates X_i, Y_i, Z_i (see Figure 2.1) for $\forall t \in [t_0, t_f]$

$$m\frac{d^2X}{dt^2} = -\mu m\frac{X}{R^3} + F_x, \tag{1}$$

$$m\frac{d^2Y}{dt^2} = -\mu m\frac{Y}{R^3} + F_y, \tag{2}$$

$$m\frac{d^2Z}{dt^2} = -\mu m\frac{Z}{R^3} + F_z, \tag{3}$$

$$\begin{aligned} F_x = {} & F\left[\cos\beta\sin\alpha\left(\cos\Omega\cos\theta - \sin\Omega\cos I\sin\theta\right) + \sin\beta\sin\Omega\sin I - \right. \\ & \left.\cos\beta\cos\alpha\left(\cos\Omega\sin\theta + \sin\Omega\cos I\cos\theta\right)\right], \end{aligned} \tag{4}$$

$$\begin{aligned} F_y = {} & F\left[\cos\beta\sin\alpha\left(\sin\Omega\cos\theta + \cos\Omega\cos I\sin\theta\right) - \sin\beta\cos\Omega\sin I - \right. \\ & \left.\cos\beta\cos\alpha\left(\sin\Omega\sin\theta - \cos\Omega\cos I\cos\theta\right)\right], \end{aligned} \tag{5}$$

$$F_z = F\left(\cos\beta\sin\alpha\sin I\sin\theta + \cos\beta\cos\alpha\sin I\cos\theta + \sin\beta\cos I\right). \tag{6}$$

The V_N, V_T and V_R are the normal, transversal and radial velocity components, respectively. Their accelerations are a_N, a_T and a_R. These equations in orbital coordinates

(radial R, transverse T, and binormal N) of Figure 2.1 are:

$$ma_R(t) = F\cos(\beta(t)+\Delta\beta(t))\sin(\alpha(t)+\Delta\alpha(t)) - \frac{\mu m}{R^2(t)}, \quad (7)$$

$$ma_T(t) = F\cos(\beta(t)+\Delta\beta(t))\cos(\alpha(t)+\Delta\alpha(t)), \quad (8)$$

$$ma_N(t) = F\sin(\beta(t)+\Delta\beta(t)), \quad (9)$$

$$a_R(t) = \dot{V_R} - \frac{V_T^2}{R} - \frac{V_N^2}{R}, \quad (10)$$

$$a_T(t) = \dot{V_T} + \frac{V_R V_T}{R} - V_N\dot{I}\cos\theta - V_N\dot{\Omega}\sin I\sin\theta, \quad (11)$$

$$a_N(t) = \dot{V_N} + \frac{V_R V_N}{R} + V_T\dot{I}\cos\theta + V_T\dot{\Omega}\sin I\sin\theta, \quad (12)$$

$$V_R = \dot{R}, \quad (13)$$

$$V_T = R(\dot{\Omega}\cos I + \dot{\theta}), \quad (14)$$

$$V_N = R(-\dot{\Omega}\sin I\cos\theta + \dot{I}\sin\theta), \quad (15)$$

$$\theta = \omega + f, \quad (16)$$

where $\Delta\alpha$ and $\Delta\beta$ are the errors in the "pitch" and in the "yaw" angles, respectively. In this way, for each implementation of the orbital transfer arc, values of α and β are chosen, whose errors are inside the range, that produce the direction for the overall minimum fuel consumption. If we consider mass time-variable, for example, linear variation, so,

$$m(t) = m(t_o) + \dot{m}(t - t_o) \quad (17)$$

with $\dot{m} < 0$ and

$$F \cong \mid \dot{m} \mid c. \quad (18)$$

The motion Equations (1),(2),(3) etc. must be modified to include the force associated to mass variation.

4) Given the initial and final orbits, and the parameters of the problem $m(t_o), c, \ldots$ these equations were obtained by: 1) writing in coordinates of the dexterous rectangular reference system with inertial directions $OX_iY_iZ_i$ the Newton's laws for the motion of a satellite S with mass m, with respect to this reference system, centered in the Earth's center of mass O with X_i axis toward the Vernal point, X_iY_i plane coincident with Earth's Equator,and Z_i axis toward the Polar Star approximately; 2) rewriting them in coordinates of the dexterous rectangular reference system with radial, transverse, binormal directions $SRTN$, centered in the satellite center of mass S; helped by 3) a parallel system with $OX_oY_oZ_o$ directions, centered in the Earth's center of mass O, X_o axis toward the satellite S, X_oY_o plane coincident with the plane established by the position $\vec{R}$ and velocity $\vec{V}$ vectors of the satellite, and Z_o axis perpendicular to this plane; and helped by 4) the instantaneous Keplerian coordinates $(\Omega, I, \omega, f, a, e)$. These equations were later rewritten and simulated by using 5) 9 state variables, defined and used by Biggs [19, 20] and Prado [21].

3 Orbital Continuous Transfer under Thrust Deviations – General Equations

The cause/effect relation between the thrust vector directions deviations and the semi-major axis of the final orbit can be found if we consider the mechanical energy of the space vehicle under thrusters burns. This dynamics is under action of two forces: natural force (gravity) and nonnatural force (due to the thrusters). Our algebraic approach for the semi-major axis deviations is done through the rate of change of the space vehicle mechanical energy with respect to the time, which is equal to the power applied by forces components in the transverse, radial and normal directions. We considered the Earth mass and the space vehicle mass as punctual. Also we considered the thrust to be nonideal in direction, transfering the deviations effects to the vehicle dynamics. Their energy rate of change are:

$$\frac{dE_M(t)}{dt} = F\cos\alpha(t)\cos\beta(t)v_T(t) + F\sin\alpha(t)\cos\beta(t)v_R(t) + F\sin\beta(t)v_N(t). \qquad (19)$$

In the Equation (19) the powers are included applied by forces components in the transverse, radial and normal directions, without the thrust deviations. During the time interval Δt, we integrated and found the change of the mechanical energy,

$$\Delta E_M(t_1,t_2) = E_M(t_2) - E_M(t_1) = \int_{t_1}^{t_2} F[\cos\alpha(t)\cos\beta(t)v_T(t) + \sin\alpha(t)\cos\beta(t)v_R(t) + \sin\beta(t)v_N(t)]dt = \frac{-\mu m}{2a(t_2)} + \frac{\mu m}{2a(t_1)} \qquad (20)$$

with $a(t_i)$ the semi-major axis of the space vehicle orbit in the instant i. This mechanical energy change, Equation (20), can be computed for one transfer under "pitch", $\Delta\alpha(t)$ and "yaw", $\Delta\beta(t)$ deviations. So,

$$\Delta E'_M(t_1,t_2) = E'_M(t_2) - E'_M(t_1) = \int_{t_1}^{t_2} F[\cos(\alpha(t)+\Delta\alpha(t))\cos(\beta(t)+\Delta\beta(t))v'_T(t)]dt + \int_{t_1}^{t_2} F\sin(\beta(t)+\Delta\beta(t))v'_N(t)dt + \int_{t_1}^{t_2} F[\cos(\beta(t)+\Delta\beta(t))\sin(\alpha(t)+\Delta\alpha(t))v'_R(t)]dt = \frac{-\mu m}{2a'(t_2)} + \frac{\mu m}{2a'(t_1)}. \qquad (21)$$

The terms in $(')$ denotes functions under thrust deviations influence. We define $\Delta_2 E_M$ as change of the mechanical energy change, that is, the difference between its values with and without thrust deviations. So, taking the difference between Equations (20) and (21)

and using a small mathematical manipulation,

$$\Delta_2 E_M(t_1,t_2) \equiv \Delta E'_M(t_1,t_2) - \Delta E_M(t_1,t_2) = \frac{-\mu m}{2a'(t_2)} + \frac{\mu m}{2a'(t_1)} + \frac{\mu m}{2a(t_2)} + \frac{-\mu m}{2a(t_1)} =$$

$$\int_{t_1}^{t_2} F[\cos(\beta(t)+\Delta\beta(t))\sin(\alpha(t)+\Delta\alpha(t))v'_R(t) - \sin\alpha(t)\cos\beta(t)v_R(t)]dt +$$

$$\int_{t_1}^{t_2} F[\sin(\beta(t)+\Delta\beta(t))v'_N(t) - \sin\beta(t)v_N(t)]dt +$$

$$\int_{t_1}^{t_2} F[\cos(\alpha(t)+\Delta\alpha(t))\cos(\beta(t)+\Delta\beta(t))v'_T(t) - \cos\alpha(t)\cos\beta(t)]v_T(t)dt. \quad (22)$$

4 $\Delta\alpha(t)$ and $\Delta\beta(t)$ Not Correlated with the Transverse, Radial and Normal Velocities (Uniform Deviations)

Equation (22) is general, but we need to realize the integrations to realistic space missions conditions. In this way, we consider that the direction deviations are not correlated (in the time) with the transversal, radial and normal velocities components. That is, during the burn time, the thrust vector deviations have not functional dependence with space vehicle velocity. Besides this, we consider that the semi-major axis in the initial instant to the initial and final orbits are equal. This condition is physically reasonable, because during the initial instant there is no time to the deviations affect the semi-major axis.

To find the cause/effect relation, we apply the expectation operator, $\mathcal{E}$, (or the first moment, or mean) over the Equation (22). In this way, we select the mean of the functions inside the integrations. We consider the probabilistic approach, where the mean over the physical functions is very good to represent the dynamic phenomena under deviations, define through probabilistic errors function (Gaussian, Uniform, etc.). This approach is applicable in the space technology, because the direction deviations are due to the several unpredictable reasons such as: vehicle mass center displacement, due to the fuel consumption or movable parts as solar panels, antennas, booms, pendulums, etc., and their angular deviations. These deviations and others in the thrust magnitude cause resultant nonideal force, which do not pass through the vehicle mass center. So, the linear and/or angular misalignments displace the vehicle with respect to its nominal directions. The technological implementations has shown that these deviations can be modeled through the uniform and gaussian probability function. We assume that stochastic processes are ergotic. So, the expectation operator (mean in the ensemble) commutes with the integral operator (in time). Besides this, the function F and the trigonometric functions are deterministic in time.

The non-correlation of the deviations with the velocities allows us to decompose the expectation operator as one product of the individual expectatins for the product of the functions. Therefore, taking the expectation, $\mathcal{E}$, and doing some algebraic manipulation, we have

$$\mathcal{E}[\Delta_2 E_M(t_1,t_2)] = [Q_{11}+Q_{22}][\mathcal{E}[\cos\Delta\beta(t)\cos\Delta\alpha(t)]-1] + [Q_{12}+Q_{21}][\mathcal{E}[\cos\Delta\beta(t)\sin\Delta\alpha(t)]-1] + [Q_{31}+Q_{42}][\mathcal{E}[\sin\Delta\beta(t)\cos\Delta\alpha(t)]-1] + [Q_{32}+Q_{41}][\mathcal{E}[\sin\Delta\beta(t)\sin\Delta\alpha(t)]-1] + Q_{93}[\mathcal{E}[\cos\Delta\beta(t)]-1] + Q_{10}[\mathcal{E}[\sin\Delta\beta(t)]-1] + [Q_{51}+Q_{52}+Q_{61}+Q_{71}+Q_{72}+Q_{82}], \quad (23)$$

where Q_{ij} are quadratures in sines and cosines. Besides this, we consider that the velocities effects inside the interval $[-\Delta\alpha_{max}, \Delta\alpha_{max}]$ in the same time are,practically, balanced, because the deviations occur between values maxima and minima inside them. That is, the velocities with and without deviations have, in mean, very close values. So,

$$\mathcal{E}[v'_{R,T,N}(t)] = v_{R,T,N}(t_1). \tag{24}$$

We consider the important approach of the $\Delta\alpha(t)$ and $\Delta\beta(t)$ are random-bias deviations with uniform distribution inside the interval $[-\Delta\alpha_{max}, \alpha_{max}]$, that is, $\Delta\alpha(t) = \Delta\alpha(t_1) = \Delta\alpha$ and $\Delta\beta(t) = \Delta\beta(t_1) = \Delta\beta$ (systematic deviations) through the orbital transfers. Besides this, we consider that the pitch and yaw deviations are not correlated with each other (it occurs in the practice) and that their values in anterior instant (due to thrusters action) are not correlated with their values in posterior instant (due to thrusters action again). This last effect was analized in 2004 by Jesus and Santos [16] in numerical approach. They modeled the consuming of the thrusters through it. Hier, we do not consider this effect. Therefore, applying the expectation operator over the first term (not correlated) of the Equation (23), for example,

$$\mathcal{E}\{\cos\Delta\alpha(t_1)\} = \frac{1}{2\Delta\alpha_{max}}\int_{\Delta\alpha_{max}}^{\Delta\alpha_{max}} \cos\Delta\alpha d(\Delta\alpha) = \frac{1}{2\Delta\alpha_{max}}\sin[\Delta\alpha]_{\Delta\alpha_{max}}^{\Delta\alpha_{max}} = \frac{\sin\Delta\alpha_{max}}{\Delta\alpha_{max}} \tag{25}$$

and

$$\mathcal{E}[\sin\Delta\beta(t_1)] = \mathcal{E}[\sin\Delta\alpha(t_1)] = 0. \tag{26}$$

If we compute the expectation over all the terms of the Equation (23), we obtain

$$\Delta_2 E_M(t_1,t_2) = C_1[[\frac{\sin\Delta\alpha_{max}}{\Delta\alpha_{max}}][\frac{\sin\Delta\beta_{max}}{\Delta\beta_{max}}] - 1] + C_2[[\frac{\sin\Delta\beta_{max}}{\Delta\beta_{max}} - 1] + Q_{T1} - Q_{10} + Q_{T2} \tag{27}$$

or, writting in Taylor expansion to the $\sin\Delta\alpha$, $\sin\Delta\beta$, we obtain

$$\mathcal{E}\{\Delta_2 E_M(t_1,t_2)\} = C_1\sum_{n=0}^{\infty}(-1)^n\frac{1}{(2n+1)!}\Delta\alpha_{max}^{2n}.\sum_{n=0}^{\infty}(-1)^n\frac{1}{(2n+1)!}\Delta\beta_{max}^{2n} + C_2\sum_{n=0}^{\infty}(-1)^n\frac{1}{(2n+1)!}\Delta\beta_{max}^{2n} + Q_T, \tag{28}$$

where Q_T, C_1 and C_2 are quadratures. The expectation over the left side of the Equation (23) provide

$$\mathcal{E}\{\Delta_2 E_M(t_1,t_2)\} = \mathcal{E}\{\frac{\mu m}{2a(t_2)} - \frac{\mu m}{2a'(t_2)}\} = \frac{\mu m}{2}\frac{1}{a(t_2)}\mathcal{E}\{\frac{\Delta a(t_2)}{a'(t_2)}\}. \tag{29}$$

If we expand Equation (29) about the rate $\frac{\Delta a(t_2)}{a(t_2)}$, we get

$$\mathcal{E}\{\Delta_2 E_M(t_1,t_2)\} = \frac{\mu m}{2}[\frac{1}{a^2(t_2)}\mathcal{E}\{\Delta a(t_2)\} - \frac{1}{a^3(t_2)}\mathcal{E}\{\Delta^2 a(t_2)\} + \frac{1}{a^4(t_2)2!}\mathcal{E}\{\Delta^3 a(t_2)\} - \frac{1}{a^5(t_2)3!}\mathcal{E}\{\Delta^4 a(t_2)\} + \ldots] = \frac{\mu m}{2}\sum_{n=1}^{\infty}(-1)^{n+1}\frac{1}{a^{n+1}(t_2)(n-1)!}\mathcal{E}\{\Delta^n a(t_2)\}, \quad (30)$$

where, $\Delta a(t_2)$=$a'(t_2) - a(t_1)$. So,

$$\sum_{n=1}^{\infty}(-1)^{n+1}\frac{1}{a^{n+1}(t_2)(n-1)!}\mathcal{E}\{\Delta^n a(t_2)\} = [C_4 + C_3\sum_{n=0}^{\infty}(-1)^n\frac{1}{(2n+1)!}\Delta\alpha_{max}^{2n}].\sum_{n=0}^{\infty}(-1)^n\frac{1}{(2n+1)!}\Delta\beta_{max}^{2n} + C_5. \quad (31)$$

Equation (31) is the cause/effect relation between thrust vector pitch and yaw direction deviations and semi-major axis deviation of the final orbit. It shows that the direction deviations affect directly the transfer maneuvers. It is nonlinear relation in even power of the maxima deviations terms

$$C_3 = \frac{2C_1}{\mu m}; C_5 = \frac{2C_2}{\mu m}; C_5 = \frac{2Q_T}{\mu m}. \quad (32)$$

Equations (30) and (31) can be expandied, that is,

$$\mathcal{E}\{\Delta_2 E_M(t_1,t_2)\} = C_7 - \frac{C_3}{3!}(\Delta\alpha_{max}^2 + \Delta\beta_{max}^2) + \frac{1}{5!}(C_3\Delta\alpha_{max}^4 + C_6\Delta\beta_{max}^4) + \frac{1}{7!}(C_3\Delta\alpha_{max}^6 + C_6\Delta\beta_{max}^6) + \frac{1}{(3!)^2}(\Delta\alpha_{max}\Delta\beta_{max})^2 + \frac{1}{(5!)^2}(\Delta\alpha_{max}^2\Delta\beta_{max}^2)^2 + \frac{1}{(7!)^2}(\Delta\alpha_{max}^3\Delta\beta_{max}^3)^2 - \frac{C_3}{(3!5!)}(\Delta\alpha_{max}^2\Delta\beta_{max}^4 + \Delta\alpha_{max}^4\Delta\beta_{max}^2) + \frac{C_3}{(3!7!)}(\Delta\alpha_{max}^2\Delta\beta_{max}^6 + \Delta\alpha_{max}^6\Delta\beta_{max}^2) + \frac{C_3}{(5!7!)}(\Delta\alpha_{max}^4\Delta\beta_{max}^6 + \Delta\alpha_{max}^6\Delta\beta_{max}^4) + \ldots \quad (33)$$

The space missions conditions request direction deviations inside the practical interest range, that is, maximum two degree. So, for small deviations we can neglect high power terms. In this condition we can choose $n = 0$ for the expansion

$$\mathcal{E}\{\Delta a(t_2)\} = K_1 - K_2\Delta\alpha_{max}^2 - K_2\Delta\beta_{max}^2. \quad (34)$$

This is the first order nonlinear cause/effect relation between thrust direction deviations and semi-major axis. It is one revolution paraboloid. Our paper [18] in 2004 showed numerical simulation results of these superposed direction deviations case and found a revolution paraboloid deformed inside general deviations pitch and yaw range and revolution paraboloid not deformed inside the space missions practical interest range. This algebraic results confirm it (Figures 4.1, 4.2, 4.3, 4.4).The deviations in modulus thrust (DES1),in pitch direction (DES2) and in yaw direction (DES3). These deviations are modeled as operational (white-noise) and systematic (random-bias).

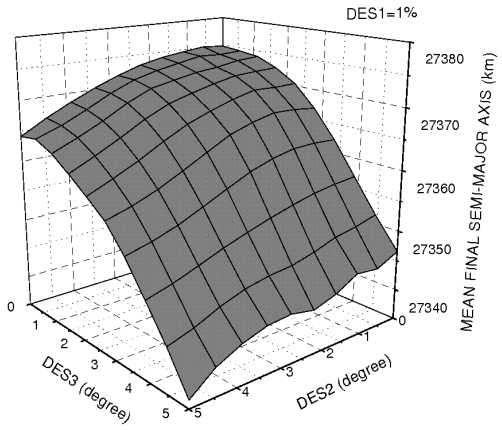

Figure 4.1: Noncoplanar Transfer under Operational Deviations.

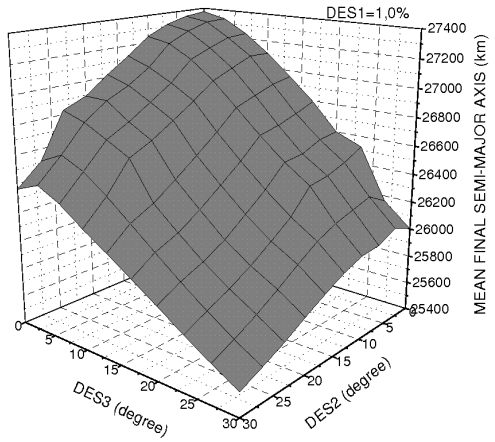

Figure 4.2: Noncoplanar Transfer under Systematic Deviations.

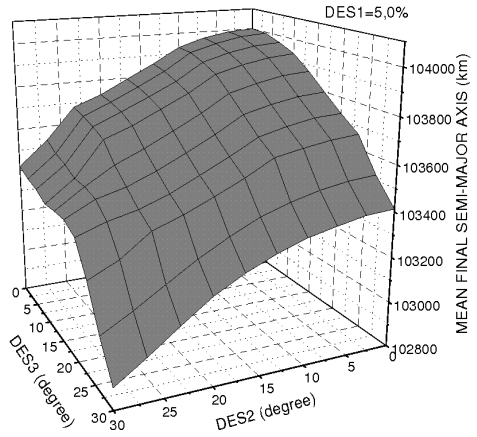

Figure 4.3: Coplanar Transfer under Operational Deviations.

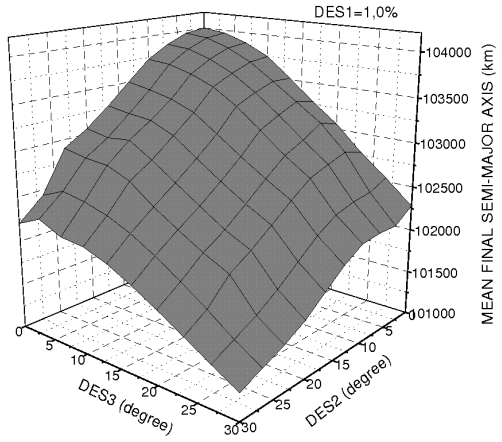

Figure 4.4: Coplanar Transfer under Systematic Deviations.

5 $\Delta\alpha(t)$ and $\Delta\beta(t)$ Not Correlated with the Transverse, Radial and Normal Velocities (Gaussian Deviations)

The procedures for the $\Delta\alpha(t)$ and $\Delta\beta(t)$ with Gaussian distribution inside the interval $[-\Delta\alpha_{max}, \Delta\alpha_{max}]$ and $[\Delta\alpha_{max}, \Delta\alpha_{max}]$ are the same for the uniform distribution. Therefore, applying the expectation operator over the first term (not correlated) of the Equation (23) for the Gaussian distribution, for example, we have

$$\mathcal{E}\{\cos\Delta\alpha(t_1)\} = \int_{-\infty}^{\infty} \cos\Delta\alpha \frac{\exp^{-\frac{(\Delta\alpha)}{2\sigma_\alpha}}}{\sqrt{2\pi}\sigma_\alpha} d(\Delta\alpha) = \exp^{\frac{-{\sigma_\alpha}^2}{2}} = \sum_{n=0}^{\infty} (-1)^n \frac{\sigma_\alpha^{2n}}{2^n n!}. \tag{35}$$

The expectation of the sinos terms are zero. So, we can obtain the nonlinear cause e effect relation between thrust direction gaussian deviations and the semi-major axis,

$$\sum_{n=1}^{\infty} (-1)^{n+1} \frac{1}{a^{n+1}(t_2)(n-1)!} \mathcal{E}\{\Delta^n a(t_2)\} =$$
$$[C_4 + C_3 \sum_{n=0}^{\infty} (-1)^n \frac{\sigma_\alpha^{2n}}{(2^n)n!}]. \sum_{n=0}^{\infty} (-1)^n \frac{\sigma_\beta^{2n}}{(2^n)n!} + C_5, \tag{36}$$

where σ_α and σ_β are standard pitch and yaw deviations, respectively. Equation (36) is similar to Equation (31), that is, the nonlinear cause/effect relation do have dependence with the probability deviations function.

So, for small deviations we can neglect high power terms. In this condition we can choose $n = 0$ for the expansion

$$\mathcal{E}\{\Delta a(t_2)\} = K_3 - K_4 \frac{\sigma_\alpha^2}{2} - K_5 \frac{\sigma_\beta^2}{2}. \tag{37}$$

6 $\Delta\alpha(t)$ Correlated with Transverse, Radial and Normal Velocities

In this case, we cannot decompose the expectation operator as a product of the individual expectations for the trigonometric functions of the $\Delta\alpha(t)$ and $\Delta\beta(t)$ and the velocities components, because now they are correlated. The procedures are the same done until this point, except that we must evaluate the expectation of the products of the different variables, without decomposing them. Besides this, we consider the $\Delta\alpha(t)$ and $\Delta\beta(t)$ random-bias deviations, that is, $\Delta\alpha(t)$=constant=$\Delta\alpha(t_1)$=$\Delta\alpha$ and $\Delta\beta(t)$=constant=$\Delta\beta(t_1)$=$\Delta\beta$. After many mathematical manipulations we found the following equation, for both cases, uniform and Gaussian distribution,

$$I_{t,r,n} = \int_{t_2}^{t_1} \mathcal{E}\{(\cos\Delta\alpha)(\cos\Delta\beta){v'}_{t,r,n}(t)\dot{f}'_{t,r,n}(t)\}dt. \tag{38}$$

We know that the integral of the odd functions for symmetrical distributions is null. But Equation (38) has even product of the functions. The odd functions inside the product are not known, but we can modeled its product as one even function, for example, $\cos\Delta\alpha$. Besides this, we consider that the I, Ω, θ, $\dot{I}$ and $\dot{\Omega}$ effects inside the $[-\Delta\alpha_{max}, \Delta\alpha_{max}]$ and $[-\Delta\beta_{max}, \Delta\beta_{max}]$ intervals in the same time are, practically, balanced, because the deviations occur between values maxima and minima inside them.

That is, these instantaneous Keplerian coordinates values with and without deviations are, in mean, very close values. So,

$$\mathcal{E}\{\dot{I}'(t)\cos\theta'(t)\} = \dot{I}(t_1)\cos\theta(t_1), \tag{39}$$

$$\mathcal{E}\{\dot{\Omega}'(t)\sin I'(t)\sin\theta'(t)\} = \dot{\Omega}(t_1)\sin I(t_1)\sin\theta(t_1). \tag{40}$$

Other important approach in this way is to consider for Equations (9) and (11) that the expectation of the product is equal to the product of the expectations of the functions, so that

$$\mathcal{E}\{\frac{(\cos\Delta\alpha)(\cos\Delta\beta)}{(r')^2(t)}\} = \mathcal{E}\{(\cos(\Delta\alpha)(\cos\Delta\beta)\frac{1}{(r')^2(t)}\} \cong$$
$$\mathcal{E}\{\cos\Delta\alpha\}\mathcal{E}\{\cos\Delta\beta\}\mathcal{E}\{\frac{1}{(r')^2(t)}\} = \frac{\mathcal{E}\{\cos\Delta\alpha\}\mathcal{E}\{\cos\Delta\beta\}}{r^2(t)}. \tag{41}$$

The final forms are:

$$\sum_{n=1}^{\infty}(-1)^{n+1}\frac{1}{a^{n+1}(t_2)}\mathcal{E}\{\Delta^n a(t_2)\} = \lambda_1 + \lambda_2\Delta\alpha_{max} + \lambda_3\Delta\beta_{max} +$$
$$\lambda_4\Delta\alpha_{max}\Delta\beta_{max} - \lambda_5\Delta\alpha_{max}^2 - \lambda_6\Delta\alpha_{max}^2\Delta\beta_{max} - \lambda_7\Delta\beta_{max}^2\Delta\alpha_{max} +$$
$$\lambda_8\Delta\alpha_{max}^2\Delta\beta_{max}^2 + \lambda_9\Delta\alpha_{max}^4 + \lambda_{10}\Delta\alpha_{max}^5 -$$
$$\lambda_{11}\Delta\alpha_{max}\Delta\beta_{max}^4 - \lambda_{12}\Delta\alpha_{max}^2\Delta\beta_{max}^4 + \lambda_{13}\Delta\alpha_{max}^4\Delta\beta_{max}^2 +$$
$$\lambda_{14}\Delta\alpha_{max}^4\Delta\beta_{max}^4 + \ldots \tag{42}$$

for the uniform deviations and

$$\sum_{n=1}^{\infty}(-1)^{n+1}\frac{1}{a^{n+1}(t_2)}\mathcal{E}\{\Delta^n a(t_2)\} = f_1 + f_2\sigma_\alpha + f_3\sigma_\beta + f_4\sigma_\alpha\sigma_\beta - f_5\sigma_\alpha^2$$
$$-f_6\sigma_\alpha^2\sigma_\beta - f_7\sigma_\beta^2\sigma_\alpha + f_8\sigma_\alpha^2\sigma_\beta^2 + f_9\sigma_\alpha^4 + f_{10}\sigma_\alpha^5 - f_{11}\sigma_\alpha\sigma_\beta^4 - f_{12}\sigma_\alpha^2\sigma_\beta^4$$
$$+f_{13}\sigma_\alpha^4\sigma_\beta^2 + f_{14}\sigma_\alpha^4\sigma_\beta^4 + \ldots \tag{43}$$

for the Gaussian deviations.

The coefficients λ_i, λ_{ij}, f_i and f_{ij} are mathematical operations (sums, products and sums of the products) between quadratures in sines and cosines of the pitch and yaw angles.

If we compute the first order terms, Equations (42) and (43), and consider deviations inside the practical range for the space missions, we obtain, for the both cases,

$$\mathcal{E}\{\Delta\alpha(t_2)\} = C_1 + C_2\Delta\alpha_{max} + C_3\Delta\beta_{max} + C_4\Delta\alpha_{max}\Delta\beta_{max} - C_5\Delta\alpha_{max}^2 \tag{44}$$

for the uniform deviations and

$$\mathcal{E}\{\Delta\alpha(t_2)\} = C_6 + C_7\sigma_\alpha + C_8\sigma_\beta + C_9\sigma_\alpha\sigma_\beta - C_{10}\sigma_\alpha^2 \tag{45}$$

for the Gaussian deviations.

These results show once again the nonlinear relationship between cause and effect since n=1 of the expansions.

We modeled in the Equation (38) the product of the not known odd functions as an even function equal to the $\cos\Delta\alpha$. If we choose it as the $\cos\Delta\beta$ the results are different. So, with the same previous algebraic proceedings, we have

$$\sum_{n=1}^{\infty}(-1)^{n+1}\frac{1}{a^{n+1}(t_2)}\mathcal{E}\{\Delta^n a(t_2)\} = \lambda'_1 + \lambda'_2\Delta\alpha_{max} + \lambda'_3\Delta\beta_{max} + \lambda'_4\Delta\alpha_{max}\Delta\beta_{max} - \lambda'_5\Delta\alpha^2_{max} - \lambda'_6\Delta\beta^2_{max} - \lambda'_7\Delta\alpha^2_{max}\Delta\beta_{max} - \lambda'_8\Delta\beta^3_{max} + \lambda'_9\Delta\alpha^4_{max} + \lambda'_{10}\Delta\beta^4_{max} + \lambda'_{11}\Delta\alpha^2_{max}\Delta\beta^2_{max} - \lambda'_{12}\Delta\alpha^2_{max}\Delta\beta^3_{max} - \lambda'_{13}\Delta\alpha^2_{max}\Delta\beta^4_{max} - \lambda'_{14}\Delta\beta^6_{max} + \lambda'_{15}\Delta\alpha^2_{max}\Delta\beta^6_{max} + \dots \quad (46)$$

for the uniform deviations, and

$$\sum_{n=1}^{\infty}(-1)^{n+1}\frac{1}{a^{n+1}(t_2)}\mathcal{E}\{\Delta^n a(t_2)\} = f'_1 + f'_2\sigma_\alpha + f'_3\sigma_\beta + f'_4\sigma_\alpha\sigma_\beta - f'_5\sigma^2_\alpha - f'_6\sigma^2_\beta - f'_7\sigma^2_\alpha\sigma_\beta - f'_8\sigma^3_\beta + f'_9\sigma^4_\alpha + f'_{10}\sigma^4_\beta + f'_{11}\sigma^2_\alpha\sigma^2_\beta - f'_{12}\sigma^2_\alpha\sigma^3_\beta - f'_{13}\sigma^2_\alpha\sigma^4_\beta - f_{14}\sigma^6_\beta + f'_{15}\sigma^2_\alpha\sigma^6_\beta + \dots \quad (47)$$

for the Gaussian deviations.

These results for the space missions interest deviations range are

$$\mathcal{E}\{\Delta\alpha(t_2)\} = C_{11} + C_{12}\Delta\alpha_{max} + C_{13}\Delta\beta_{max} + C_{14}\Delta\alpha_{max}\Delta\beta_{max} - C_{15}\Delta\alpha^2_{max} - C_{16}\Delta\beta^2_{max}, \quad (48)$$

$$\mathcal{E}\{\Delta\alpha(t_2)\} = C_{17} + C_{18}\sigma_\alpha + C_{19}\sigma_\beta + C_{20}\sigma_\alpha\sigma_\beta - C_{21}\sigma^2_\alpha - C_{11}\sigma^2_\beta. \quad (49)$$

These results show, again, the nonlinear relation between the thrust deviations and the mean semi-major axis uncertainess. The difference between this case, correlated with cossine of the yaw, is that, in the practical interest range, it occurs the $-\cos\Delta\beta^2_{max}$ contribution. It is the out-plane angle deviation and the nonlinear relation in the space missions interest must avoid it, because the in-plain maneuvers are fuel-optimal.

7 Conclusions

Our results show the nonlinear relations between thrust superposed pitch and yaw direction deviations and the final mean semi-major axis. We analysed the correlated and not correlated deviations with the satellite velocity. In all the cases, the relation shows a progressive deformation of the trajectory due these deviations. This dependence is presented as a revolution paraboloid in the space mission practical interest in the range deviations and the deformed revolution paraboloid in general case. In the space mission interest the relation is dominated by $(\Delta\alpha_{max})^2$ term for the α-correlation and $(\Delta\beta_{max})^2$ and $(\Delta\alpha_{max})^2$ terms for the β-correlation. We suggest the first correlation for the transfers maneuvers under fuel consumption optimal. Besides this, these algebraic results confirm the exhaustive numerical simulation realized before in all the deviations ranges. These results do not depend of the trajectory.

References

[1] Goddard, R.H. A method of reaching extreme altitudes. In: *Smithsonian Inst. Publish. Misc. Collect* (1919), Vol. 17, No.2, P. 1-10.

[2] Hohmann, W. Die Erreichbarkeit der Himmelkörper. Munique: s.e., 1925. 1v.

[3] Hoelker, R. F. and Silber, R. The Bi-Elliptic Transfer between circular co-planar orbits. Balistic Missile Agency, Redstone Arsenal, Alabama, Army, EUA, 1959.

[4] Lawden, D. F. Optimal Programming of Rocket Thrust Direction. *Astronautica Acta* **1** (1955) 41–56.

[5] Kluever, C. A. and Tanck, G.S. A Feedback Control Law for Stationkeeping with On-off Thrusters. *Advances in the Astronautical Sciences* **97**(3) (1997) 387–399.

[6] Javorsek II, D. and Longuski, M. J. Velocity Pointing Errors Associated with Spinning Thrusting Spacecraft. AIAA Paper 99-452, AIAA/AAS Astrodynamics Conference, Girdwood, Alaska, August 16-19, 1999.

[7] Vassar, R. H. and Sherwood, R. B. Formationkeeping for a Pair of Satellites in a Circular Orbit. *Journal of Guidance, Control and Dynamics* **8**(2) (1985) 235–242.

[8] Ulybyshev, Y. Long Term Formation Keeping of Satellite Constellation Using Linear-Quadratic Controller. *Journal of Guidance, Control and Dynamics* **21**(1) (1998) 109–115.

[9] Duboshin, G. N. The Existence and Stability of the Equilibrium Points of a Triaxial Rigid Body Moving Around Another Triaxial Rigid Body. *Astronom. Zh.* **2**(35) (1958) p. 265.

[10] Barkin, Y. V. Oblique Regular Motions of a Satellite and Certain Subtle Effects in the Motion of the Moon and PHOBOS. *Kosm. Issled.* **1**(15) (1985) p. 26.

[11] Beletskii, V. V. and Ponomareva, O. N. A Parametric Analysis of Relative Equilibrium Stability in the Gravitational Field. *Kosm. Issled.* **5**(28) (1990) p. 664.

[12] Wang, L.S., Krishnaprasad, P. S. and Maddocks, J. Hamiltonian Dynamics of a Rigid Body in a Central Gravitational Field. *Celestial Mechanics* (50) (1991) p. 349.

[13] Wang, L.S., Maddocks, J. and Krishnaprasad, P. S. Relative Equilibrium and Stabilities of Spring - Connected Bodies in an Central Gravitational Field. *Journal Astronaut. Sci.* **4**(40) (1992) p. 449.

[14] Maciejewski, A. Redution, Relative Equilibria and Potential in the two Rigid Bodies Problem. *Celestial Mechanics and Dynamics Astronomy* **63** (1995) 1–28.

[15] Jesus, A. D. C. Statistical Analysis of the Orbital Maneuveres with Continuous Propusion under Thrust Vector Errors. Doctoral Thesis. INPE. São José dos Campos, São Paulo, Brazil, 1999.

[16] Jesus, A. D. C. and Santos, F. B. M. Study about the Correlated Thrust Vector Deviations in Continuous Orbital Maneuvers. In: *Advances in Space Dynamics*. Vol.4: Celestial Mechanics and Astronautics, 2004, P. 187–197.

[17] Jesus, A. D. C., Santos, F. B. M., Souza, M. L. O. and Prado, A. F. B. A. Study of the Nonimpulsive Orbital Maneuvers Feasibility due to the Restrictions of the Fuel Consumption and the Thruster Power. In: *Advances in Space Dynamics*. Vol. 4: Celestial Mechanics and Astronautics, 2004, P. 209–220.

[18] Jesus, A. D. C. and Santos, F. B. M. Continuous Trajectories under Superposed of the Thrust Vector Deviations. In: *Advances in Space Dynamics*. Vol. 4: Celestial Mechanics and Astronautics, 2004, P. 199–208.

[19] Biggs, M.C.B., The Optimisation of Spacecraft Orbital Manoeuvres. Part I: Linearly Varying Thrust Angles. Connecticut, USA: The Hatfield Polytechnic, Numerical Optimisation Centre, 1978. 24 p. (The Hatfield Polytechnic - Tecnical Report 98).

[20] Biggs, M.C.B., The Optimisation of Spacecraft Orbital Manoeuvres. Part II: Using Pontryagin's Maximum Principle. Connecticut, USA: The Hatfield Polytechnic, Numerical Optimisation Centre, 1979. 27p. (The Hatfield Polytechnic - Tecnical Report 101).

[21] Prado, A.F.B.A., Análise, Seleção e Implementação de Procedimentos que Visem Manobras Ótimas de Satélites Artificiais. Master Dissertation. Instituto Nacional de Pesquisas Espaciais (INPE), São José dos Campos, São Paulo, Brasil, 1989 (INPE-5003-TDL/397).

Nonlinear Dynamics and Systems Theory, **6** (4) (2006) 367–387

Deterministic Chaos in a System Generator – Piezoceramic Transducer

T.S. Krasnopolskaya [1] and A.Yu. Shvets [2*]

[1] *Institute of Hydromechanics, National Academy of Sciences of Ukraine, 03057, Zheljabova Str., 8/4, Kyiv, Ukraine*
[2] *NTUU Kyiv Polytechnic Institute, 03057, Pobedy ave., 37, Kyiv, Ukraine*

Received: January 11, 2006; Revised: September 28, 2006

Abstract: New models and properties of piezoceramic transducer due to the interaction with the excitation device of limited power-supply are built and investigated in details. The special attention is given to examination of origin and development of the deterministic chaos in this system. It is shown, that a major variety of effects typical for problems of chaotic dynamics is inherent in the system. The presence of several types of chaotic attractors is established and the existence of hyper-chaos is revealed. Various scenarios of passage from the regular regimes to chaotic are explored. Explicitly phase portraits and Poincaré sections and maps of of chaotic attractors are investigated. Their spectral densities and distributions of invariant measures are obtained and explored.

Keywords: *Limited excitation; piezoeffect; chaotic attractor; Lyapunov exponents; Poincaré section and mapping.*

Mathematics Subject Classification (2000): 37D45, 37G35, 37L30, 74B99.

1 Introduction

Functioning of many important and mission-critical devices of various engineering machines, including transformers, is based on the effect of coupling of mechanical and electrical fields in piezoceramic media [2, 3, 8, 26, 27, 28, 23]. Hence, creation of a general mathematical theory of electroelastic processes in such media under arbitrary conditions of mechanical and electrical loading is important, both in scientific and applied aspects. Such theory for many piezoceramic devices and constructions is created by A.F. Ulitko and his school [3, 8, 26, 27, 28]. However, in these theories, and in other publications, a problem of behaviour of electroelastic fields is considered only for conditions of forced

* Corresponding author: alex.shvets@bigmir.net

and free oscillations, when the piezoelectric ceramics is under the action of applied mechanical and electrical fields of given values. Thus a problem of influence of dissipation and radiation of energy under oscillations of coupled fields of the device remains outside of many considerations. If the transducer with electroelastic coupled field is mounted in a medium with resistance, as happens in operation of sound emitters, then radiation of energy changes an electric field in the power generator, as opposed to the "ideal" case when no losses occur happen. This adjustment can be essential and lead to unexpected dynamic conditions or be negligibly small — it depends on outer power of the generator compared as with an emitting power. Examination of new effects in dynamics of piezoceramic coupled fields and in functioning of the power generator, which are caused by "sensitivity" of cumulative systems to radiation of energy is, without a doubt, of significant scientific interest. This is a case of so-called limited or non-ideal excitation [12, 24, 25] when supply power is of the same order as the power consumed by a loading piezoceramic transducer. In this case the electric generator is said to have limited power, i.e. a power comparable with the power radiated or consumed by piezoceramic coupled field. The present paper is devoted to the analysis of interaction effects, collectively called the effect of Sommerfeld–Kononenko [12, 13, 15, 16, 17, 18, 19, 24, 25], in oscillations of the piezoceramic transducer and in the mechanism of its excitation — the generator of the electric current of limited power-supply. A new mathematical model of interaction of the generator and the piezoceramic transducer submerged in a hydromedium with resistance is constructed. The coupling of processes in the transformer and the energy source (the generator) leads to the qualitatively new effects in their dynamics that cannot be seen using a model of the problem with unlimited or so-called "ideal" excitation — primarily the possibility of appearance of deterministic chaotic regimes, which are theoretically impossible in a problem with ideal excitation (when corresponding mathematical models of such a problem have dimensionality of phase spaces equal to two, a possibility of chaos origination is excluded).

2 Construction of a mathematical model

Let us consider a piezoceramic rod transducer, which is loaded on the acoustic medium and to which electrodes the electrical voltage is affixed, raised by the LC–generator (Figure 2.1). The selection of the generator of such type is caused by the renaissance of its application observable now in the up-to-date technique. This is related with facts that the electrovacuum-tube (analogue) devices ensure higher metrological characteristic on to comparison with the numeral devices. The origin of the Cartesian coordinate system is in the middle of the rod; from its surfaces S_- and S_+, which are perpendicular to axis oz, acoustic signals radiate into the medium. We will examine the longitudinal vibrations of a round rod of length $2h$ and cross-sectional area S, with longitudinal polarization.

According to the theory of longitudinal deformations [8, 27] the piezoeffect constitutive relations have the form

$$\epsilon_z = s_{33}\sigma_z + d_{33}E_z, \qquad D_z = \epsilon_{33}E_{,z} + d_{33}\sigma_z, \tag{1}$$

where ϵ_z is a longitudinal deformation; σ_z is the mechanical stress; E_z is the intensity of the electric field; D_z is an induction of this field; and $s_{33}, d_{33}, \epsilon_{33}$ are constants.

When studying the acoustic frequency region, we used the equations of a quasistatic

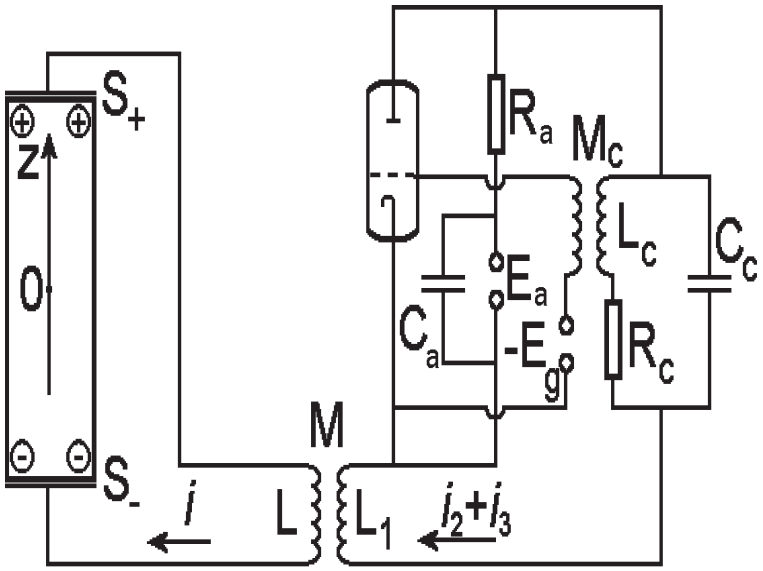

Figure 2.1: Scheme of viewed system.

field. Here, they could be written as

$$\frac{\partial D_z}{\partial z} = 0, \qquad E_z = -\frac{\partial \Psi}{\partial z}, \tag{2}$$

where Ψ is an electrical potential.

We shall add to equations (1)–(2) the Cauchy relation $\epsilon_z = \dfrac{\partial u}{\partial z}$ and the equation of the rod vibrations

$$\frac{\partial \sigma_z}{\partial z} = \rho \frac{\partial^2 u}{\partial t^2}, \tag{3}$$

where $u = u(z,t)$ is the longitudinal displacement of the rod, ρ is its density.

The boundary conditions, when the rod is under an acoustic load impedance η_0, are as follows

$$\sigma_z = -\eta_0 \frac{\partial u}{\partial t}, \qquad \Psi = \pm V(t), \qquad z = \pm h. \tag{4}$$

The voltage in the electrodes of the rod is $2V(t)$. It is a known function of time in the problem of "forced" vibrations of the transducer and "unlimited" power from the generator. The system of equations (1)–(4) represents a complete description of "forced" vibrations with ideal excitation, when $2V(t)$ is a harmonic function of time. But $2V(t)$ is the voltage in a real physical circuit and a current

$$i = -\frac{\partial (S_z)}{\partial t}$$

flows through the rod. The current i of the transformer with the rod is related with a current of the generator $i_2 + i_3$ according to the differential equation

$$2V + L\frac{di}{dt} = M\frac{d(i_2 + i_3)}{dt}. \tag{5}$$

For comparison we may present this relation for the case of the absence of the rod, namely

$$L\frac{di}{dt} = M\frac{d(i_2+i_3)}{dt}.$$

So, the presence of the rod in the circuit changes the disturbance to the voltage in every part of the circuit. The addition of a rod is like the addition of some capacity (the input electrical impedance at the rod transducer can be calculated to some approximation from so - called geometrical capacity) [2]. We must have a different value i for the circuit with the transducer as compared with that without it. If i is small and $2V \gg L\frac{di}{dt}$ (in this case, $2V \approx M\frac{d(i_2+i_3)}{dt}$) then we have an ideal excitation of the transducer. When $2V$ is comparable with $L\frac{di}{dt}$, the statement does a given value of $2V(t)$ not hold about, because i will also influence regimes of the generator through a transformer (i influences the current i_2+i_3).

A vacuum-tube generator is the classical example of a self-exciting system [21]. Let us write Kirchhoff's equations for each branch of the tube generator current [13, 15]. First of all we assume, that the generator works in the soft condition, i.e.

$$i_a = I_0 + I_1(e_g + De_a) - I_3(e_g + De_a)^3, \tag{6}$$

where i_a is the anode current, e_g is the tube grid voltage; e_a is the anodic voltage; D is the penetration factor of the tube; I_0, I_1, I_3 are constant parameters of the tube.

The equations of currents of the generator are

$$\begin{gathered} i_a = i_1 + i_2 + i_3, \quad e_a - E_a + R_a i_1 = 0, \quad e_g + E_g - M_c\frac{di_2}{dt} = 0, \\ L_c\frac{di_2}{dt} + R_c i_2 = \frac{1}{C_c}\int i_3\,dt, \\ e_a + L_c\frac{di_2}{dt} + R_c i_2 + L_1\frac{d(i_2+i_3)}{dt} = 0. \end{gathered} \tag{7}$$

The system of equations (6)–(7) describes interior processes in a vacuum-tube generator. These equations are nonlinear with respect to e_g (usually D is a small value), we can reduce them to a single equation. Introducing a new variable

$$\phi(t) = \int_0^t (e_g - E_g)dt \tag{8}$$

(here $-E_g$ is the constant component of the voltage e_g), we obtained the following nonlinear equation for the function ϕ

$$\frac{d^2\phi}{dt^2} + \omega_0^2\phi = a_1\frac{d\phi}{dt} + a_2\left(\frac{d\phi}{dt}\right)^2 - a_3\left(\frac{d\phi}{dt}\right)^3, \tag{9}$$

where

$$a_1 = \frac{M_c}{L_cC_c}\left[I_1 - \frac{R_cR_aC_c - L_c}{R_a(M_c - DL_c)} + \frac{R_cL_1}{R_a^2M_c} - 3I_3(E_g)^2\right], \quad a_2 = 3\frac{M_cI_3E_g}{L_cC_c}, \quad a_3 = \frac{M_cI_3}{L_cC_c}.$$

Besides

$$\omega_0^2 = \frac{R_a + R_k}{R_a L_k C_k}$$

and ω_0 is a frequency of the generator in the linear theory.

If the generator is connected to the electric circuit of the transformer, the last equation of the system (7) changes to the following

$$e_a + L_c \frac{di_2}{dt} + R_c i_2 + L_1 \frac{d(i_2 + i_3)}{dt} = M \frac{di}{dt}. \tag{10}$$

Now for inner processes in the generator a such new equation for the function ϕ should be fulfilled

$$\ddot{\phi} + \omega_0^2 \phi = a_0 \dot{\phi} + a_2 \dot{\phi}^2 - a_3 \dot{\phi}^3 - a_4 V(t), \tag{11}$$

where

$$a_0 = a_1 - \frac{M^2 R_c}{L_c C_c L R_a^2}, \quad a_4 = \frac{2MM_c}{LR_a L_c C_c}.$$

Thus, the operation of the generator and the creation of a voltage $2V(t)$ are described not by the equation (9), but by the system of fourth order equations (11) and (5), where the value of i depends on the mechanical deformations of the rod.

For such deformations and the electric field we have the following system of equations

$$c^2 \frac{\partial^2 u}{\partial z^2} = \frac{\partial^2 u}{\partial t^2}, \quad \frac{\partial^2 \Psi}{\partial z^2} = \frac{k^2}{d_{33}(1-k^2)} \frac{\partial^2 u}{\partial z^2}, \tag{12}$$

where $c = [\rho s_{33}(1-k^2)]^{-1/2}$ is a velocity of longitudinal conjugate waves in the rod; $k = d_{33}(\epsilon_{33} s_{33})^{-1/2}$.

Let's present longitudinal oscillations of the rod in the form of the sum of eigenmodes, namely [22]

$$u(z,t) = \sum_{i=1}^{N} f_i(t) \sin \mu_i z. \tag{13}$$

Here μ_i is a solution of the equation $\mu_i h \cos \mu_i h - k2 \sin \mu_i h = 0$.

In this case for the voltage Ψ we shall have [2]

$$\Psi(z,t) = f(t) z + \frac{k^2}{d_{33}(1-k^2)} \sum_{i=1}^{N} f_i(t) \sin \mu_i z. \tag{14}$$

Thus the current i, flowing through the rod is equal to

$$i = -\frac{\partial (S D_z)}{\partial t} = S\epsilon_{33}(1-k^2)\dot{f} = S\epsilon_{33} \frac{(1-k^2)}{h} \left[\dot{V} - \frac{k^2}{d_{33}(1-k^2)} \sum_{i=1}^{N} \dot{f}_i \sin \mu_i h \right]. \tag{15}$$

Using boundary conditions (4), we obtain the following relations for eigenmodes of oscillations

$$-\frac{s_{33} h \eta_0}{d_{33}} \sum_{i=1}^{N} \dot{f}_i(t) \sin \mu_i h = V(t) \tag{16}$$

and

$$i = \frac{S\epsilon_{33}(1-k^2)}{h} \dot{V}(t) + \frac{\epsilon_{33} k^2}{h^2 \eta_0} V(t). \tag{17}$$

Substituting these expressions in (5), we find that voltage $2V(t)$, applied to the electrodes of the transducer should be determined as the solution of the system of equations

$$\begin{aligned} \ddot{\phi} + \omega_0^2\phi &= a_1\dot{\phi} + a_2\dot{\phi}^2 - a_3\dot{\phi}^3 - a_4V(t), \\ \ddot{V}(t) + \omega_1^2V(t) &= a_5\phi + a_6\dot{\phi} - a_7\dot{V}(t). \end{aligned} \tag{18}$$

Here

$$\omega_1^2 = \frac{2h}{LS\epsilon_{33}(1-k^2)}, \quad a_5 = -\frac{M\omega_1^2R_c(R_a+R_c)}{2M_cR_aL_c}, \quad a_6 = -\frac{M\omega_1^2R_c}{2M_cR_a}, \quad a_7 = \frac{k^2}{\eta_0hS(1-k^2)}.$$

After the determination of $V(t)$, longitudinal oscillations of the rod $u(t) = \sum_{i=1}^{N} f_i(t)\sin\mu_i z$ are defined by the following equation

$$\frac{\partial^2u}{\partial t^2} = c^2\frac{\partial^2u}{\partial z^2} - \frac{d_{33}}{s_{33}h\rho}V(t)\delta(z-h) + \frac{d_{33}}{s_{33}h\rho}V(t)\delta(z+h), \tag{19}$$

where $\delta(z)$ is the delta-function.

If we neglect the inverse influence of transducer oscillations (mechanical and electrical) on functioning of the generator ($a_4 = 0$), in other words, if we neglect the effect of Sommerfeld - Kononenko, the system of equations (18) breaks up into two equations, each of which has dimension of a phase space equal to two. First of them is the self-exciting equation and can be solved irrespectively of the second. The second equation, featuring vibrational processes in the rod, is linear. In this case possible attractors of the system of equations (18) always are the regular one. Therefore, in this situation functioning of the generator and radiation of waves by the transducer in acoustic medium correspond to regular (probably complex enough) processes.

If $a_4 \neq 0$, dimension of a phase space of the equation system (18) is equal to four. In this case in the system both regular, and chaotic attractors can exist [14, 21, 20]. Thus, the basic possibility of existence of chaotic regimes in the generator and excitation of chaotic waves in acoustic medium is caused by the effect of Sommerfeld–Kononenko.

3 Investigation of the steady-state regimes of interaction

For determination of the possible steady-state regimes of interaction in the system (18) we use the dimensionless variables

$$\xi = \frac{\phi\omega_0}{E_g}, \quad \frac{d\xi}{d\tau} = \zeta, \quad \beta = \frac{V}{E_g}, \quad \frac{d\beta}{d\tau} = \gamma, \quad \tau = \omega_0 t. \tag{20}$$

Then the system of equations (18) can be written in the form

$$\begin{aligned} \frac{d\xi}{d\tau} &= \zeta, \quad \frac{d\zeta}{d\tau} = -\xi + \alpha_1\zeta + \alpha_2\zeta^2 - \alpha_3\zeta^3 + \alpha_4\beta, \\ \frac{d\beta}{d\tau} &= \gamma, \quad \frac{d\gamma}{d\tau} = \alpha_5\xi + \alpha_6\zeta - \alpha_0\beta - \alpha_7\gamma, \end{aligned} \tag{21}$$

where the coefficients are equal to

$$\begin{aligned} \alpha_0 = \frac{\omega_1^2}{\omega_0^2}, \quad \alpha_1 = \frac{a_0}{\omega_0}, \quad \alpha_2 = \frac{a_2E_g}{\omega_0}, \quad \alpha_3 = \frac{a_3E_g^2}{\omega_0}, \\ \alpha_4 = -\frac{a_4}{\omega_0}, \quad \alpha_5 = \frac{a_5}{\omega_0^3}, \quad \alpha_6 = \frac{a_6}{\omega_0^2}, \quad \alpha_7 = \frac{a_7}{\omega_0}. \end{aligned}$$

First of all we investigate equilibrium states of the system (21). All of them are defined as solutions of non-linear algebraic coupled equations

$$\begin{aligned} &\zeta = 0, \quad -\xi + \alpha_1\zeta + \alpha_2\zeta_2 - \alpha_3\zeta_3 + \alpha_4\beta = 0, \\ &\gamma = 0, \quad \alpha_5\xi + \alpha_6\zeta - \alpha_0\beta - \alpha_7\gamma = 0. \end{aligned} \tag{22}$$

At realization of the requirement $\alpha_0 = \alpha_4\alpha_5$ this system has the infinite set of solutions which are defined by the formulas

$$\zeta = 0, \quad \xi = \alpha_4\beta, \quad \gamma = 0, \quad \beta = r,$$

where r is any real number not equal to zero. At realization of the requirement

$$\alpha_0 \neq \alpha_4\alpha_5 \tag{23}$$

the system (22) has the single trivial solution $\xi = 0, \quad \zeta = 0, \quad \beta = 0, \quad \gamma = 0$. This solution corresponds to the zero equilibrium state, which at realization of a requirement (23), will be a single equilibrium state of the system.

According to the criterion of Hurwitz, sufficient conditions for asymptotic stability of a zero equilibrium state can be written in the form

$$\alpha_7 - \alpha_1 > 0, \tag{24}$$

$$1 + \alpha_0 - \alpha_1\alpha_7 > 0, \tag{25}$$

$$\alpha_7 - \alpha_4\alpha_6 - \alpha_0\alpha_1 > 0, \tag{26}$$

$$\alpha_6 - \alpha_4\alpha_5 > 0, \tag{27}$$

$$\begin{aligned} &(\alpha_7 - \alpha_1)(1 + \alpha_0 - \alpha_1\alpha_7)(\alpha_7 - \alpha_4\alpha_6 - \alpha_0\alpha_1) \\ &\quad - (\alpha_7 - \alpha_4\alpha_6 - \alpha_0\alpha_1)^2 - (\alpha_7 - \alpha_1)^2(\alpha_6 - \alpha_4\alpha_5) > 0. \end{aligned} \tag{28}$$

Thus, at realization of the requirement (23) and not realization of at least one of inequalities (24)–(28) single equilibrium state of system (21) is unstable. In this case all trajectories of the system starting from a neighborhood of an origin of coordinate phase spaces, eventually abandon this neighborhood and due to dissipativity of the system, aspire to some limiting sets — attractors, which, as we shall see in the following, can be both regular and chaotic.

As the system of equations (21) is a non-linear system of the fourth order differential equations, all its further examinations will be done by means of numerical methods. The basic method of determination of solutions of the system (21) is the fourth or fifth order method of Runge–Kutta with the application of correcting procedure of Dormand–Prince [9], which ensures precision of the order $O(10^{-8})$ – $O(10^{-15})$. In the construction of phase portraits of the steady-state regimes the special attention was given to non-admission of their contortions by trajectories of transients process. For calculation of a spectrum of Lyapunov characteristic exponents (LCE) of attractors the algorithm of Benettin, etc. [4, 14, 21, 11] was applied. The influence of atypical trajectories on quantities of Lyapunov characteristic exponents was excluded. For construction of the Poincaré sections and mappings for attractors of the system the method of Hénon [10, 14] was applied, and for calculation of spectral densities the method of Filon was used [7].

Extensive numerical experiments were carried out with the purpose of finding the regions of exsistence of chaotic solutions. We assume that the generator works with the

following parameters:

$$\begin{gathered} E_g = 700V, \quad E_a = 2000V, \quad I_1 = 6.5 \times 10{-}5A/V, \quad I_3 = 5.184 \times X{\times}10{-}9A/V3, \\ D = 0.015, \quad R_a = 160\Omega, \quad R_c = 10\Omega, \quad L_c = 0.094H, \\ C_c = 1.0465\, mmF, \quad M_c = 0.275H, \quad M = 1H, \quad L = 100H. \end{gathered} \tag{29}$$

Here X is the dimensionless bifurcation parameter.

In this case the coefficients of system (21) are equal to

$$\begin{gathered} \alpha_0 = 0.995, \quad \alpha_1 = 0.0535, \quad \alpha_2 = 0.63 \times X, \quad \alpha_3 = 0.21 \times X, \\ \alpha_4 = -0.103, \quad \alpha_5 = -0.0604, \quad \alpha_6 = -0.12, \quad \alpha_7 = 0.01. \end{gathered} \tag{30}$$

We want to underline especially, that the values of parameters in formulas (29 - 30) correspond to real characteristics of LC-generators and piezoceramic transducers [2, 28]. For the chosen parameters of the system (21) it has a single zero equilibrium state which is unstable in the sense of Lyapunov.

Let's determine divergence ($\operatorname{div} F$) of the system (21). It is obvious, that it can be found using the formula

$$\operatorname{div} F = \alpha_1 + 2\alpha_2\zeta - 3\alpha_3\zeta^2 - \alpha_7. \tag{31}$$

As is seen from the formula (31) in a general case divergence will be a sign-alternating quantity. Taking into account parameters of system (30) it is possible to write the expression for divergence as

$$\operatorname{div} F = 0.63X\zeta(2 - \zeta) + 0.0435. \tag{32}$$

If the parameter X is positive then, up to 0.0435, divergence of system will be positive during those moments of time, when the phase variable ζ satisfies the inequality $2 > \zeta > 0$. Therefore, in cotrast to systems with a constant negative divergence, the question about local change in time of the phase volume of the system near a particular solution demands additional explanations. As is known [1], the given phase volume changes in time according to the expression

$$V(t) = V(t_0)e^{(\overline{\operatorname{div} F})t} = V(t_0)e^{(\lambda_1+\lambda_2+\lambda_3+\lambda_4)t}, \tag{33}$$

where $V(t)$ is the phase volume, λ_i is a Lyapunov characteristic exponent of an attractor, and in expression $\overline{\operatorname{div} F}$ the line denotes averaging in time. The carried out calculations have shown that the sum of Lyapunov characteristic exponents for all (examined further in the article) regular and chaotic attractors of system (21) will be negative. Therefore, negative will be averaged in time divergence of the system, though at some intervals of time it can be positive. It means, that all attractors of the systems (21) have zero limiting volumes.

Let's consider the bifurcations which are taking place in the system (21), when the parameter X is changing. We shall give special attention to the origin of chaotic attractors, their detailed exposition and scenarios of transitions from the regular regimes to the chaotic one. As is known, the basic practical criterion of existence of a chaotic attractor is the presence in a spectrum of LCE of at least one of the positive exponent [21, 14]. In Figure 3.1 a dependence of the maximal, distinct from zero, Lyapunov characteristic exponent on the parameter X is shown. Referring to Figure 3.1, there is a series

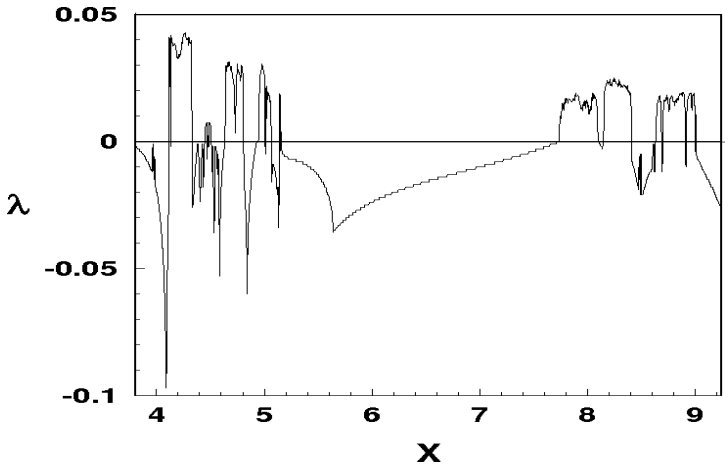

Figure 3.1: Dependence of the maximal Lyapunov characteristic exponent λ on X.

of X intervals in which the maximal Lyapunov exponent is positive. Hence, in these intervals there are chaotic attractors. Intersection points of this diagram with horizontal coordinate axis correspond to bifurcation values of parameter X.

In Figure 3.2 the phase-parametric characteristic of system (so-called bifurcation tree) is given. This characteristic is constructed as a function of coordinate ξ. Phase-parametric characteristics regarding other coordinates of the system are qualitatively similar to given in Figure 3.2. The light sites of this tree "crone" correspond to periodic regimes of the steady-state oscillations of the system (21), and densely blacked out - to chaotic. Points of a bifurcation, at which transition from regular periodic regime to the nonregular chaotic one occurs are precisely visible.

Let's now consider these changes of regimes in more details. At changing of the parameter X value in a segment $9.3 \geq X \geq 9.01$ in the system there is a stable limit cycle with the signature of a LCE spectrum which looks like ("0″, " −″, " −″, " −″). That is, the maximal Lyapunov exponent of the cycle is zero, and three others are negative. A three-dimensional projection of the phase portrait of this cycle, its Poincaré section by the plane $\beta = 0$ and the spectral density constructed in logarithmic scale, are given, accordingly, in Figure 3.3.a-b, Figure 3.4.a. The given figures are constructed at the value $X = 9.01$. Poincaré section and the spectral density have a structure typical for the regular regimes. A signal sent by the transducer to the medium in this case is periodic.

At $X = 9.005$ instead of a limit cycle as a result a saddle-knot or the tangential bifurcation a chaotic attractor arises in the system. In the signature of the LCE spectrum of the attractor the positive maximal exponent appears and it becomes: (" +″, "0″, " −″, " −″). In Figures 3.4.b, 3.5.a-b, 3.6.a the three-dimensional projection of the attractor phase portrait , its Poincaré section and mapping and the spectral density (Fourier spectrum) constructed at the value $X = 8.955$ are given, accordingly. Transition from the regular attractor to chaotic is carried out through an intermittency of the first type in the sense of Pomeau–Manneville [5]. When we move to a point of a bifurcation, the unstable cycle comes nearer to the limit cycle. In a point of bifurcations both cycles merge and disappear. Trajectories of system leave for remote fields of a

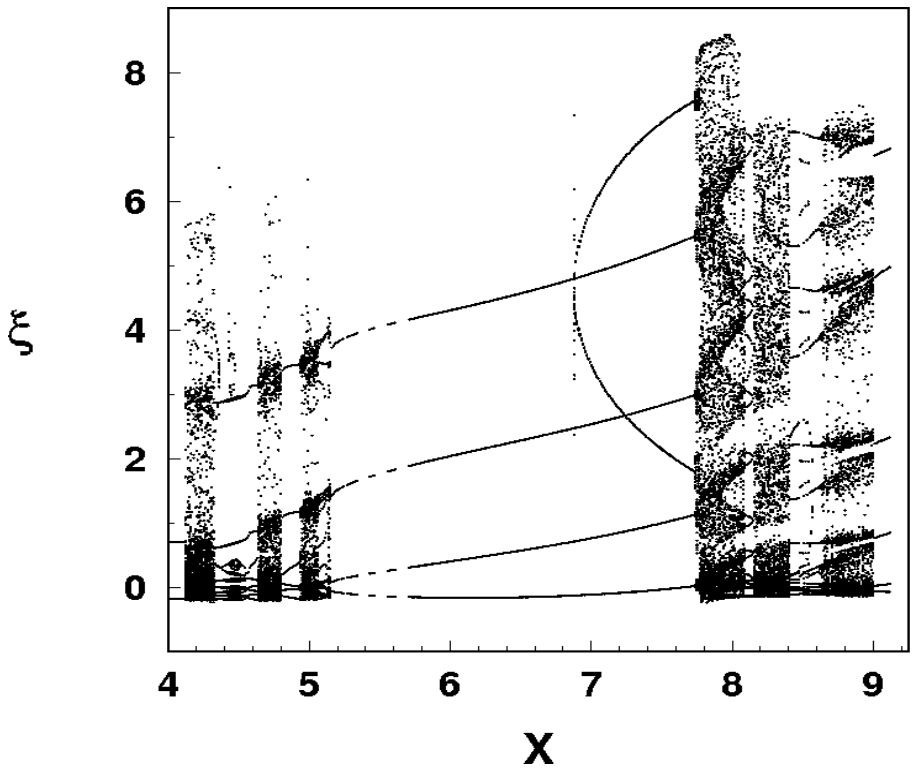

Figure 3.2: Phase-parametric characteristic of the system.

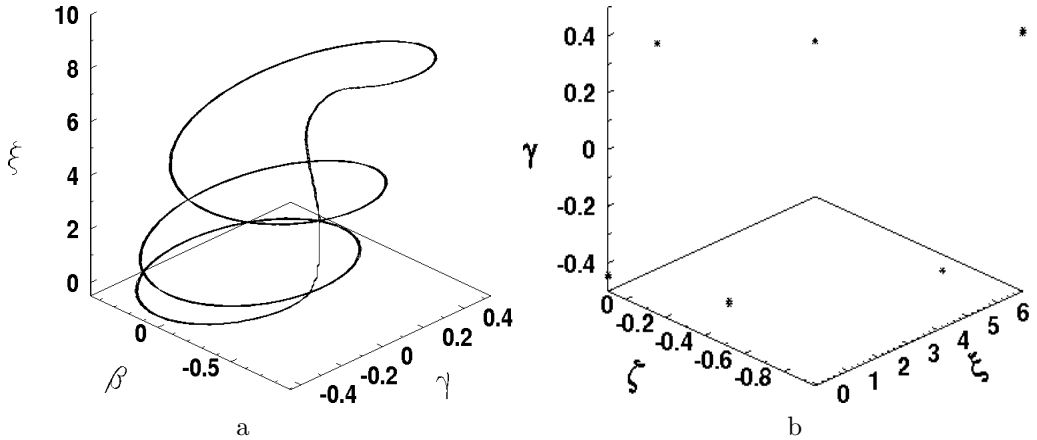

Figure 3.3: Projection of the phase portrait *(a)* and Poincaré section by the plane $\beta = 0$ *(b)* at $X = 9.01$.

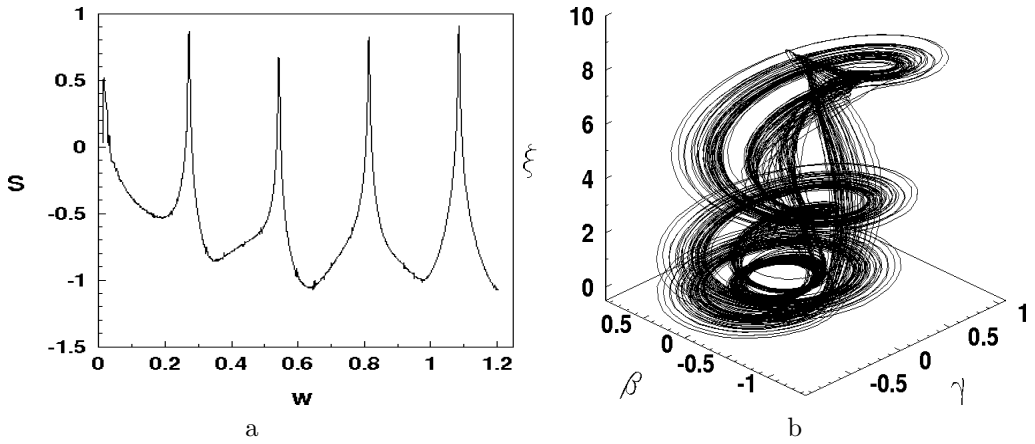

Figure 3.4: Spectral density at $X = 9.01$ *(a)* and the projection of the phase portrait at $X = 8.955$ *(b)*.

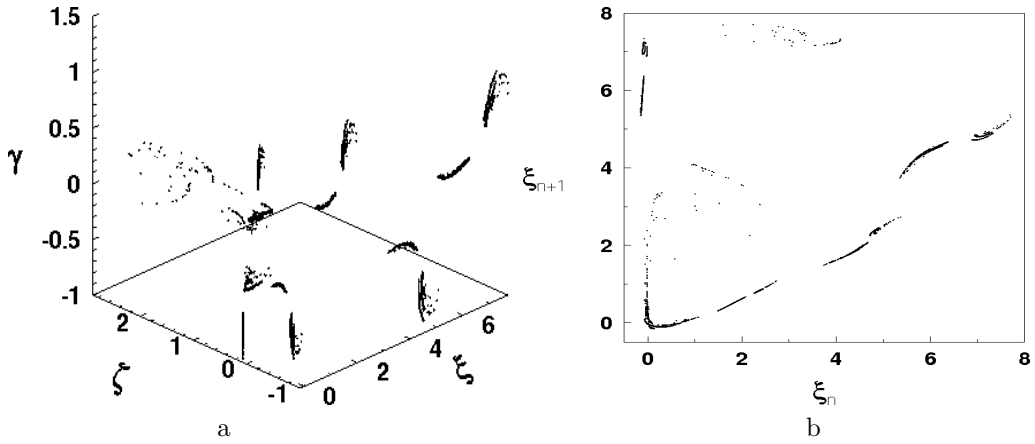

Figure 3.5: Poincaré section by the plane $\beta = 0$ *(a)* and mapping *(b)* at $X = 8.955$.

phase space. Then, because the system (21) is stable in the sense of Lagrange (by its dissipativity) and in the sense of Poisson (as a regime is steady-state) and is unstable in the sense of Lyapunov (a positive Lyapunov exponent exists), a process of reinjections happens, when returnings of trajectories to neighborhood of the vanished limit cycle happen, then again they leave and return end so on. Laminar phase of this intermittency is the motion in enough small neighborhood of the vanished limit cycle, and turbulent phase is unpredictable roamings around the coils of a spiral chaotic attractor (see Figure 3.4.b). Transition to chaos through an intermittency is also testified by the structure of a bifurcation tree in a neighbourhood of the point $X = 9.01$.

Poincaré section and mapping represent some chaotic point sets, which are grouped inside of several domains having quasiribbon structure. The view of Poincaré mapping shows, that the system (21) can be roughly enough approximated by means of the one-dimensional mapping that will essentially simplify its investigation. The view of this mapping (which can be substituted by a set of one-dimensional parabolic and horseshoe-

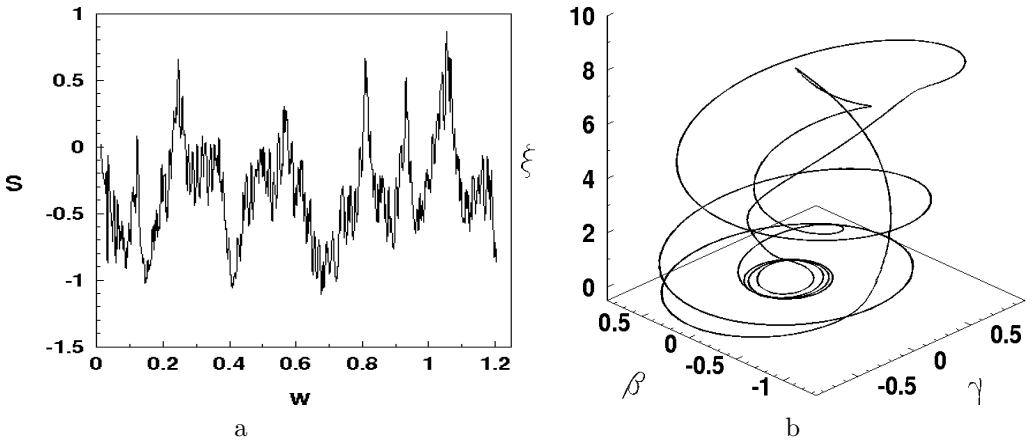

a b

Figure 3.6: Spectral density at $X = 8.955$ *(a)* and a projection of a phase portrait at $X = 8.41$ *(b)*.

shaped lines) is one more proof that the system has a chaotic regime [14]. A spectrum of an attractor is continuous, but with apparent enough peaks. A continuity of Fourier spectrum also testifies a chaotic character of the given attractor. Chaotic attractors of such type exist in the system (21) at $9.005 \geq X \geq 8.645$. A signal generated by the transducer to the medium at such X will be chaotic.

Now consider several types of the attractors existing in the system (21). At $8.645 > X \geq 8.41$ a stable limit cycle exists in the system. A projection of a phase portrait of such cycle is given in Figure 3.6.b. This cycle has more complex structure, than the cycle given in Figure 3.3.a. Besides it has approximately six times larger period, than a cycle given in Figure 3.3.a. At the value $X \simeq 8.405$ this cycle disappears, due to a tangent bifurcation, and the chaotic attractor of new type is born (whose projection of the phase portrait is constructed at value $X = 8.25$ and is given in Figure 3.7.a). Transition from the regular attractor to the chaotic one, as before, is carried out through the first type intermittency in the sense of Pomeau–Manneville according to the described above scenario. However, unlike the previous described chaotic attractor (Figure 3.4.b), here we have a more continuous covering by turbulent splashes of an attractor trajectories of its phase volume. The signature of the LCE spectrum of this chaotic attractor looks like: ("+", "0", "−", "−").

In Figure 3.7.b Poincaré section of this attractor is shown. It represents a chaotic point set the number of which constantly increases with the time of numerical integration time of the system. However for this type of chaotic attractors its Poincaré section loses quasiribbon structure.

In Figure 3.8.a one more important characteristic of chaotic attractors is shown, namely a distribution of an invariant measure of Krylov–Bogolyubov on the attractor phase portrait. The given figure is constructed by so-called technique of coding by grey color tones as stated in [14]. The invariant measure is a quantitative characteristic of the residence time of a representation point of attractor trajectories in the given region of the phase volume. More dark parts in the figure correspond to regions in which representation point of trajectories spends a majority of time. As is apparentl from Figure 3.8.a, the trajectories spend the largest part of time in the neighborhoods of

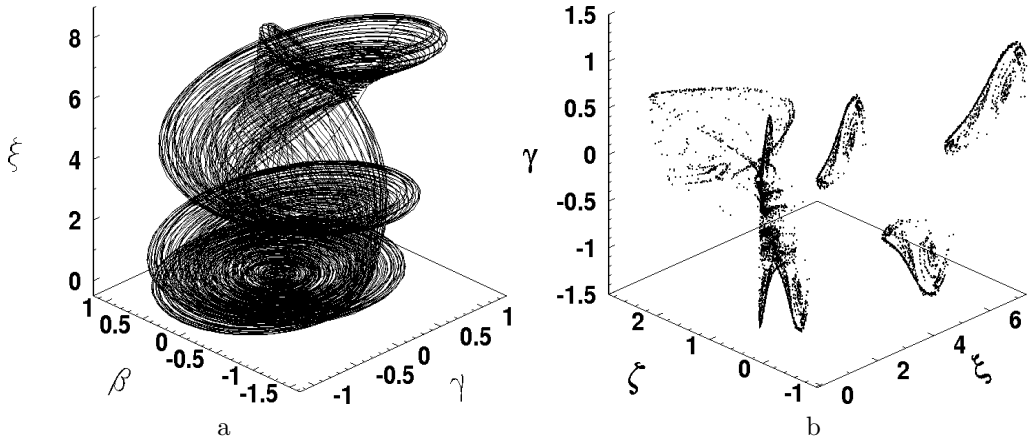

Figure 3.7: Projection of the phase portrait *(a)* and Poincaré section by the plane $\beta = 0$ *(b)* at $X = 8.25$.

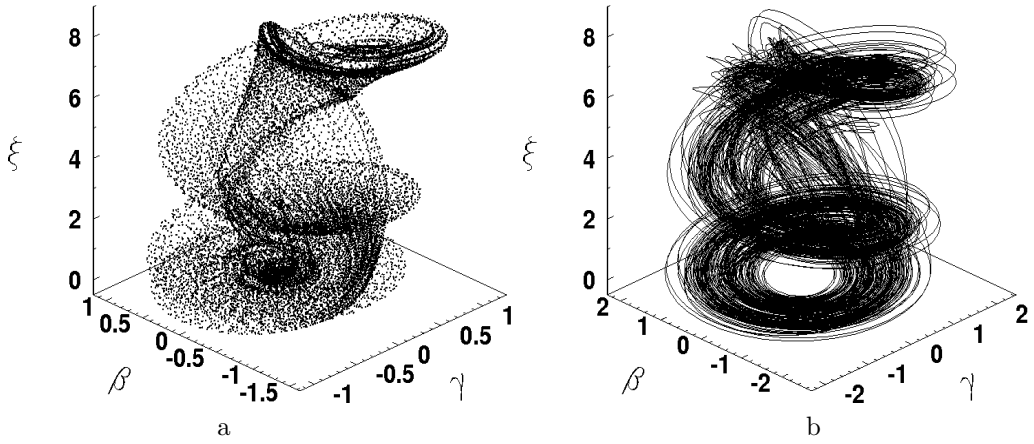

Figure 3.8: Distribution of an invariant measure at $X = 8.25$ *(a)* and projection of the phase portrait at $X = 7.85$ *(b)*.

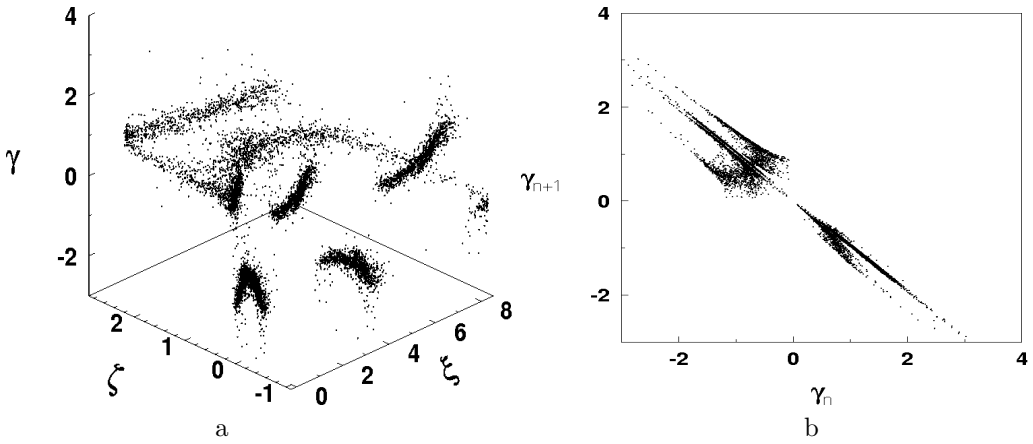

Figure 3.9: Poincaré section by the plane $\beta = 0$ *(a)* and mapping *(b)* at $X = 7.85$.

the vanished limit cycle that is the testimony of larger duration of laminar phases in comparison with the turbulent ones. Moreover, this figure is one more verification of realization of the intermittency scenario at transition from the regular regime to chaotic.

At the value $X = 7.86$ an extremely interesting bifurcation of a type "chaos–chaos" happens, when as a result of the complex mechanisms of interactions of a chaotic attractor with the saddle limiting cycles existing in pool of its attraction, in the system (21) an attractor arises whose signature of LCE spectrum looks like ("+", "+", "0", "−"). This attractor has two positive Lyapunov exponents. Such attractor is called hyper-chaotic [14]. Such type attractors exist only in dynamic systems, dimensionality of which in phase space is more or equal to four, and are characterized by the presence in LCE spectrum of not less than two positive Lyapunov exponents. Presence of two positive exponents indicates the existence in a phase space of two directions in which the close phase trajectories of an attractor diverge. All above-considered chaotic attractors have only one direction of divergence of the close phase trajectories. In Figure 3.8.b the projection of a phase portrait of a hyper-chaotic attractor is shown for $X = 7.85$. A phase portrait of such attractor has a "hole" in its lower ring spirals.

In Figures 3.9.a-b the Poincaré section and mapping of a hyper-chaotic attractor are shown. As can be seen the observed structures have more complicated chaotic point sets than those in (Figures 3.5.a-b and Figure 3.7.b). The one-dimensional approximation of mapping of Poincaré ia out of the question. Further in Figures 3.10.a-b the distribution of invariant Krylov-Bogolyubov's measure and the spectral density of the hyper-chaotic attractor are given, accordingly. As is apparent from Figure 3.10.a, now the hyper-chaotic attractor possesses more uniform distribution of invariant measure than the attractor existing at $X = 8.25$. Distribution of the spectral density of the hyper-chaotic attractor is , as before, continuous, however in it separate peaks practically disappear. Hyper-chaotic attractors exist in rather small interval of changing of the parameter X, namely, $7.86 \geq X \geq 7.745$. At the further decreasing of X they disappear and in the system a stable limit cycle arises again.

As can be seen in Figure 3.1, there are some more intervals of the parameter X changing in which chaotic attractors exist. The further examinations made possible to find out still some more transitions from the regular motions to chaotic through

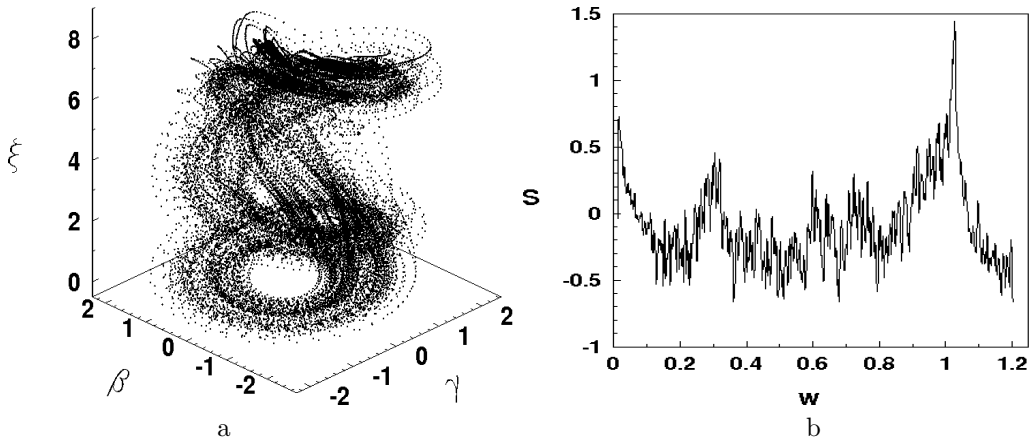

Figure 3.10: Distribution of an invariant measure *(a)* and a spectral density *(b)* at $X = 7.85$.

intermittency. Besides, transitions to chaos have been discovered through cascade of bifurcations of doubling of a period [6].

Let's consider one more type of the chaotic attractor discovered in system (21). Attractors of such type exist in system at $4.325 \geq X \geq 4.115$. Transition from the regular condition to chaotic here, as well as in several previous cases, is carried out under the scenario of an intermittency of the first type. The signature of LCE spectrum of such attractor looks like: (" $+''$, "$0''$, " $-''$, " $-''$). In Figures 3.11.a-b, 3.12.a-b the three-dimensional projection of the attractor phase portrait, its Poincaré section by the plane $\beta = 0$, Poincaré mapping and a spectral density constructed at the value $X = 4.255$are shown respectively . As can be seen from these figures, the phase portrait of a chaotic attractor has varied noticeably, on which merging of rings of its spirals has happened. Amplitudes of oscillations of phase variables have decreased. But, at the same time, as is apparent from Figure 3.1, the maximal Lyapunov characteristic exponent for this attractor is approximately twice as large as corresponding exponents for the above chaotic attractors. It testifies to much greater velocity of divergence of the close phase trajectories. Disposition of points in Poincaré cross-section has considerably varied, however, it is still some chaotic point set. Mapping of coordinate ξ vaguely resemble corresponding mapping, given in Figure 3.5.b, however, a disposition of points on mapping, given in Figure 3.12.a, testifies about impossibility of any one-dimensional approximation in this case. Fourier spectrum of an attractor (Figure 3.12.b) has continuous structure and is characterised by the absence of peaks.

The comparative analysis of behaviour of the system "generator – transducer" in the case of an ideal excitation, when we neglect influence of a transducer on functioning of the generator, attracts a significant interest. This is the case of zero coefficient α_4 in the system of equations (21). In Figure 3.13.a-b phase portraits are given for attractors of the systems (21) constructed at $\alpha_4 = 0$, $X = 8.25$ (Figure 3.13.a) and $\alpha_4 = 0$, $X = 7.85$ (Figure 3.13.b). In both cases attractors of system are limit cycles. Meanwhile under the nonideal excitation, which always takes place by virtue of the law of conservation of energy, the system will be in chaotic (at $X = 8.25$) or in hyper-chaotic (at $X = 7.85$) regimes. Moreover, the case of an ideal excitation is characterised by appreciable diminution of vibration amplitudes of phase variables, especially of the variables

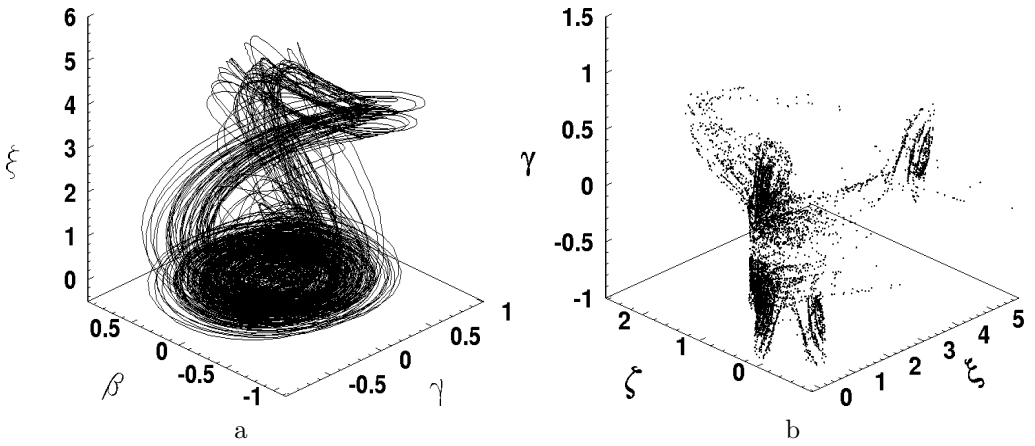

Figure 3.11: Projection of a phase portrait *(a)* and Poincaré section by the plane $\beta = 0$ *(b)* at $X = 4.255$.

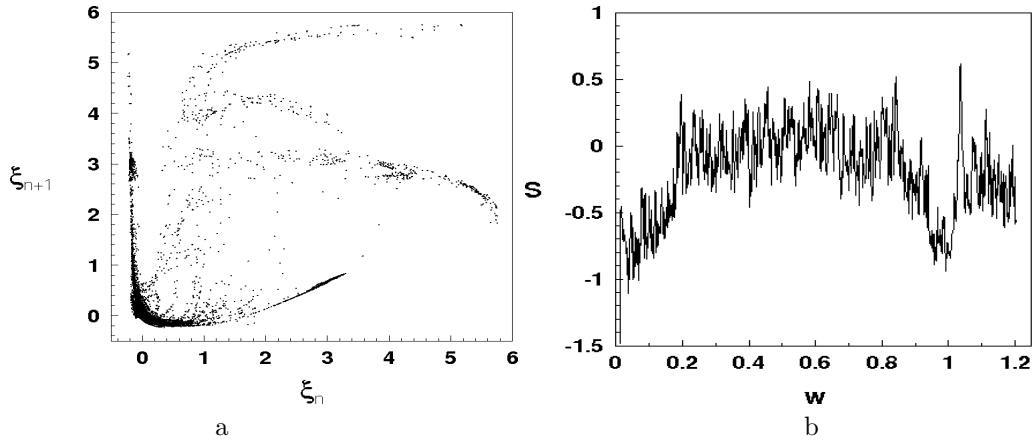

Figure 3.12: Poincaré mapping *(a)* and spectral density *(b)* at $X = 4.255$.

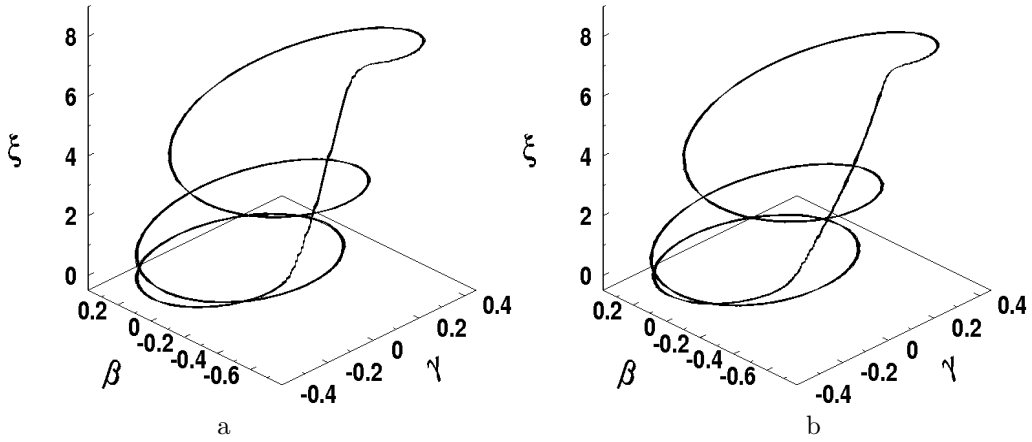

Figure 3.13: Projection of a phase portrait at $X = 8.25$, $\alpha_4 = 0$ *(a)* and projection of a phase portrait at $X = 7.85$, $\alpha_4 = 0$ *(b)*.

β, γ which describe oscillations of the transducer. Thus, the neglection of nonidealness of excitation leads to the significant errors in exposition of process of interaction of transducer and generator both quantitative, and, what is more essential, qualitative. For example, instead of expected periodic regimes of interaction the system actually will be in a hyper-chaotic regime.

Further an examination of the bifurcations which are taking place at a changing of parameter α_4 (which, as it has just been noted, characterizes interaction between transducer and generator) has been carried out. In the computer experiments values of parameters of system were defined by formulas (30) except for the parameter α_4 which was taken as bifurcation one and was variable. For parameter X it was supposed, that $X = 7.82$. Such value of parameter X previously corresponded to the case of hyper-chaos in the system.

In Figure 3.14 dependence of the maximal, distinct from zero, Lyapunov characteristic exponent of the system λ on the values α_4 is given. As is apparent from the figure, there are intervals of α_4 in which values of λ will be positive. In these intervals the system has chaotic attractors. At $\alpha_4 = 0$ the system (21) has stable limited cycle, whose phase portrait practically coincides with phase portrait of a cycle given in Figure 3.13.b. However, already at very small changing of α_4 value, namely at $\alpha_4 = -0.004$, the maximal Lyapunov characteristic exponent becomes positive, that testifies about origin of the chaotic attractor. As we see, even very small interaction between subsystems, the generator and the transducer, leads to occurrence of chaos.

Let's consider the bifurcations happening in the system (21) at increasing of α_4. At $\alpha_4 = -0.138$ in system a stable limit cycle exists. Further, at increase of value α_4, on very small interval $(-0.138, -0.13515)$ in the system there is a cascade of bifurcations of period doubling, which comes to an end with origin of a chaotic attractor at $\alpha_4 = -0.1351$. A projection of a phase portrait of this attractor, its Poincaré section and mapping, and also distribution of the spectral density, constructed at $\alpha_4 = -0.135$, are given respectively in Figures 3.15.a–b, 3.16a–b.

Here the transition from the regular regime to chaotic here is carried out in correspondence with Feigenbaum's scenario [6]. We would like to emphasize, that this attractor is

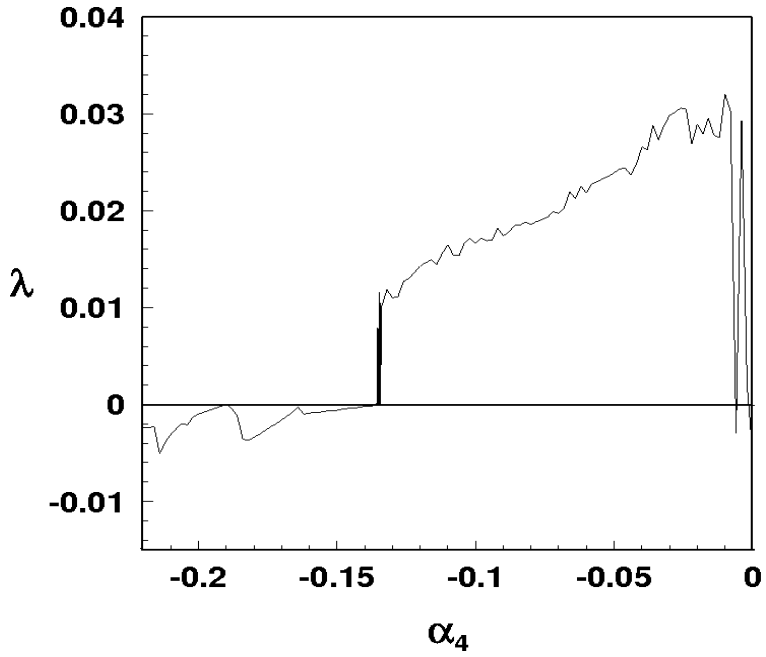

Figure 3.14: Dependence of the maximal Lyapunov characteristic exponent λ on the parameter α_4.

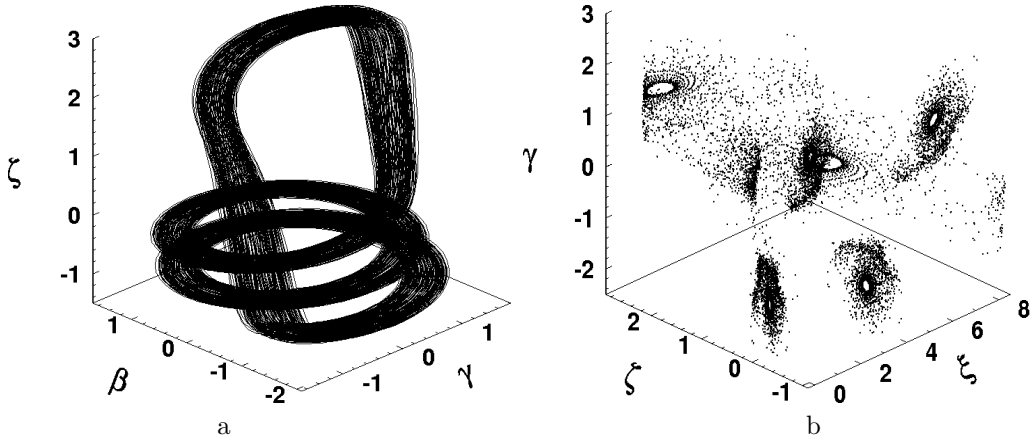

Figure 3.15: Projection of a phase portrait *(a)* and Poincaré section by the plane $\beta = 0$ *(b)* at $\alpha_4 = -0.135$.

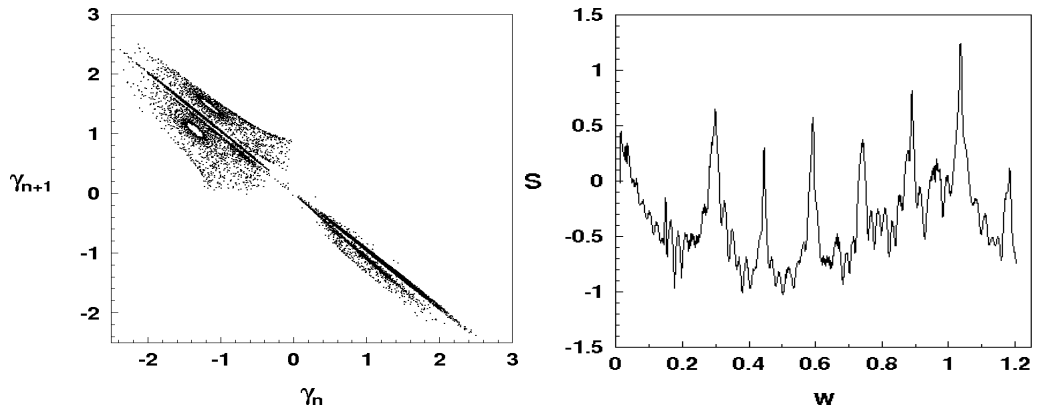

Figure 3.16: Mapping *(a)* and spectral density *(b)* at $\alpha_4 = -0.135$.

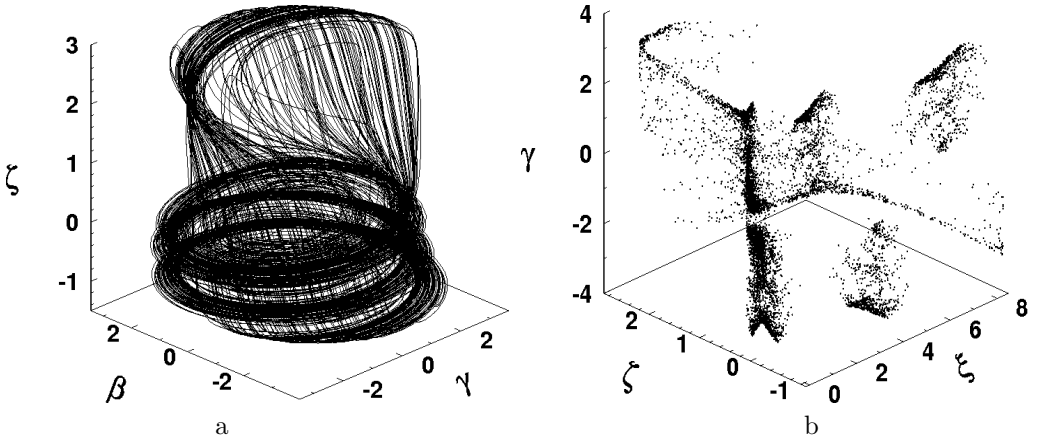

Figure 3.17: Projection of a phase portrait *(a)* and Poincaré section by the plane $\beta = 0$ *(b)* at $\alpha_4 = -0.025$.

hyper-chaotic as it has two positive Lyapunov characteristic exponents. Phase portrait of this attractor noticeably differs from the hyper-chaotic attractor considered above. At the same time Poincaré section and mapping possess some qualitative simularity with the cases of hyper-chaos shown in Figure 3.9 a–b. Essential differences are found in Fourier spectrum of the given attractor. It is continuous, but, at the same time, the spectrum peaks are precisely pronounced. They are "the memories" about harmonics of vanished limit cycles. This the hyper-chaotic attractor exists in system in the very small interval $(-0.1351, -0.1348)$ of α_4. Then in the system there is "a window of periodicity" which again is replaced by hyper-chaotic attractor at $\alpha_4 = -0.1344$. Arising attractor is qualitatively similar to a hyper-chaotic attractor, given in Figure 3.8.b. Further increase of α_4 leads to the bifurcation "hyper-chaos — chaos", as a result of which, at $\alpha_4 = -0.058$, a chaotic attractor arises. The signature of LCE spectrum of given attractor looks like: ("+", "0", "−", "−"). In Figure 3.17.a a projection of a phase portrait and Poincaré section of attractors of this type constructed at value $\alpha_4 = -0.025$ are given, accordingly. Chaotic attractors similar to that given in Figure 3.17 exist in the system (21) at $-0.058 \leq \alpha_4 \leq -0.004$. Then, at $\alpha_4 > -0.004$, the regular attractor — a limit cycle arises again in the system.

4 Conclusion

Thus, in the present work a series of new effects has been discovered, caused by process of interaction of oscillation regimes in piezoceramic transducer and setting electric generator, and obtained on the basis of the constructed new mathematical model.

In the given deterministic system some types of chaotic attractors were revealed, including the hyper-chaotic one. It is shown, that the system possesses a significant variety of existing in it steady-state regimes of interaction, their properties, and also scenarious of transition from the regular conditions to chaotic. It was established that existence of the deterministic chaos in the system is caused only by interaction between subsystems (generator and transducer), instead of their independent properties.

These effects are applicable at the analysis of the regular and chaotic regimes of functioning of electrodynamic, electromagnetic and piezoceramic vibrators with the limited excitation.

Acknowledgments

The authors are very grateful to Prof. A.M. Samoilenko for extensive discussions and illuminative conversations.

References

[1] Anishchenko, V.S., Astakhov, V.V, Nieman, A.B, Vadivasova, T.E. and Schimansky–Geier, L. *Nonlinear Dynamics of Chaotic and Stochastic Systems*. Springer, Berlin, 2003.

[2] Auld, B.A. *Acoustic Fields and Waves in Solids*. John Wiley & Sons, New York, 1973.

[3] Bazenov, V.M. and Ulitko, A.F. Examination dynamic behaviour of a piezoceramic stratum at instantaneous electrical loading. *Appl. Mech.* **11**(1) (1975) 22–27. [Russian]

[4] Benettin, G., Galgani, L., Strelcyn, J.M. Kolmogorov entropy and numerical experiments. *Phys. Rev. A*. **14** (1976) 2338–2342.

[5] Berge, P., Pomeau, Y. and Vidal, C.H. *Order within chaos.* John Wiley & Sons, New York, 1984.

[6] Feigenbaum, M.J. Quantative universality for a class of nonlinear transformations. *J. Stat. Phys.* **19**(1) (1978) 25–52.

[7] Filon, L.N.G. On a quadrature formula for trigonometric integrals. *Proc. R. Soc. Edinburgh* **49** (1929) 38–47.

[8] Grinchenko, V.T., Ulitko, A.F. and Shulga N.A. *Electroelasticity.* Naukova Dumka, Kiev, 1989. [Russian]

[9] Hairer, E., Norsett, S.P. and Wanner, G. *Solving ordinary differential equations. Nonstiff problems.* Springer–Verlag, Berlin, 1987.

[10] Hénon, M. On the numerical computation of Poincaré maps. *Physica. D.* **5** (1982) 412–415.

[11] Khaki–Sedigh, A., Ataei, M., Lohmann, B. and Lucas, C. Adaptive Calculation of Lyapunov Exponents from Time Series Observations of Chaotic Time Varying Dynamical Systems. *Nonlinear Dynamics and Systems Theory* **4** (2004) 145–159.

[12] Kononenko, V.O. *Vibrating systems with a limited power supply.* Iliffe Books, London, 1969.

[13] Kononenko, V.O. and Krasnopolskaya, T.S. The vacuum tube generator in to system of excitation of mechanical oscillations. *Vibrotechnics* **28** (4) (1977) 105–120. [Russian]

[14] Kouznetsov, S.P. *Dynamic chaos.* Physmatlit, Moscow, 2001. [Russian]

[15] Krasnopolskaya, T.S. Independent excitation mechanical oscillations by the electrodynamic vibrator. *Sov. Appl. Mech.* **13**(2) (1977) 108–113.

[16] Krasnopolskaya, T.S. and Shvets, A.Yu. Chaos in dynamics of machines with a limited power-supply. In: *8-th World Congr. on the theory of machines and mechanisms.* Prague: Czechoslovak Acad. Sci., Vol. 1, 1991, 181–184.

[17] Krasnopolskaya, T.S. and Shvets, A.Yu. Chaos in vibrating systems with limited power-supply. *Chaos* **3** (1993) 387–395.

[18] Krasnopolskaya, T.S. and Shvets, A.Yu. Chaotic surface waves in limited power-supply cylindrical tank vibrations. *J. Fluids and Structures* **8** (1994) 1–18.

[19] Krasnopolskaya, T.S. Acoustic chaos caused by Sommerfeld effect. J. Fluids and Structures **8** (1994) 803–815.

[20] Martynyuk, A.A. Stability of Dynamical Systems in Metric Space. *Nonlinear Dynamics and Systems Theory* **5** (2005) 157–168.

[21] Neimark, J.I. and Landa, P.S. *Stochastic and chaotic oscillations.* Nauka, Moscow, 1987. [Russian]

[22] Rayleigh, W. *Theory of Sound.* Macmillan, London, 1877.

[23] Perel, V.Y. and Palazotto, A.N. A Nonlinear Model of Composite Delaminated Beam with Piezoelecric Actuator, with Account of Nonpenetration Constraint for the Delamination Crack Faces. *Nonlinear Dynamics and Systems Theory* **4** (2004) 161–194.

[24] Sommerfeld, A. Beitrage zum dynamischen ausbau der festigkeislehre. *Zeitschrift des Vereins Deutscher Ingenieure* **46** (1902) 391–394.

[25] Timoshenko, S. *Vibration Problems in Engineering.* Van Nostrand Co., New York, 1928.

[26] Ulitko, A.F. The Conjugate undular processes in piezoceramic skew fields at the electrical discharge. *Acoustical Bull.* **2**(1) (1999) 60–73. [Russian]

[27] Ulitko, A.F. *Vector Decomposition in the Space Theory Elasticities.* Akademperiodica, Kiev, 2002. [Russian]

[28] Zharii, O.Yu. Normal mode expansions in dynamic electroelasticity and their application to electromechanical energy conversion. *J. Acoust. Soc. Am.* **91**(1) (1992) 57–68.

Nonlinear Dynamics and Systems Theory, **6** (4) (2006) 389–400

A Survey on Space Trajectories in the Model of Three Bodies

A.F.B.A. Prado*

Instituto Nacional de Pesquisas Espaciais,
São José dos Campos, 12227-010, Brazil

Received: January 12, 2004; Revised: Revised: April 4, 2005

Abstract: This paper presents a survey on space trajectories in the circular restricted three-body problem. In this situation, a spacecraft moves under the gravitational forces of two bodies, which are assumed to be in circular orbits. First of all, there is a search for orbits that can be used to transfer a spacecraft from one body back to the same body or to transfer a spacecraft from one body to the respective Lagrangian points L_4 and L_5. The method employed is to solve the Two-Point Boundary Value Problem. The close approach between the spacecraft and the celestial bodies involved is also studied in the three-dimensional space. Then, the gravitational capture is studied. It is a characteristic of some dynamical systems, like the three- or four-body system, where a hyperbolic orbit around a celestial body can be transformed in an elliptic orbit without the use of any propulsive system.

Keywords: *Astrodynamics; orbital maneuvers; restricted problem; gravitational capture; swing-by; Lagrangian points.*

Mathematics Subject Classification (2000): 70F07, 70F15, 70M20.

1 Introduction

This paper has the goal of making a survey of trajectories to make orbital transfers of a spacecraft that is travelling in space under the gravitational forces of two bodies. It presents some results available in the literature, as well as some unpublished results in the direction.

First of all, it is considered the problem of finding transfer orbits in the restricted problem. Several situations are studied individually. A family of transfer orbits that can transfer a spacecraft from the Moon back to the Moon again (passing close to the

* Corresponding author: prado@dem.inpe.br

Lagrangian point L_3 in most of the cases) with minimum fuel consumption is considered. The family of transfer orbits from the Moon back to the Moon that requires an impulse with magnitude lower than the escape velocity from the Moon is studied and explained separately. Then, an extension is made to study similar trajectories for the Sun-Earth system, including a new suggestion to build a cycler transportation between the Earth and the Lagrangian point L_4.

After that, a swing-by maneuver in three dimensions is studied. The swing-by maneuver is a very popular technique used to decrease fuel expenditure in space missions. The most usual approach to study this problem is to divide the problem in three phases dominated by the "two-body" celestial mechanics. Other models used to study this problem are the circular restricted three-body problem (see [1 – 3]) and the elliptic restricted three-body problem [4]. In the present paper, the swing-by maneuvers are also studied under the model given by the three-dimensional circular restricted three-body problem. Particular attention is given to study the inclination change due to this maneuver.

Finally, the problem of gravitational capture in the regularized restricted three-body problem is studied. For gravitational capture it is understood a phenomenon where a massless particle changes its two-body energy around one of the primaries from positive to negative. This capture is always temporary and, after some time, the two-body energy changes back to positive and the massless spacecraft leaves the neighborhood of the primary. The importance of this temporary capture is that it can be used to decrease the fuel expenditure for a mission going from one of the primaries to the other, like an Earth-Moon mission [5]. The goal is to apply an impulse to the spacecraft during this temporary capture to accomplish a permanent capture. Since the goal of this impulse is to decrease the two-body energy of the spacecraft, its magnitude will be smaller if applied during this temporary capture.

2 Mathematical Model

For the research performed in this paper, the equations of motion for the spacecraft are assumed to be the ones valid for the well-known three-dimensional restricted circular three-body problem. The standard dimensionless canonical system of units is used, which implies that: the unit of distance is the distance between M_1 and M_2; the mean angular velocity (ω) of the motion of M_1 and M_2 is assumed to be one; the mass of the smaller primary (M_2) is given by $\mu = \dfrac{m_2}{m_1 + m_2}$ (where m_1 and m_2 are the real masses of M_1 and M_2, respectively) and the mass of M_2 is $(1 - \mu)$; the unit of time is defined such that the period of the motion of the two primaries is 2π and the gravitational constant is one. There are several systems of reference that can be used to describe the three-dimensional restricted three-body problem [6]. In this paper the rotating system is used. In the rotating system of reference, the origin is the center of mass of the two massive primaries. The horizontal axis (x) is the line that connects the two primaries at any time. It rotates with a variable angular velocity in such way that the two massive primaries are always on this axis. The vertical axis (y) is perpendicular to the (x) axis. In this system, the positions of the primaries are: $x_1 = -\mu,\ x_2 = 1 - \mu,\ y_1 = y_2 = 0$. In this

system, the equations of motion for the massless particle are [6]:

$$\ddot{x} - 2\dot{y} = x - (1-\mu)\frac{x+\mu}{r_1^3} - \mu\frac{x-1+\mu}{r_2^3}, \tag{1}$$

$$\ddot{y} + 2\dot{x} = y - (1-\mu)\frac{y}{r_1^3} - \mu\frac{y}{r_2^3}, \tag{2}$$

$$\ddot{z} = -(1-\mu)\frac{z}{r_1^3} - \mu\frac{z}{r_2^3}, \tag{3}$$

where r_1 and r_2 are the distances from M_1 and M_2.

3 Transfer Orbits in the Restricted Problem

The problem considered here is the problem of finding trajectories between two points that are fixed in the rotating coordinate system. This is the famous TPBVP (two point boundary value problem). There are many orbits that satisfy this requirement, and the way used in this research to find families of solutions is to specify a time of flight for the transfer. Then, the problem becomes the Lambert's three-body problem, that can be formulated as: "Find an orbit (in the three-body problem context) that makes a spacecraft to leave a given point A and go to another given point B, arriving there after a specified time of flight". Then, by varying the specified time of flight, it is possible to find a whole family of transfer orbits and study them in terms of the ΔV required, energy, etc. The transfers considered here are all restricted to the plane of motion of the two primaries.

Several families made of different trajectories to make a transfer from M_2 back to the M_2 and to the Lagrangian points are shown in [7] for the Earth-Moon system and in [8] for the Sun-Earth system. A new pair of transfers from the Moon back to the Moon is showed in Figure 3.1, one involving a hyperbolic transfer (faster) and one involving an elliptic transfer (slower).

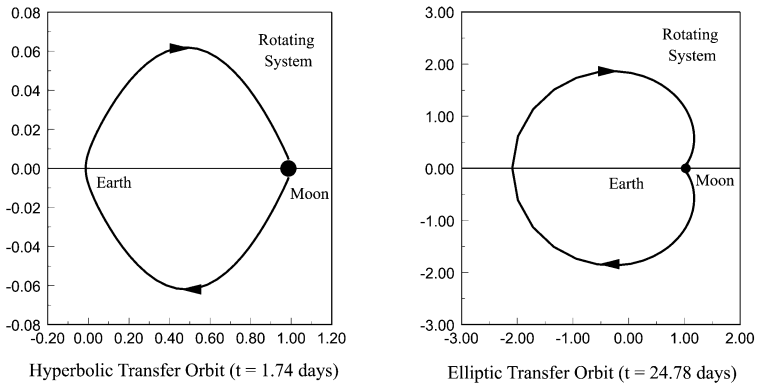

Figure 3.1: Transfer orbits in the Earth-Moon system, as seen in the rotating frame.

An interesting type of transfer was found [7] that requires an impulse with a magnitude lower than the escape velocity from the Moon. This possibility is opened by the restricted three-body problem model. It uses the perturbation of the third-body

(the Earth in this case) to help the massless particle to escape from the Moon (the first body), and it decreases the ΔV required for the maneuver. Remember that the escape velocity is defined as the velocity required to escape one celestial body considering the system governed by the "two-body" celestial mechanics. Figure 3.2 shows one of those transfers. The initial conditions in canonical units for this trajectory are: $x = 0.987871437$, $y = -0.004786681$, $\dot{x} = 2.220000000$, $\dot{y} = 0.000000000$, $V_{esc} = 2.251139608$, $\Delta V - V_{esc} = -0.031139608$, where V_{esc} is the escape velocity from the Moon.

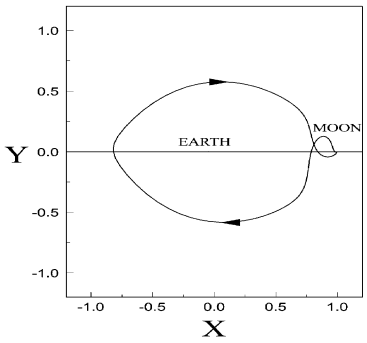

Figure 3.2: Transfer from the Moon back to the Moon with $\Delta V - V_{esc} < 0$.

Figure 3.3 shows a transfer from the Moon to the Lagrangian points and back to the Moon, also from [7]. This trajectory pass twice by the Lagrangian points visited. The initial conditions in canonical units for this trajectory are: $x = 0.987871437$, $y = -0.004500000$, $\dot{x} = -0.100000000$, $\dot{y} = -3.063600000$, $V_{esc} = 2.321739099$, $\Delta V - V_{esc} = 0.743349025$.

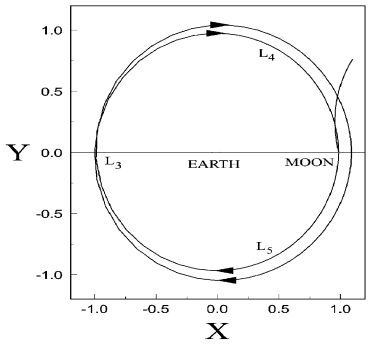

Figure 3.3: Transfer from the Moon to the Lagrangian points.

Several trajectories to transfer a spacecraft between the Earth and the Lagrangian points with minimum ΔV are shown in [8]. In the present paper one of them is shown in details, because it generates results for the construction of a cycler transportation between the triangular Lagrangian points and the Earth. The spacecraft leaves the Earth and visits the Lagrangian points in the order L_4 (in 1.81 years), L_3 (in 5.49 years),

L_5 (in 9.20 years) and then it returns to the Earth's neighborhood (in 11.00 years). Figure 3.4 shows the first two revolutions of this trajectory. The particular important point of this orbit is that after the close approach with the Earth (in the end of the first revolution) the spacecraft starts a new tour to the Lagrangian points, in the reverse order. Integrating this trajectory for a longer time it is possible to see that the first five revolutions have alternating directions of motion.

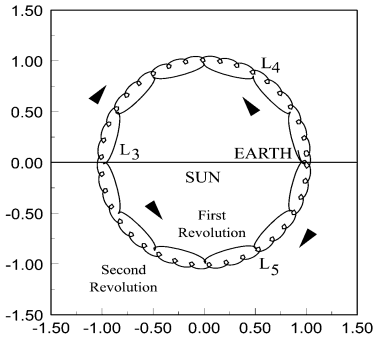

Figure 3.4: Trajectory linking the Earth and the Lagrangian points.

The "swing-by" that reverses the direction of motion discovered in this trajectory can be used to build a cycler transportation system between the Earth and the Lagrangian point L_5 as shown in [8]. In the present paper, an extension is made to build a cycler system for the Lagrangian point L_4, by using the mirror image theorem [9]. It is necessary to find the mirror image of the trajectory linking the Earth and the Lagrangian point L_5. Figure 3.5 shows this trajectory.

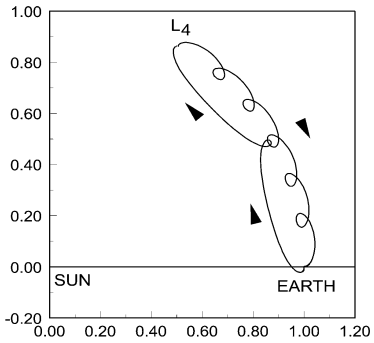

Figure 3.5: The cycler system between the Earth and L_4.

Note that the mirror image of the legs for an Earth-bound trip in now a L_4-bound trip and the mirror image of the L_5-bound leg is now the Earth-bound leg. The time-line for a complete cycler is: $t = 0$: The spacecraft leaves L_4 from rest (as seen in the rotating frame) with an impulse of $\Delta V = 0.0274$ (816 m/s); $t = 5.82$ years: The spacecraft arrives at the Earth, makes a swing-by to reverse the sense of motion and it starts going back to L_4; $t = 7.62$ years: The spacecraft arrives at L_4. A new impulse of $\Delta V = 0.0377$

(1003.8 m/s) is applied to send it back to the Earth and to start the cycler again.

4 The Swing-By in Three Dimensions

The three dimensional swing-by maneuver consists of using a close encounter with a celestial body to change the velocity, energy, and angular momentum of a smaller body (a comet or a spacecraft). Figure 4.1 shows the sequence for this maneuver and some important variables.

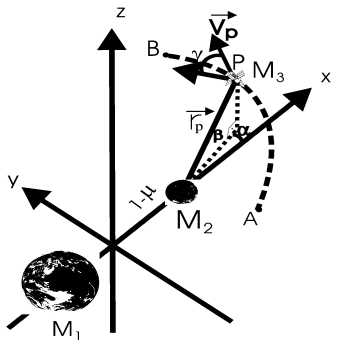

Figure 4.1: The swing-by in three dimensions.

It is assumed that the system has three bodies: a primary (M_1) and a secondary (M_2) body with finite masses that are in circular orbits around their common center of mass and a third body with negligible mass (the spacecraft) that has its motion governed by the two other bodies. The spacecraft leaves the point A, passes by the point P (the periapsis of the trajectory of the spacecraft in its orbit around M_2) and goes to the point B. The points A and B are chosen in a such way that the influence of M_2 at those two points can be neglected and, consequently, the energy can be assumed to remain constant after B and before A (the system follows the two-body celestial mechanics). The initial conditions are clearly identified in Figure 4.1: the periapsis distance r_p (distance measured between the point P and the center of M_2), the angles α and β and the velocity V_p. The distance r_p is not to scale, to make the figure easier to understand.

The result of this maneuver is a change in velocity, energy, angular momentum and inclination in the Keplerian orbit of the spacecraft around the central body. A numerical algorithm to solve the problem has the following steps:

(1) Arbitrary values for the parameters r_p, V_p, α, β and γ are given.

(2) With these values the initial conditions in the rotating system are computed. The initial position is the point (X_i, Y_i, Z_i) and the initial velocity is (V_{xi}, V_{yi}, V_{zi}),

where:

$$X_i = 1 - \mu + r_p \cos(\beta)\cos(\alpha), \tag{4}$$

$$Y_i = r_p \cos(\beta)\sin(\alpha), \tag{5}$$

$$Z_i = r_p \sin(\beta), \tag{6}$$

$$V_{xi} = -V_p \sin(\gamma)\sin(\beta)\cos(\alpha) - V_p \cos(\gamma)\sin(\alpha) + r_p \cos(\beta)\sin(\alpha), \tag{7}$$

$$V_{yi} = -V_p \sin(\alpha)\sin(\gamma)\cos(\alpha) + V_p \cos(\gamma)\sin(\alpha) - r_p \cos(\beta)\sin(\alpha), \tag{8}$$

$$V_{zi} = V_p \cos(\beta)\sin(\gamma). \tag{9}$$

(3) With these initial conditions, the equations of motion are integrated forward in time until the distance between M_2 and the spacecraft is larger than a specified limit d. At this point the numerical integration is stopped and the energy (E_+) and the angular momentum (C_+) after the encounter are calculated.

(4) Then, the particle goes back to its initial conditions at the point P, and the equations of motion are integrated backward in time, until the distance d is reached again. Then the energy (E_-) and the angular momentum (C_-) before the encounter are calculated.

An interesting question that appears in this problem is what happens to the inclination of the spacecraft due to the close approach. Some results regarding this question for the Earth-Moon system are shown in [10]. To investigate this fact the inclination of the trajectories were calculated before and after the closest approach. To obtain the inclinations the equation $\cos(i) = C_z/C$ is used, where C_z is the Z-component of the angular momentum and C is the magnitude of the total angular momentum. Figure 4.2 shows some new results for the case $\gamma = 0$ in the Sun-Jupiter system. This constraint is assumed, because it is the most usual situation in interplanetary research, since the planets have orbits that are almost coplanar. The horizontal axis represents the angle α, and the vertical axis represents the angle β. The variation in inclination is shown in the contour plots. All the angles are expressed in degrees.

Several conclusions come from those results:

(i) when $\beta = 0^\circ$ (planar maneuver) the variation in inclination can have only three possible values: $\pm 180^\circ$, for a maneuver that reverse the sense of its motion, or 0° for a maneuver that does not reverse its motion. Those numerical results agree with the physical-model, since the fact that $\beta = 0^\circ$ implies in a planar maneuver that does not allow values for the inclination other than 0° or 180°;

(ii) when $\beta = \pm 90^\circ$ the variation in inclination is very close to zero;

(iii) when $\alpha = 0^\circ$ or $\alpha = 180^\circ$ there is no change in the inclination. This is in agreement with the fact that a maneuver with this geometry does not change the trajectory at all;

(iv) when the periapsis distance or the velocity at periapsis increases, the effects of the swing-by in the maneuver are reduced. In the plots shown, this can be verified by the fact that the area of the regions where the variation in inclination is close to zero increases.

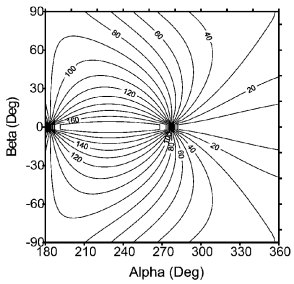

Inclination before swing-by for $r_p = 0.000137595$, $V_p = 4.0$.

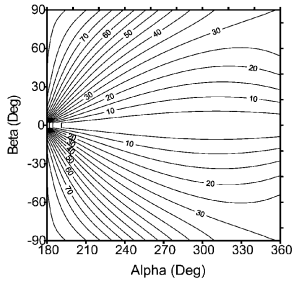

Inclination after swing-by for $r_p = 0.000137595$, $V_p = 4.0$.

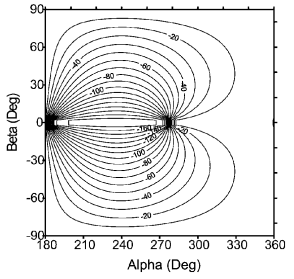

Variation in Inclination for $r_p = 0.000137595$ and $V_p = 4.0$.

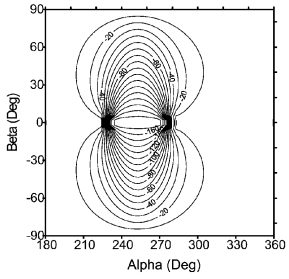

Variation in Inclination for $r_p = 0.000137595$ and $V_p = 5.0$.

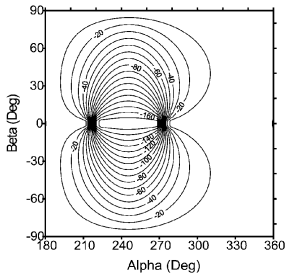

Variation in Inclination for $r_p = 0.000183460$ and $V_p = 4.0$.

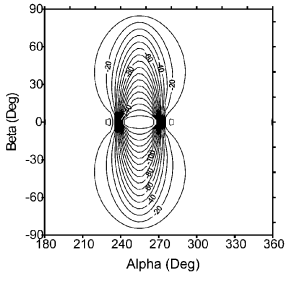

Variation in Inclination for $r_p = 0.000183460$ and $V_p = 5.0$.

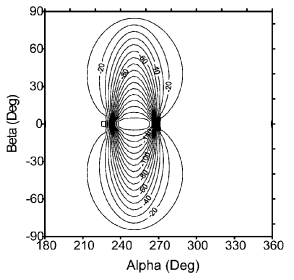

Variation in Inclination for $r_p = 0.000275190$ and $V_p = 4.0$.

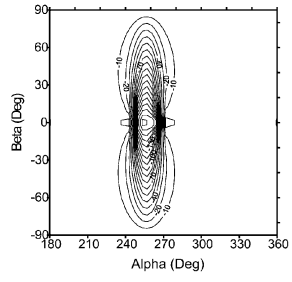

Variation in Inclination for $r_p = 0.000275190$ and $V_p = 5.0$.

Figure 4.2: Inclination change resulted from a close approach in the Sun-Jupiter system.

5 The Gravitational Capture

Then, attention is given to the problem of gravitational capture. For gravitational capture it is understood a phenomenon where a massless particle changes its two-body energy around one of the primaries from positive to negative. This capture is always temporary and, after some time, the two-body energy changes back to positive and the massless spacecraft leaves the neighborhood of the primary. Studies related to this problem are available in [5] and [12 – 16]. The importance of this temporary capture is that it can be used to decrease the fuel expenditure for a mission going from one of the primaries to the other, like an Earth-Moon mission. The goal is to apply an impulse to the spacecraft during this temporary capture to accomplish a permanent one. Since the impulse decrease the two-body energy of the spacecraft, its magnitude will be smaller if applied during this temporary capture. An important application of this technique can be found in trajectories to the Moon with fuel consumption smaller than the fuel required by the [17] transfer [18 – 21, 5]. In this paper the main concern is to study the forces involved in this maneuver. The main force is the gravitational force due to the central body, in this case, the Moon. The others forces are perturbations on the movement of the massless particle. So, to understand the behavior of the perturbing forces, an analysis was made by measuring the components of each force. The chosen components are in the radial, transversal and in the direction of motion of the massless particle. In the radial direction, the positive sign means that the force is acting opposite to the direction of the body. In the transversal direction, the positive sign indicates that the force is acting in the counter-clockwise direction. In the direction of motion, the force is positive when it is being applied in the direction of the movement of the particle.

Figure 5.1 shows one of those trajectories and the forces acting in the spacecraft in every moment of time. The curves are:

(1) gravitational radial force;
(2) gravitational transversal force;
(3) centripetal radial force;
(4) centripetal transversal force;
(5) resultant radial force;
(6) resultant transversal force;
(7) gravitational force in the direction of motion;
(8) centripetal force in the direction of motion;
(9) resultant force in the direction of motion.

In the radial direction the force due to the Earth has a negative sign. This means that the force is pushing the spacecraft to an opposite direction to the Moon. So, it is slowing down the object. In the transversal direction, this force is also negative, which means that it is accelerating the spacecraft in the clock-wise direction. In the direction of motion the sign is also negative, breaking the spacecraft all the time. The centripetal force acts in an opposite direction from the gravity force due to the Earth, but with smaller absolute values. So the net result is due to the gravity force of the Earth, which makes the vehicle to reduce its velocity. The resultant on the transversal direction accelerates the spacecraft in the clock-wise direction. It is visible that the components radial and in the direction of motion of the forces are very close to each other. This is a consequence of the fact that the trajectory is close to radial in most of the trajectory.

The most relevant component is in the direction of motion. This component of the resulting forces shows that, independent of where the particle came, it is breaking the

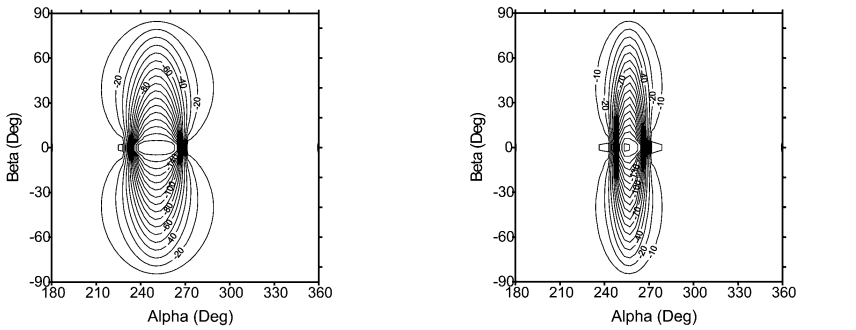

Figure 5.1: Trajectory with $C_3 = -0.2\text{e}$, $\alpha = 0^\circ$ at perilune and the forces.

particle all the time. The transversal component ever tries to pull the particle to the Earth-Moon axis. The radial component of the resultant force has the same effect of the component in the direction of motion. It also shows that the particle is loosing radial velocity when approaching the central body. These forces slow down the spacecraft working opposite to the movement of the spacecraft. This is equivalent of applying a continuous propulsion force against the motion of the spacecraft. In the radial direction the gravitational force due to the Earth and the centripetal force tends to equilibrium, but ever rest some work against the movement. This is also true for the component in the direction of motion. In the transversal direction the forces pull the particle to the Earth-Moon axis. Understanding these behaviors explains why a particle with a velocity slower than the escape velocity can escape from the Moon. It is the opposite case for the capture and it happens for all the cases studied. Some analytical results with respect to this problem are available in [22].

6 Conclusions

In this paper, trajectories in the planar restricted three-body problem with near-zero ΔV to move a spacecraft between any two points in the group formed by the Earth and the Lagrangian points L_3, L_4, L_5 in the Earth-Moon and Earth-Sun systems are found. It is shown how to apply these results to build a cycler transportation system to link all the points in this group. For the Sun-Earth system, it is also shown how to use one or more "swing-by" with the Earth to build a cycler transportation system between the Earth and the Lagrangian points L_4 and L_5, with small ΔV required for maneuvers in nominal operation.

Looking at the results for the Earth-Moon system, we can conclude that:

(i) there are trajectories with ΔV near the escape velocity to move a spacecraft from the Moon back to the Moon in the Earth-Moon system, using the restricted three-body problem as a model;

(ii) there is a new type of trajectory for this transfer that requires a ΔV under the escape velocity;

(iii) there are trajectories connecting the Moon and the Lagrangian points L_3, L_4 and L_5;

(iv) there are trajectories that make consecutive close approaches with the Earth and the Moon.

Those orbits are shown in this paper and they can be used in three situations:

(a) to transfer a spacecraft from the Moon back to the Moon;

(b) to transfer a spacecraft from the Moon to the respective Lagrangian points L_3, L_4 and L_5;

(c) to transfer a spacecraft to an orbit that passes close to the Moon and to the Earth several times, with the goal of building a transportation system between these two celestial bodies.

The three-dimensional restricted three-body problem is also used to study the swing-by maneuver. The effects of the close approach in the inclination of the spacecraft is studied and the results show several particularities, like: $\beta = 0^\circ$ allows only $\pm 180^\circ$, and 0° for Δi, $\beta \pm 90^\circ$ or $\alpha = 0^\circ$ or 180° implies in $\Delta i = 0^\circ$, etc.

Some particularities of the gravitational capture problem are also studied and the forces acting are also shown. This study answers some questions about the phenomena. Two of the forces are relatively weak, and they act as disturbing forces: the gravitational force due to Earth and the centrifugal force. These forces working together slow down the spacecraft with a force in the opposite direction of the spacecraft's motion. This is equivalent of applying a continuous propulsion force against the motion of the spacecraft. In the radial direction the gravitational force due to Earth and the centripetal force tends to equilibrium, but ever rest some work against the gravitation of the central body. It is also true for the components in the direction of motion for these forces. In the transversal direction, the forces pull the particle to the Earth-Moon axis. The understandings of these behaviors explain why a particle with a velocity slower than the escape velocity can escape from the Moon. It is the opposite case for the capture and it happens for all the cases studied.

Acknowledgements

The author is grateful to the Foundation to Support Research in the São Paulo State (FAPESP) for the research grant received under Contract 2003/03262-4 and to CNPq (National Council for Scientific and Technological Development) for the Grant 300828/2003-9.

References

[1] Broucke, R.A. The celestial mechanics of gravity assist. *AIAA Paper 88-4220*, August, 1988.

[2] Broucke, R.A. and Prado, A.F.B.A. Jupiter swing-by trajectories passing near the Earth. *Advances in the Astronautical Sciences* **82**(2) (1993) 1159–1176.

[3] Prado, A.F.B.A. *Optimal Transfer and Swing-By Orbits in the Two- and Three-Body Problems*. Ph.D. Dissertation, University of Texas at Austin, Austin, TX, 1993.

[4] Prado, A.F.B.A. Close-approach trajectories in the elliptic restricted problem. *J. Guidance, Control and Dynamics* **20**(4) (1997) 797–802.

[5] Yamakawa, H. *On Earth-Moon Transfer Trajectory with Gravitational Capture*. Ph.D. Dissertation, University of Tokyo, Tokyo, Japan, 1992.

[6] Szebehely, V.G. *Theory of Orbits*. Academic Press, New York, 1967.

[7] Prado, A.F.B.A. and Broucke, R.A. Transfer orbits in the Earth-Moon system using a regularized model. *J. Guidance, Control and Dynamics* **19**(4) (1996) 929–933.

[8] Prado, A.F.B.A. and Broucke, R.A. Transfer orbits in restricted problem. *J. Guidance, Control and Dynamics* **18**(3) (1995) 593–599.

[9] Miele, A. Theorem of image trajectories in the Earth-Moon space. *Astronautica Acta* **6** (1960) 225–232.

[10] Felipe, G. and Prado, A.F.B.A. Study of the inclination change in three-dimensional swing-by trajectories. In: *Abstracts of the 22^{nd} Int. Symposium on Space Technology and Science*. Morioka, Japan, 28 May – 04 June, 2000, 60 (Paper 00-j-02).

[11] Prado, A.F.B.A. An analytical description of the close approach maneuver in three dimensions. *51^{th} Int. Astronautical Congress (Paper IAF-00-A.5.05)*. Rio de Janeiro, Brazil, 1 – 7 October, 2000.

[12] Yamakawa, H., Kawaguchi, J., Ishii, N. and Matsuo, H. A numerical study of gravitational capture orbit in Earth-Moon system. *AAS paper 92-186*, 1992.

[13] Vieira Neto, E. and Prado, A.F.B.A. A study of the gravitational capture in the restricted-problem. *Proc. of the Int. Symposium on Space Dynamics*. Toulouse, France, 19 – 23 June, 1995, 613–622.

[14] Vieira Neto, E. and Prado, A.F.B.A. Time-of-flight analyses for the gravitational capture maneuver. *J. Guidance, Control and Dynamics* **21**(1) (1998) 122–126.

[15] Vieira Neto, E. and Prado, A.F.B.A. Forças que atuam na captura gravitacional temporária. *IX Colóquio Brasileiro de Dinâmica Orbital*. Águas de Lindóia, Brazil, 16 – 20 November, 1998, 30.

[16] Vieira Neto, E. *Estudo Numérico da Captura Gravitacional Temporária Utilizando o Problema Restrito de Três Corpos*. Ph.D. Dissertation, Instituto Nacional de Pesquisas Espaciais, São José dos Campos, Brazil, 1999.

[17] Hohmann, W. *Die Erreichbarheit der Himmelskorper*. Oldenbourg, Munich, 1925.

[18] Belbruno, E.A. Lunar capture orbits, a method of constructing Earth Moon trajectories and the Lunar Gas mission. *AIAA-87-1054, 19th AIAA/DGLR/JSASS Int. Electric Propulsion Conference*. Colorado Springs, Colorado, May, 1987.

[19] Belbruno, E.A. Examples of the nonlinear dynamics of ballistic capture and escape in the Earth-Moon system. *AIAA-90-2896, AIAA Astrodynamics Conference*. Portland, Oregon, August, 1990.

[20] Belbruno, E.A. Ballistic Lunar capture transfer using the fuzzy boundary and solar perturbations: a survey. In: *Proc. for the Int. Congress of SETI Sail and Astrodynamics*. Turin, Italy, 1992.

[21] Krish, V. *An Investigation Into Critical Aspects of a New Form of Low Energy Lunar Transfer, the Belbruno-Miller Trajectories*. Master's Dissertation, Massachusetts Inst. of Technology, Cambridge, MA, 1991.

[22] Prado, A.F.B.A. A semi-analytical study of the gravitational capture. In: *Proc. of the Int. Symposium Space Dynamics*. Biarritz-France, 26 – 30 June, 2000, P.299–308.

Nonlinear Dynamics and Systems Theory, **6** (4) (2006) 401–409

Deployment Considerations for Spacecraft Formation at Sun-Earth L2 Point

G. Radice *

Department of Aerospace Engineering, University of Glasgow
GLASGOW, G12 8QQ, UK

Received: July 19, 2005; Revised: September 18, 2006

Abstract: The coordination and control of a constellation of spacecraft, flying a few meters from one another, dictates several interesting design requirements, including efficient architectures and algorithms for formation acquisition, reorientation and resizing. The spacecraft must perform these transitions without interfering or colliding into each other. Furthermore position keeping is fundamental for formation efficiency. This paper presents an optimal deployment of the DARWIN formation using the potential function control technique in the vicinity of the Sun-Earth L2 point. The method hinges on defining a potential function from the geometric configuration of the constellation together with any collision avoidance requirement. A review of the fundamentals of relative motion and dynamics is presented before describing the features of the different control algorithms and validating the method using Lyapunov's theorem. The potential function method has been used to control both translational and rotational control. Obstacles, in the shape of other satellites and constrained payload pointing directions have been included. Finally it will be shown that the attitude control algorithm can be successfully used to avoid plume impingement that can have catastrophic consequences for the mission.

Keywords: *Formation flying; Lyapunov functions; rotational control.*

Mathematics Subject Classification (2000): 70E55, 70F15, 70M20.

* Corresponding author: gradice@aero.gla.ac.uk

1 Introduction

Over the past decade, the introduction of cost reduction policy by the major space agencies caused a paradigm shift in the design of scientific satellites, as the primary metric by which spacecraft were judged switched from purely performance to specific performance or performance per unit cost [Cyrus and Miller, 1997]. Several new technologies, including multifunctional structures, micro-electro-mechanical systems, nano-technology and distributed satellite systems, have the potential to revolutionise the field of satellite design. In particular in the field of distributed satellite systems, that is systems based on dividing the tasks among several light and small satellites, two approaches exist: constellations and formations. The difference between the two methods lies in the relative positioning between satellites. Constellations are positioned relative to an object, such as the Earth, while in formations spacecraft are positioned relative to each other. Each satellite communicates with the others and shares the processing, communications, and payload or mission functions. Thus the cluster of satellites forms a "virtual satellite". This concept promises many benefits, including greater utility and flexibility by allowing the cluster to reconfigure and optimise its geometry for a given mission, enhanced survivability, and increased reliability.

In general terms, the formation-flying approach has the following advantages: the opportunity of completing space observation missions without large and expensive ground infrastructures, reducing operational costs. The deeper covering of the phenomena under observation, since different instruments, under different points of view, inspect it at the same time. By substituting one large complex satellite with a group of small satellites, a better flexibility is achieved, with the chance of reconfiguring the system in case of malfunction, thus avoiding the mission failure. The failure of one spacecraft will not compromise the mission. The employment of identical platforms within the constellation allows a standardisation of the manufacturing, thus reducing production costs. The system functionality is not extremely dependent from technology: it is possible to launch a temporary formation with state-of-the-art instruments and later increasing the system performance by adding one or more spacecraft to the formation. On the other hand, the development of formation-flying presents the following technological challenges: accurate sensors are needed to allow a precise determination of the state of the system in order to control the formation. High precision in spacecraft coordination is indispensable in order to avoid troubles linked with the reciprocal distances among the elements of the formation, most of all collisions between the satellites.

Current studies in spacecraft formation control vary from individual satellite control to the use of stochastic algorithms [Gurfil et al., 2002]. The main problem to be addressed in formation control is that of workload. For small, Earth centred formations, individual control is a viable options. As the satellite number and operational distance from Earth increase, methods that automate the control processes become a necessity. The method proposed here aims, to drastically reduce the workload required to control the formation. The potential function control method represents a means of both estimating the desired states of a spacecraft's location, and autonomously correct and control these states. It is based on Lyapunov's method for stability analysis and its efficiency in the problem of collision avoidance is due to the fact that it aims to avoid a particular condition rather than to reach a state of equilibrium.

2 Formation Flight Dynamics

We will now introduce the model used for formation dynamics, including the simplifications used. We assume that the Sun-Earth system is not disturbed by the inclusion of a third infinitively small body. The whole system rotates with a constant angular velocity ω, about the baricentre G, the position of which is a function of the Earth mass m_{E} and the Sun mass m_{S} as shown in Figure 2.1. The Earth is in a circular orbit around the Sun at distance R_{ES}. Additionally, Sun and Earth are supposed to be perfect spherical bodies.

The acceleration of a spacecraft M in the inertial frame R_0 is:

$$\mathbf{a}_{M/R_0} = \mathbf{a}_{M/R} + \mathbf{a}_{M\in R/R_0} + 2\mathbf{\Omega}_{R/R_0} \times \mathbf{v}_{M/R}\,,$$

where $\mathbf{a}$ denotes an acceleration, $\mathbf{v}$ a velocity and Ω an angular velocity. In the local frame the acceleration becomes:

$$\mathbf{a}_{M/R_0} = \begin{bmatrix} \ddot{x} \\ \ddot{y} \\ \ddot{z} \end{bmatrix} - \omega^2 \begin{bmatrix} R_{GL2} + x \\ 0 \\ z \end{bmatrix} - 2\omega \begin{bmatrix} \dot{z} \\ 0 \\ -\dot{x} \end{bmatrix}, \tag{1}$$

where R_{GL2} is the distance from G to L2.

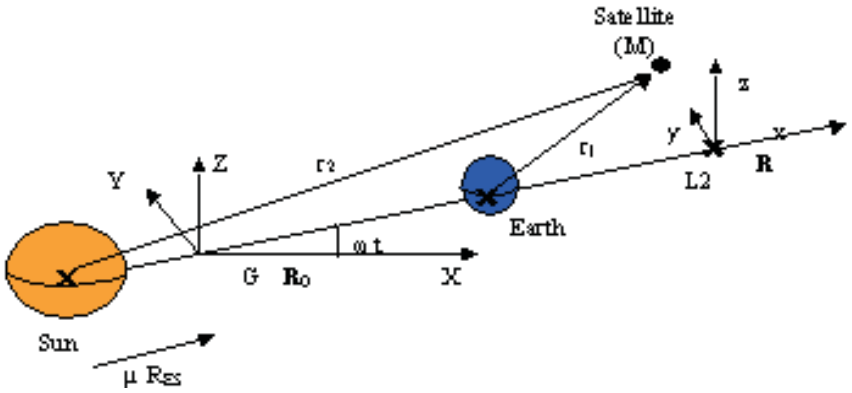

Figure 2.1: Geometric Configuration.

The forces f acting on the spacecraft are gravitational attraction and non-Newtonian. Because of the small size of satellites we confuse their centre mass with their gravitational centre. Therefore the equations of motion of a satellite are:

$$\mathbf{a}_{M/R_0} = -\mu_E \frac{\mathbf{r}_1}{\|\mathbf{r}_1\|^3} - \mu_S \frac{\mathbf{r}_2}{\|\mathbf{r}_2\|^3} + f,$$

where μ_{E} and μ_{S} are respectively the earth and the sun gravitational constants. In

component form the equations of motion become:

$$\begin{aligned} \ddot{x} - 2\omega\dot{z} - \omega^2(R_{\mathrm{GL2}} + x) + \frac{\mu_{\mathrm{E}}(R_{\mathrm{EL2}} + x)}{r_1^3} + \frac{\mu_{\mathrm{S}}(R_{\mathrm{SL2}} + x)}{r_2^3} &= f_{\mathrm{x}}, \\ \ddot{y} + \left(\frac{\mu_{\mathrm{E}}}{r_1^3} + \frac{\mu_{\mathrm{S}}}{r_2^3}\right) y &= f_{\mathrm{y}}, \\ \ddot{z} + 2\omega\dot{x} - \omega^2 z + \left(\frac{\mu_{\mathrm{E}}}{r_1^3} + \frac{\mu_{\mathrm{S}}}{r_2^3}\right) z &= f_{\mathrm{z}}, \end{aligned} \tag{2}$$

where R_{EL2} and R_{SL2} respectively the distances from the Earth and the Sun to the L2 point.

It is clear that these equations are non-linear as r_1 and r_2 hinge on the satellite position into the local frame. Moreover, the x and z variables are coupled whereas y is independent [Alfriend et al., 2002]. The majority of studies dealing with formation flying adopt linear equations of motion. The linearisation is very accurate since the distances of the satellites from the L2 point are very small compared to the distances between the L2 point and the Earth and the Sun [Hamilton et al., 2002]. The linearisation yields:

$$\begin{aligned} \ddot{x} - 2\omega\dot{z} - (\omega^2 + 2\mu_0^2)x &= f_{\mathrm{x}}, \\ \ddot{y} + \mu_0^2 y &= f_{\mathrm{y}}, \\ \ddot{z} + 2\omega\dot{x} + (\mu_0^2 - \omega^2)z &= f_{\mathrm{z}}, \end{aligned} \tag{3}$$

with

$$\mu_0^2 = \frac{\mu_{\mathrm{S}}}{R_{\mathrm{SL2}}^3} + \frac{\mu_{\mathrm{E}}}{R_{\mathrm{EL2}}^3}.$$

Equation (3) will be used to model the relative motion of each satellite from the reference orbit.

3 The Potential Function Control Method

A dynamical system is stable in the sense that it returns to equilibrium after any perturbation, if and only if, there exists a Lyapunov function; some scalar function $V(x)$ of the state with the following properties.

Let $\dot{x} = f(x),\ f(0) = 0$ and $0 \in \Omega \subset \Re^n$. If there exists a C^1 function $V:\ \Omega \to \Re$ such that:

(1) $V(0) = 0$;

(2) $V(x) > 0\ \forall x \in \Omega,\ x \neq 0$;

(3) $\dot{V}(x) \leq 0\ \forall x \in \Omega$,

than $x = 0$ is locally stable. Furthermore, if

(4) $\dot{V}(x) < 0\ \forall x \in \Omega,\ x \neq 0$,

then $x = 0$ is locally asymptotically stable. This theorem can be easily modified by replacing (3) by $\dot{V}(x) \geq 0$ for limited times, which implies that $\dot{V}(x) \leq 0$ after a certain time and then the initial theorem is fulfilled.

The method then consists in controlling V to fulfil Condition 3 of Lyapunov's theorem. The time derivative of V is:

$$\dot{V} = \nabla f \cdot \mathbf{v},$$

where $\mathbf{v}$ is the velocity of the spacecraft. The velocity of the spacecraft will be controlled as:

$$\mathbf{v}_{\text{desired}} = -k \frac{\nabla V}{\|\nabla V\|},$$

where $\frac{\nabla V}{\|\nabla V\|}$ is the unit vector normal to the isopotential surface and k is a shaping parameter which regulates the amplitude of $\mathbf{v}_{\text{desired}}$, which is then analytic. When the control is switched on, the time derivative of the potential function is forced to be equal to:

$$\dot{V} = -\, k\, \|\nabla V\|,$$

which is non-positive thus fulfilling Lyapunov's theorem. Thus the cluster converges to the goal position avoiding collisions. Through the desired velocity, the path followed by the satellite is completely defined by the potential function. To optimise the time of the deployment and the fuel consumption this function must be shaped cleverly. Also, the velocity desired must be obtained efficiently despite of bounded thrusters and imperfect sensors.

3.1 Translational control

The component that controls the spacecraft translations will guide towards the goal positions while avoiding collisions. The attractive component, $V_{\text{a Trans}}$ is a function of the distance between the current spacecraft position and the desired final position while the repulsive component, $V_{\text{rep Trans}}$ is a function of the current spacecraft position and the obstacle position:

$$V_{\text{a Trans}} = \tfrac{1}{2}(\mathbf{r} - \mathbf{r}_f)^2 \quad V_{\text{rep Trans}} = A_{\text{T}}\ e^{-B_{\text{T}}(\mathbf{r}-\mathbf{r}_{\text{obs}})^2}. \tag{4}$$

With r the current spacecraft position, $\mathbf{r}_f$ the final position $\mathbf{r}_{\text{obs}}$ the obstacle position and A_{T} and B_{T} shaping parameters. One of the weak points of the potential function control method is the presence of saddle points in the potential function. The main problem consists in dimensioning the function around these points so that the satellites behave correctly there. We therefore develop a repulsive component that always maintains the same width. The parameter that controls the amplitude of the repulsive component now hinges on the distance from the target, $\mathbf{r}_{\text{target}}$, as well as the width of the obstacle d_{obs}:

$$A_{\text{T}} = \frac{1}{2}\ \frac{e^{B_{\text{T}} d_{\text{obs}}^2}}{B_{\text{T}} d_{\text{obs}}}\ \left(\mathbf{r}_{\text{target}} + \frac{1}{2B_{\text{T}} d_{\text{obs}}}\right).$$

3.2 Rotational control

The component that controls the spacecraft rotation will guide towards the desired attitude while avoiding any constrained directions. The attractive component, $V_{\text{a Rot}}$ is a function of the angular distance between the current spacecraft attitude and the desired final attitude while the repulsive component, $V_{\text{rep Rot}}$ is a function of the current spacecraft attitude and the obstacle location:

$$V_{\text{a Rot}} = \tfrac{1}{2}\ \gamma^2 \quad V_{\text{rep Rot}} = A_{\text{R}}\ e^{-B_{\text{R}}\delta^2}\ . \tag{5}$$

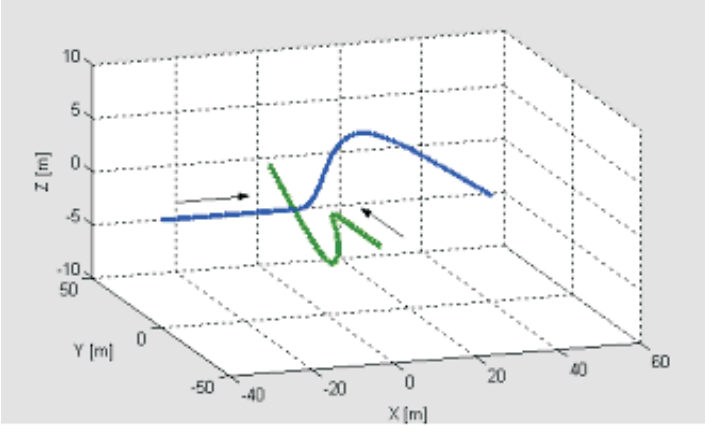

Figure 3.1: Translational Manoeuvre.

With A_{R} and B_{R} are shaping parameters and:

$$\gamma = \arccos(\mathbf{n}_{\mathrm{p}} \cdot \mathbf{n}_{\mathrm{f}}), \quad \delta = \arccos(\mathbf{n}_{\mathrm{p}} \cdot \mathbf{n}_{\mathrm{obs}}), \tag{6}$$

where $\mathbf{n}_{\mathrm{p}}$ is the unit vector along the payload axis, $\mathbf{n}_{\mathrm{f}}$ is the target unit vector and $\mathbf{n}_{\mathrm{obs}}$ is the unit vector along any avoidance directions. Once again we develop a repulsive component that always maintains the same width. The parameter that controls the amplitude of the repulsive component now hinges on the distance from the angular distance from the target, γ_{targ}, as well as the angular width of the obstacle δ_{obs}:

$$A_{\mathrm{R}} = \frac{1}{2} \frac{e^{B_{\mathrm{R}}\delta_{\mathrm{obs}}^2}}{B_{\mathrm{R}}\delta_{\mathrm{obs}}} \left(\gamma_{\mathrm{targ}} + \frac{1}{2B_{\mathrm{R}}\delta_{\mathrm{obs}}}\right).$$

In Figure 3.1 we see the avoidance action taken by two spacecraft on a colliding trajectory, while in Figure 3.2 we can see how the payload follows a trajectory from a random initial position to a desired target attitude, avoiding a constrained direction.

3.3 The potential function

We are now able to construct a Lyapunov function for each spacecraft that will guide them to their goal positions while avoiding collisions and avoiding restricted pointing directions. This function V consists of two components: attractive V_{a} and repulsive V_{rep}. Moreover, as we have seen the attractive and repulsive components will be made up of two parts each to account for the positional and attitude requirements. The potential function therefore will be:

$$V = \frac{1}{2}(\mathbf{r} - \mathbf{r}_f)^2 + \frac{1}{2}\,\gamma^2 + A_{\mathrm{T}}\; e^{-B_{\mathrm{T}}(\mathbf{r}-\mathbf{r}_{\mathrm{obs}})^2} + A_{\mathrm{R}}\; e^{-B_{\mathrm{R}}\delta^2}.$$

4 Plume Impingement Avoidance

Spacecraft thrusters send gas streams of various species onto spacecraft surfaces. The plume of gas particles emitted by thrusters may cause contamination, degradation or

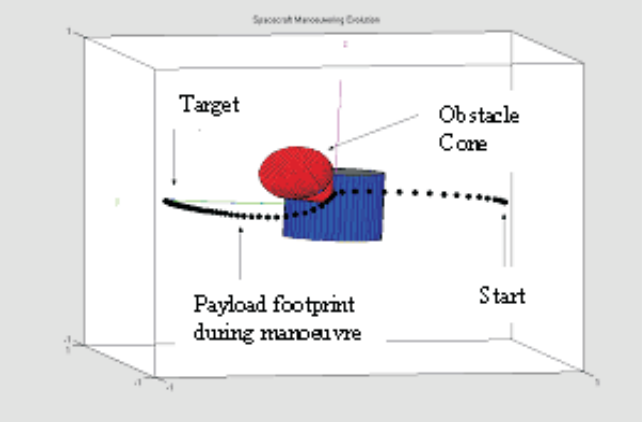

Figure 3.2: Rotational Manoeuvre.

damage to surface and can either directly or indirectly cause localized heating and contamination. Plumes and the resultant impingement phenomena are currently not well understood. Simple engineering models are used conservatively to estimate plume effects. The problem of plume impingement is a major concern for a cluster of spacecraft with close relative motion. The problem is compounded by the fact that when approaching each other, the spacecraft will have to fire the thrusters towards the incoming satellite to manoeuvre away from it. We intend to use the potential function method introduced earlier to address and solve this problem. The idea is to impart an attitude to the satellite that places the other spacecraft in a cone, where there are no exhaust particles, as shown in Figure 4.1.

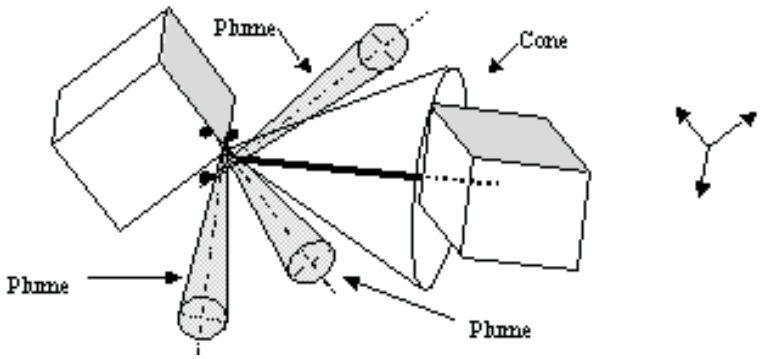

Figure 4.1: Plume Impingement Avoidance Cone.

To achieve this we make use of the potential method, and in particular the attitude control component explained in the previous section. We consider two unit vectors, $\mathbf{n}_t$ and $\mathbf{r}_s$, the first directed along the plume direction the second directed along the avoidance cone.

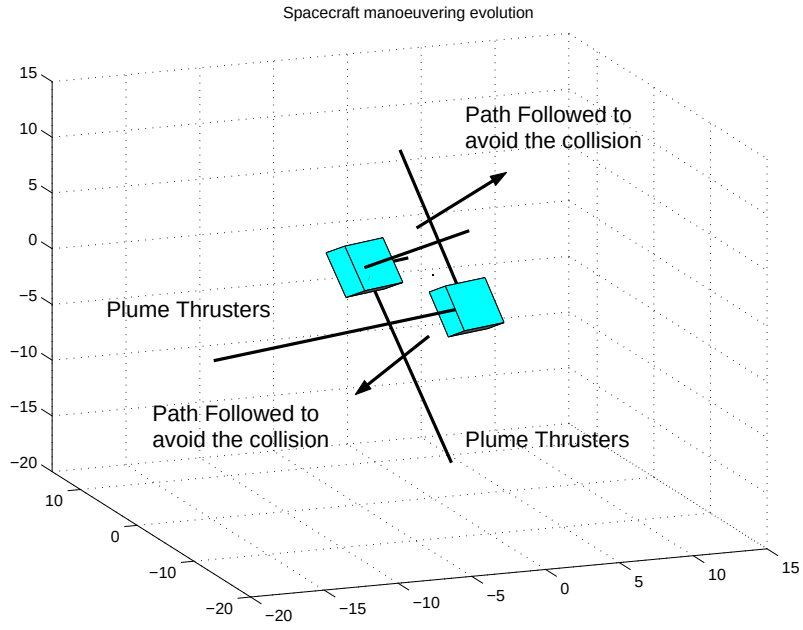

Figure 4.2: Plume impingement during deceleration phase.

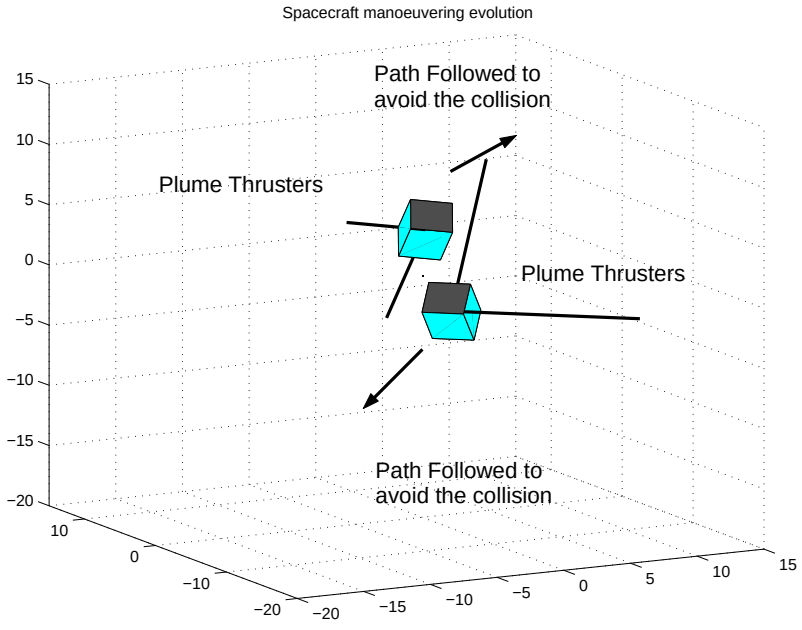

Figure 4.3: Plume impingement during avoidance phase.

The thrusters will then fire, if and only if, the plume lies outside the avoidance cone. In Figure 4.2 and 4.3 we can see that the method appears to be effective in avoiding plume impingement. At first two colliding spacecraft, decelerate their velocities, in Figure 4.2, before performing the avoidance manoeuvre, in Figure 4.3.

5 Conclusions

In this paper we have proposed some corrections to the traditional potential function control method. The strategies address the main drawback of such method, the presence of local minima. The methodology has been applied to a formation of spacecraft placed at the Sun-Earth L2 libration point. The control has been implemented for both translational and rotational movements, ensuring that the spacecraft reach the desired position with the required attitude. Obstacles, in the shape of other spacecraft or avoidance payload pointing areas have been accounted for in developing the potential function. Finally, the method has been used to avoid the possibility of plume impingement with promising results.

References

[1] Alfriend, K.T., Yan, H. and Vadali, S.R. Nonlinear considerations in satellite formation flying. *AIAA/AAS Astrodynamics Specialists Conference*, Monterey, California, USA, AIAA (2002)-4741.

[2] Cyrus, D.J. and Miller, D.W. Satellite design: past, present and future. *Int. J. Small Satellite Engineering* **1**(1) (1997).

[3] Gurifl, P., Idan, M. and Kasdin, J.N. Neurocontrol of spacecraft formation flying in the elliptic restricted three-body problem. *AIAA/AAS Astrodynamics Specialists Conference*, Monterey, California, USA, AIAA (2002)-4962.

[4] Hamilton, N.H., Folta, D. and Carpenter, R. Formation flying satellite control around the l2 sun-earth libration point. *AIAA/AAS Astrodynamics Specialists Conference*, Monterey, California, USA, AIAA (2002)-4528.

Nonlinear Dynamics and Systems Theory, **6** (4) (2006) 411–419

Numerical Search of Bounded Relative Satellite Motion

M. Sabatini [1], R. Bevilacqua [2], M. Pantaleoni [3] and D. Izzo [4*]

[1] *Department of Aerospace Engineering, University of Rome "La Sapienza"*
[2] *Department of Mathematical Models and Methods for Technology, University of Rome "La Sapienza"*
[3] *Aerospace Engineer, Alenia Spazio, Rome*
[4] *Research Fellow, Advanced Concepts Team, European Space Agency, The Netherlands*

Received: July 19, 2005; Revised: October 10, 2006

Abstract: Relative motion between two or more satellites has been studied for a long time, as the works of W.H. Clohessy and R.S. Wiltshire, dated 1960, or the studies of J. Tschauner, dated 1967, can testify. Not only these early works are milestones for the relative motion modelling, as they provide linear models whose accuracy in terms of motion prediction is granted in the simplified assumption of pure Keplerian motion, but they are also powerful tools to gain insight into the complex dynamical properties of this type of motion. These models supply conditions on the initial relative position and velocity that allow the relative orbits to be periodic, that is closed orbits. When perturbations, such as Earth oblateness and air drag effects, or even the simple nonlinearities of the keplerian gravitational attraction are taken into account in the model, an analytical solution appears more and more complicated to be derived, if not impossible. Simple relations on the initial conditions leading to periodic orbits, such as those that are well known when considering Hill-Clohessy-Wiltshire (HCW) equations, are not to be expected without introducing some simplifications. In these cases a numerical approach could still be able to locate the exact conditions that result in a minimum drift per orbit. This work investigates the possibility of using a global optimization technique to locate the initial conditions resulting into minimal drift per orbit. Before using this approach in the nonlinear problem, the methodology is tested on Hill's and Tschauner-Hempel's models, where an analytical solution is well known. The global optimizer is essentially a genetic algorithm that considers the initial relative velocities between the satellites as the chromosomes of the individuals of the population, the initial relative position is considered as given. This not only reduces the number of variables the GA has to optimize, but it also allows to search for closed relative orbits of a predefined dimension. Results show that the methodology is returning the analytical results with a satisfactorily precision and that is able to locate bounded motion also when nonlinearities become important.

* Corresponding author: Dario.Izzo@esa.int

Keywords: *Orbital mechanics; analytical Hill's solutions.*

Mathematics Subject Classification (2000): 70M20, 34C25.

Nomenclature

LVLH = Local Horizontal Local Vertical
x, y, z = relative position in LVLH frame
$\dot{x}, \dot{y}, \dot{z}$ = relative velocity in LVLH frame
subscript i= values at the initial time
subscript f= values at the final time
f = fitness function
ω_0 = angular velocity of the circular orbit
a = semi-major axis
e = eccentricity
i = inclination
Ω= RAAN
ω = argument of perigee
n = mean motion.

1 Introduction

Many efforts have been made in the last years on modelling and controlling satellites relative dynamic. In [7] conditions for relative orbits invariant with respect to the J2 perturbation are given in terms of mean orbital elements. In literature several linear models of relative dynamics including the second harmonic of the gravitational field, eccentricity and the air drag can be found (see [4, 6, 8]) but nor the analytical solution neither the initial conditions for periodic relative orbits are obtainable in most of these cases. The use of evolutionary/genetic approaches in the aerospace research, especially in mission analysis and design phase, is quite recent [5]. The difficulties encountered when using genetic algorithm in this field stand in the strong dependence that convergence speed shows upon the choice of the fitness function, the mutation and crossover probabilities, the population size and the number of generations. There is not a rigorous mathematical rule to choose these parameters in the best possible way, many times convergence can be achieved only after trial and error adjustment of the parameters with respect to the particular problem. For these reasons many think that global optimization using stochastic algorithms is more art than science. The benefits of these techniques are, though, huge. Stochastical global optimizers may approach many problems, otherwise unsolvable. A review on the use of global optimization techniques in problems related to Mission Analysis and System Design may be found in some recent studies funded under the European Space Agency ARIADNA scheme (see [2]).

2 Genetic Algorithms

Genetic Algorithms (GA) are stochastic global search methods that are based on the principle of natural selection and evolution of the species. These kinds of algorithms result to be effective for optimization problems containing different local optima with discontinuous parts between them. In these cases the calculus-based methods can converge to a local optimum rather then to the desired one. In the present paper a genetic algorithm is applied to minimize the drift per orbit in the simple case of two different linearized keplerian dynamic models. The first model of dynamics (HCW) considers a reference orbit without eccentricity (Hill-Clohessey-Wiltshire equations, [10]), the second model (TH) takes into account the eccentricity (Tschauner-Hempel equations [8] and [11]). After showing the convergence of the method to the well-known analytical conditions that exist for these simple dynamics, the algorithm is run with the nonlinear keplerian relative motion equations and considering an eccentricity value of $e = 0.3$. The relative motion is shown in the LVLH frame. The objective function chosen and maximized by the genetic algorithm has the following form

$$f(x, y, z) = -\sqrt{(x_f - x_i)^2 + (y_f - y_i)^2 + (z_f - z_i)^2} \tag{1}$$

representing the error in relative position between the initial conditions and those obtained at the end of the integration. The integration is performed over one orbital period in the linearized cases. For the nonlinear model five periods have been used to make the algorithm converge in a satisfying manner.

If a non linear dynamic, that takes into account all the possible perturbative effects, is considered, there is no clear argument that tells us information on the convexity of the objective function. On the other hand, in the Hill and T.-H. models, the objective function is expected to be convex in the $[e, \dot{y}, f]$ space. The software used for the numerical search is the online PIKAIA freely available tool (see [1]). PIKAIA uses a decimal alphabet made of 10 simple integers (0 through 9) for encoding the chromosome $(\dot{x}, \dot{y}, \dot{z})$. The mutation and crossover characteristic are the default PIKAIA's ones (see [1]).

3 Validation of the GA

3.1 Using the genetic algorithm to find analytical Hill's solutions

Considering the simple HCW equations to describe the relative dynamic between two orbiting objects we have that the analytical condition,

$$\frac{\dot{y_0}}{x_0} = -2\omega_0 \tag{2}$$

on the relative initial conditions, assures a periodic motion. If we now perform some numerical simulations considering a circular orbit with semimajor axis of 7000 km for which the above relation returns a ratio of $\frac{\dot{y_0}}{x_0} = -2.156E - 3s^{-1}$ we get the results contained in Table 3.1. The optimizer is able to converge to the global minimum that, in this case, is also the only minimum of the problem.

3.2 Using genetic algorithm to find analytical Tschauner-Hempel's solutions

As soon as we consider also the effect of the eccentricity on the relative satellite motion, the linear equations become with time periodic coefficients (Tschauner, 1967, [8]). In this

Individuals	Generations	$\frac{\dot{y}_0}{x_0}$ pikaia	Fitness function
20	50	-2.154459E-3	-2.721005E-2
20	100	-2.154459E-3	-2.721005E-2
50	100	-2.155201E-3	-1.425242E-2
100	100	-2.155892E-3	-2.164824E-3
100	500	-2.155892E-3	-2.164824E-3
100	1000	-2.155892E-3	-2.164824E-3

Table 3.1: Convergence of the GA increasing generations and population size.

case the relations between the initial conditions in order to obtain a periodic orbit are dependent on the true anomaly of the reference orbit and are quite complicated (Inalhan et al., 2002, [3]). When the true anomaly is zero, though, it is possible to write a simple analytical relation shown in Equation (3) (Inalhan et al., 2002, [3]):

$$\frac{\dot{y}_0}{x_0} = -\frac{n(2+e)}{(1-e)^{\frac{3}{2}}(1+e)^{\frac{1}{2}}} \,. \tag{3}$$

To perform the numerical simulations 100 individuals and 100 generations have been used. Higher values do not improve the quality of the solution.

Eccentricity	$\frac{\dot{y}_0}{x_0}$ eq.(1)	$\frac{\dot{y}_0}{x_0}$ pikaia	Percentage difference	Fitness function
$e = 0$	-2	-1.999999	-0.00005%	-3.4e-10
$e = 0.1$	-1.9091	-1.90899	-0.0058%	-5.2e-8
$e = 0.2$	-1.8333	-1.83339	0.00491%	-6.9e-8
$e = 0.3$	-1.7692	-1.76920	-0.000056%	-2.9e-8
$e = 0.4$	-1.7143	-1.714199	-0.005892%	-8.9e-7
$e = 0.5$	-1.6667	-1.666599	-0.006060%	-1.2e-6
$e = 0.6$	-1.625	-1.624998	-0.000123%	-3.3e-10
$e = 0.7$	-1.58823	-1.58819	-0.002519%	-4.9e-6
$e = 0.8$	-1.55556	-1.555599	0.002507%	-6.4e-5
$e = 0.9$	-1.526315	-1.526399	0.005503%	-1.6e-5

Table 3.2: GA restitution of the analytical TH conditions for different eccentricities.

The results in Table 3.2 are plotted in Figure 3.1.

As it was expected, the behaviour of the fitness function indicates an infinite number of minima but located in agreement to the Equation (3) (the real fitness has opposite sign with respect to the one here reported as the minima shown in Figure 3.2 are optimal maximum for the GA).

4 Searching Closed Relative Orbits for the Nonlinear Dynamic

When applying the above presented methodology to find the formations with minimal drift per orbit in a non linear dynamic case, problems arises in the propagation scheme that introduces difficulties in the calculation time and in the accuracy of the solution.

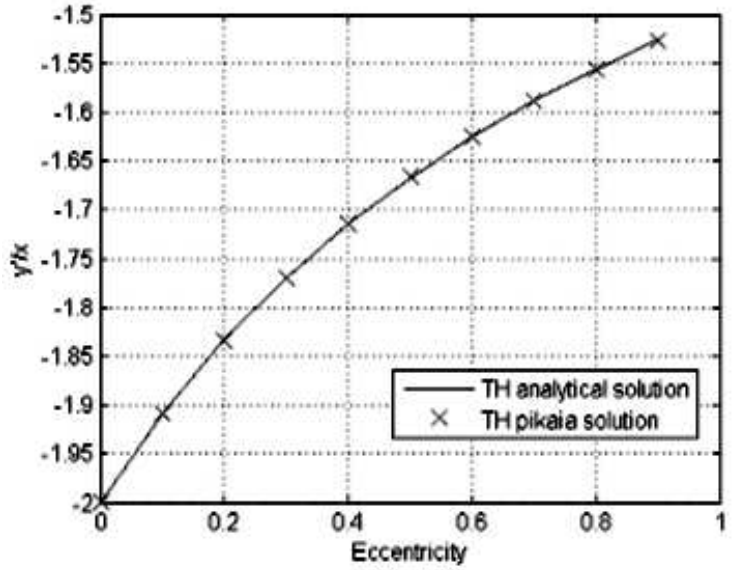

Figure 3.1: TH analytical solution vs. TH solution with GA.

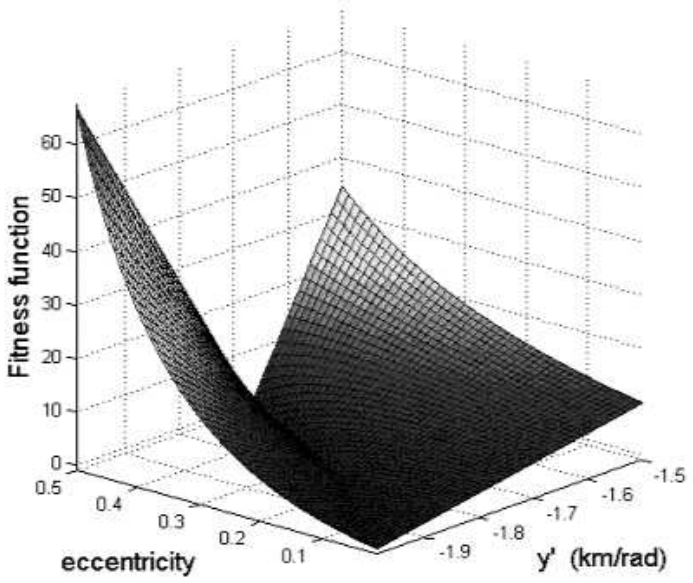

Figure 3.2: Fitness value vs. eccentricity and $\dot{y}$.

Subtracting directly the Cartesian coordinates of the two satellites can easily degrade the quality of the relative position obtained, as it subtract two very close values. In [9] an approach based on a geometric method (called unit sphere projection) is proposed. Integrating the relative dynamic in terms of orbital elements (for the Keplerian case just the true anomaly has to be used, see [9]) and subsequently translate the differences in terms $\delta x, \delta y, \delta z$ is numerically more accurate and the computation time is dramatically reduced. This approach has been used here. In Table 4.1 the used genetic parameters are reported.

Crossover probability	Mutation rate		
	initial	minimum	maximum
0.85	0.005	0.0005	0.25

Table 4.1: Genetic parameters for nonlinear approach.

After numerous trials the number of generations has been set to 500 with a population of 100 individuals and simulations have been performed for different relative orbit sizes. The initial dimension of these orbits increase from a 2 km relative position on the three axes to a 500 km one.

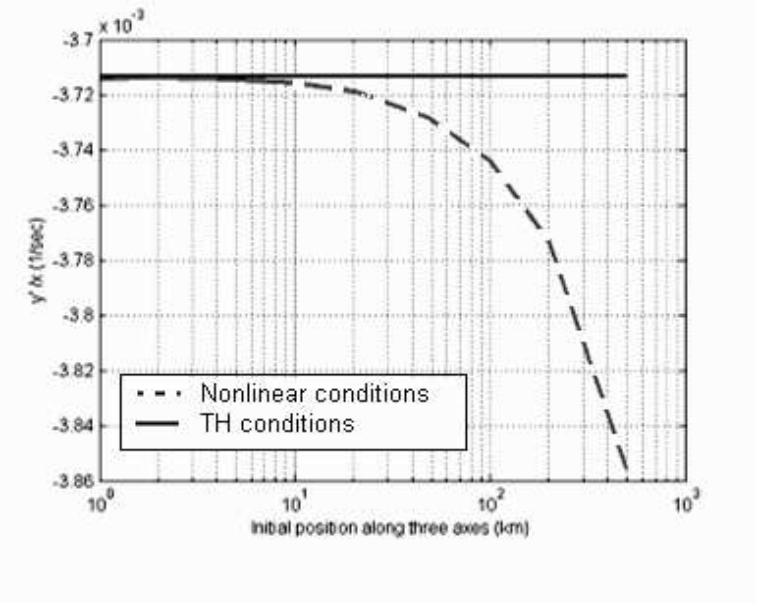

Figure 4.1: $\frac{\dot{y_0}}{x_0}$ ratio compared for the linearized and the nonlinear models (logarithmic scale on x axis).

Comparing the analytical relation of TH with the $\frac{\dot{y_0}}{x_0}$ rate obtained trough the GA it is easy to notice how the linear condition loses its capability to produce bounded orbits as the formation dimension increase. Figure 4.1 shows the comparison between the results given by Equation (3) and the one given by the genetic algorithm. As the size increases the ratio $\frac{\dot{y_0}}{x_0}$, as obtained from our numerical simulations, decreases drastically.

As expected the relation given in Equation (3) allows to obtain closed orbit only for small formations. The GA approach is therefore suitable to get the condition of periodic motion in these cases. In Figure 4.2 and Figure 4.3 a plot of ten orbits is shown as obtained propagating the initial conditions given by Equation (3) and by the GA and for two different formations of different sizes: a small one (2 km) ad a larger one (200 km).

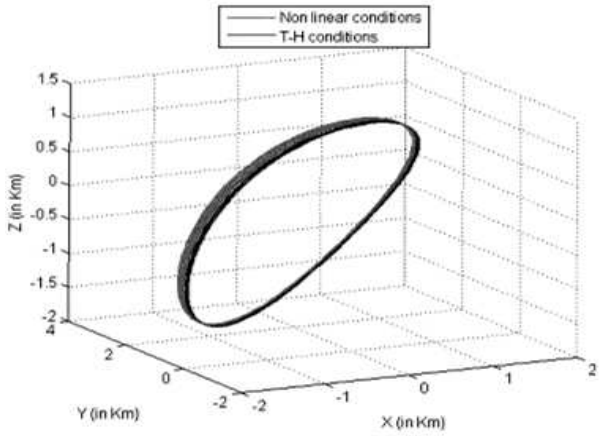

Figure 4.2: 10 orbits (TH vs. nonlinear) for low size (2 km).

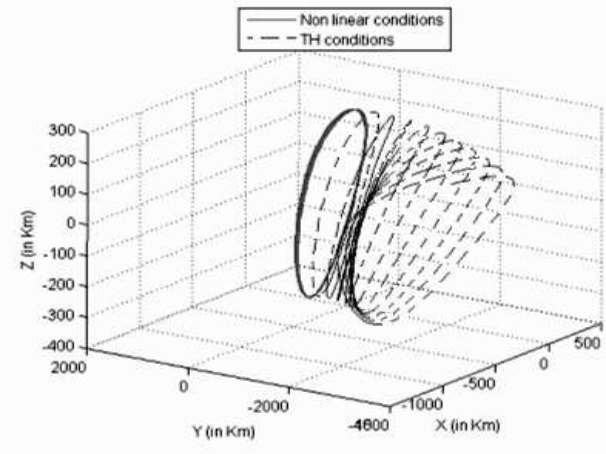

Figure 4.3: 110 orbits (TH vs. nonlinear) for high size (200 km).

As an additional proof of the GA convergence to a satisfying solution the orbital parameters of the two spacecrafts are calculated and compared in Table 4.2.

The only parameter that clearly maintains its value unchanged (considering the numerical errors) is the semi-major axis a. This result coincides with the only constrain to close a relative orbit in a Keplerian motion: the equality of the semi-major axis. In this

Vehicle N1		Vehicle N2		% difference
a	7000 km	a	7000.124 km	0.0018 %
e	0.3	e	0.2928	2.4 %
i	35	i	35.012	0.034%
Ω	35	Ω	33.99	2.9%
ω	35	ω	1.405	95.99 %

Table 4.2: Orbital parameters comparison.

way the two orbits have the same orbital period T and obviously the relative position is repeated every T seconds.

5 Conclusion

The GA strategy here used resulted to be a valid instrument to analyze the behavior of the nonlinear relative dynamics between two satellites in Keplerian orbit. After having re-obtained the Hill's and T.-H.'s solutions for bounded trajectories to check the validity of the algorithm, the GA has been run for the complete mathematical model of relative motion in Keplerian orbit. Considering the numerical approach and the limitations in terms of accuracy for the solutions, the matching period condition have been obtained for closing the relative orbit. The initial velocities generated with the genetic calculation match the analytic relation for T.-H. demonstrating the validity of the linear approach for low dimensions orbits. Increasing size results in a obliged switching to the conditions obtained numerically. Future developments of this new approach to the formation flying problem include the analysis of J2 and drag effects. The present paper represents an introduction and a validation work for the authors whose aim is to apply and study the possibilities given by the genetic algorithm to the most complete as possible model of the relative dynamics of satellites.

References

[1] Charbonneau P. and Knapp B. *A User's Guide to PIKAIA 1.0*. NCAR Technical note 418+1A (Boulder: National Centre for Atmospheric Research), 1995.

[2] Myatt, D.R., Becerra, V.M., Nasuto, S.J. and Bishop, J.M. *Advanced Global Optimisation for Mission Analysis and Design.* Final Report. Ariadna id: 03/4101. Contract Number: 18138/04/NL/MV, 2004. Available on-line: http://www.esa.int/gsp/ACT/doc/ACTRPT-ARIADNA-03-4101-Reading.pdf.

[3] Inalhan G., Tillerson M. and How J. P. Relative dynamics and control of spacecraft formations in eccentric orbits. *Journal of Guidance, Control and Dynamics* **25**(1) (2002) 48–59.

[4] Izzo D. Formation Flying linear modelling. *Proc. of the 5th Int. Conf. on Dynamics and Control of Systems and Structures in Space*, Cambridge, UK, 14–18 July 2002, 283–289.

[5] Kim Y.H. and Spencer D.B. Optimal spacecraft rendezvous using genetic algorithms. *J. Spacecraft and Rockets* **39**(6) (2002) 859–865.

[6] Izzo D., Sabatini M. and Valente C. A new linear model describing formation flying dynamics under J2 effects. *Proc. of 17th AIDAA National Congress*, Rome, ITA, 15–19 September 2003, Vol.1, 493–500.

[7] Schaub H. and Alfriend K.T. J2 invariant relative orbits for spacecraft formations. *Celestial Mechanics and Dynamical Astronomy* 79 (2001) 77–95.

[8] Tschauner J. Elliptic orbit rendezvous. *AIAA Journal* **5** (1967) 1110–1113.

[9] Vadali S.R. An analytical solution for relative motion of satellites. *Proc. of the 5th Int. Conf. on Dynamics and Control of Structures and Systems in Space*, Cambridge, UK, 14–18 July 2002, P. 309–316.

[10] Clohessy W.H. and Wiltshire R.S. Terminal guidance system for satellite rendezvous. *J. Aerospace Sciences* **27** (1960) 653–658.

[11] Tshauner J. and Hempel P. Rendezvous zu einem in Elliptischer Bahn Umlaufenden Ziel. *Acta Astronautica* **11** (1965) 104–109.

Nonlinear Dynamics and Systems Theory, **6** (4) (2006) 421–422

Contents of Volume 6, 2006

Volume 6 Number 1 March 2006

Volume 6 Number 2 June 2006

Volume 6 Number 3 September 2006

Volume 6 Number 4 December 2006

Cambridge Scientific Publishers

An International Book Series

Stability, Oscillations and Optimization of Systems

Modern stability theory, oscillations and optimization of nonlinear systems developed in respond to the practical problems of celestial mechanics and engineering has become an integral part of human activity at the end of XX century.

If, for a process or a phenomenon, for example, atom oscillations or a supernova explosion, a mathematical model is constructed in the form of a system of differential equations, the investigation of the latter is possible either by a direct (numerical as a rule) integration of the equations or by its analysis by qualitative methods.

In XX century the fundamental works by Euler (1707 – 1783), Lagrange (1736 – 1813), Poincaré (1854 – 1912), Lyapunov (1857 – 1918) and others have been thoroughly developed and applied in stability and oscillations investigation of nature phenomena and solution of many problems of technical progress.

In particular, the problems of piloted space flights and those of astrodynamics were solved due to modern achievements of stability theory and motion control. The Poincaré and Lyapunov methods of qualitative investigation of solutions to nonlinear systems of differential equations in macro-world study have been refined to a great extend though not completed. On the other hand modeling and establishing stability conditions for micro-processes are still on the stage of accumulating ideas and facts and forming the principles. One of the examples is the fact that the stability problem of thermonuclear synthesis has not been solved yet.

Obviously, this is one of the areas for application of stability and control theory in XXI century. For the development of efficient methods and algorithms in this area the interaction and spreading of the ideas and results of various mathematical theories will be necessary as well as the co-operation of scientists specializing in different fields.

The mathematical theory of optimal control (of moving objects, water resources, global process in world economy, etc.) is being developed in terms of basic ideas and results obtained in 1956 – 1961 and formulated in the Pontryagin's principle of optimality and Bellman's principle of dynamical programming. Considering manufacturing and production engineering activities, due to the difficulties of description of discrete events and hybrid processes, various heuristic and soft computing approaches have been developed for solving optimization problems. The efforts of many scholars and engineers in the framework of these ideas resulted in the efficient methods of control for many concrete systems and technological processes.

Thus, the development of classical ideas and results of stability and control theory remains the principle direction for the scholars and experts at modern stage of the mathematical theories. This fact will be demonstrated in the International Series **Stability, Oscillations and Optimization of Systems** by Cambridge Scientific Publishers Ltd.

Stability, Oscillations and Optimization of Systems provides a medium for the publication of high quality original monographs in the following areas:

Development of the theory and methods of stability analysis:

A. Stability Theory (ordinary differential equations, partial differential equations, stochastic differential equations, functional differential equations, integral equations, difference equations, etc.)
B. Dynamical Systems and Ergodic Theory (bifurcations and singularity, critical point theory, polystability, etc.)

Development of methods of the theory of nonlinear oscillations:
A. Analitical methods.
B. Qualitative methods.
C. Topological mehtods.
D. Numerical and computational methods, etc.

Development of the theory and methods of optimization of systems:
A. Optimal control of systems involving ODE, PDE, integral equations, equations with retarded argument, etc.
B. Minimax problems and nonsmooth analysis.
C. Necessary and sufficient conditions for optimality.
D. Hamilton-Jacobi theories.
E. Methods of successive approximations, etc.
F. Heuristics and metaheuristics for the optimization of ill defined and complex systems.

Applications:
A. Physical sciences (classical mechanics, including fluid and solid mechanics, quantum and statistical mechanics, plasma physics, astrophysics, etc.).
B. Engineering (mechanical engineering, aeronautical engineering, electrical engineering, chemical engineering).
C. Mathematical biology and life sciences (molecular biology, population dynamics, theoretical ecology).
D. Complex systems (synchronization, information and self-organization, collective dynamics, spatiotemporal chaos, biological and neural networks).
E. Manufacturing and production engineering.
F. Social sciences (economics, philosophy, sociology).

In the forthcoming publications of the series the readers will find fundamental results and survey papers by the experts from the worldwide which sum up the results of investigations in many directions of stability and control theory including uncertain and hybrid systems and systems with chaotic behavior of trajectories.

It is in this spirit that we see the importance of the **Stability, Oscillations and Optimization of Systems** series, and we are immensly thankful to Cambridge Scientific Publishers, Ltd. for their interest and cooperation in publishing this series.

visit us at our web site!
www.cambridgescientificpublishers